ISSN 2686-7575 (Online)

ТОНКИЕ ХИМИЧЕСКИЕ ТЕХНОЛОГИИ

Fine Chemical Technologies

- Theoretical Bases of Chemical Technology
- Chemistry and Technology of Organic Substances
- Chemistry and Technology of Medicinal Compounds and Biologically Active Substances
- Biochemistry and Biotechnology
- Synthesis and Processing of Polymers and Polymeric Composites
- Chemistry and Technology of Inorganic Materials
- Analytical Methods in Chemistry and Chemical Technology
- Mathematical Methods and Information Systems in Chemical Technology

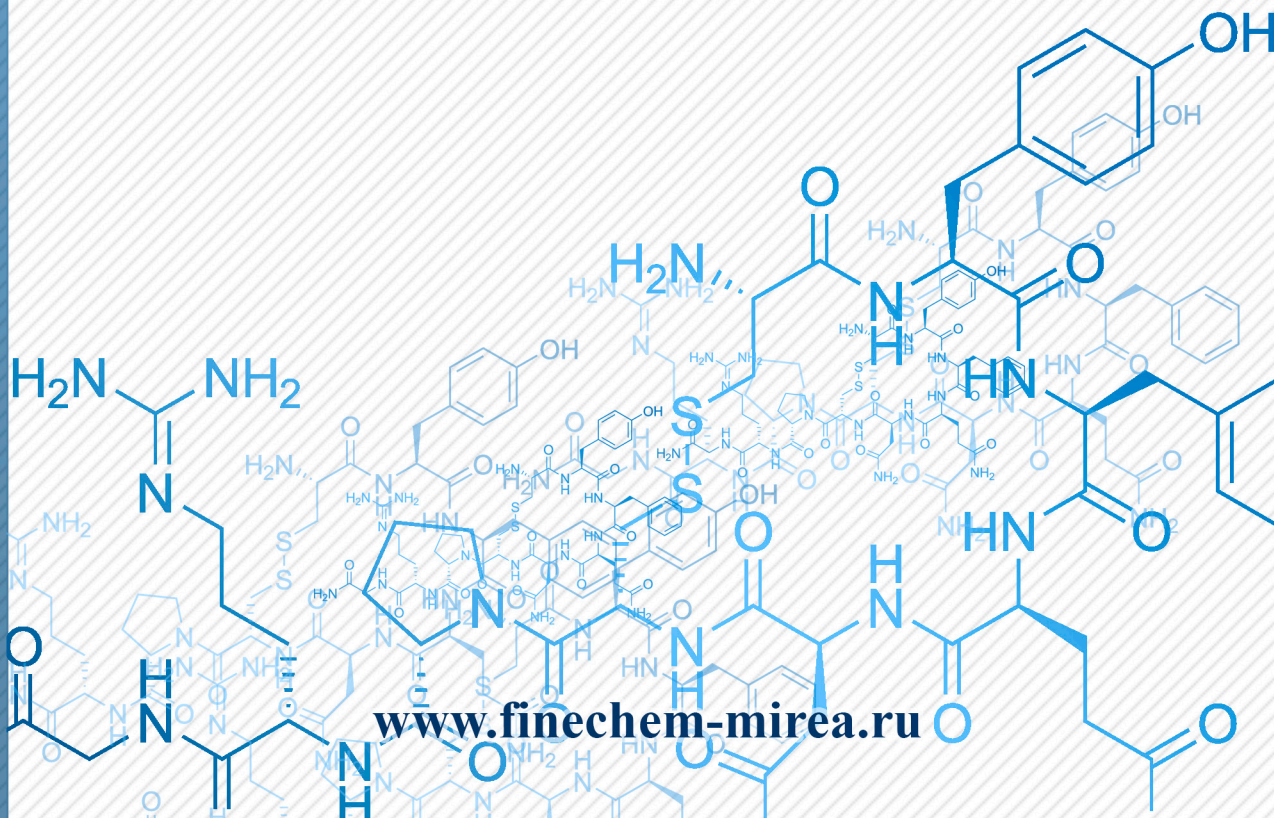

18(5)

2023

www.finechem-mirea.ru

ISSN 2686-7575 (Online)

ТОНКИЕ ХИМИЧЕСКИЕ ТЕХНОЛОГИИ

Fine Chemical Technologies

- Theoretical Bases of Chemical Technology
- Chemistry and Technology of Organic Substances
- Chemistry and Technology of Medicinal Compounds and Biologically Active Substances
- Biochemistry and Biotechnology
- Synthesis and Processing of Polymers and Polymeric Composites
- Chemistry and Technology of Inorganic Materials
- Analytical Methods in Chemistry and Chemical Technology
- Mathematical Methods and Information Systems in Chemical Technology

Tonkie Khimicheskie Tekhnologii = Fine Chemical Technologies
Vol. 18, No. 5, 2023

Тонкие химические технологии = Fine Chemical Technologies
Том 18, № 5, 2023

https://doi.org/10.32362/2410-6593-2023-18-5
www.finechem-mirea.ru

https://doi.org/10.32362/2410-6593 **ISSN 2686-7575 (Online)**

Tonkie Khimicheskie Tekhnologii = Fine Chemical Technologies 2023, Vol. 18, No. 5

The peer-reviewed scientific and technical journal Fine Chemical Technologies highlights the modern achievements of fundamental and applied research in the field of fine chemical technologies, including theoretical bases of chemical technology, chemistry and technology of medicinal compounds and biologically active substances, organic substances and inorganic materials, biochemistry and biotechnology, synthesis and processing of polymers and polymeric composites, analytical and mathematical methods and information systems in chemistry and chemical technology.

Founder and Publisher

Federal State Budget
Educational Institution of Higher Education
"MIREA – Russian Technological University"
78, Vernadskogo pr., Moscow, 119454, Russian Federation.
Publication frequency: bimonthly.
The journal was founded in 2006. The name was Vestnik MITHT until 2015 (ISSN 1819-1487).

The journal is included into the List of peer-reviewed science press of the State Commission for Academic Degrees and Titles of the Russian Federation.
The journal is indexed:
SCOPUS, DOAJ, Chemical Abstracts, Science Index, RSCI, Ulrich's International Periodicals Directory

86, Vernadskogo pr., Moscow, 119571, Russian Federation.
Phone: +7 (499) 600-80-80 (#31288)
E-mail: *seredina@mirea.ru*

The registration number ПИ № ФС 77–74580 was issued in December 14, 2018 by the Federal Service for Supervision of Communications, Information Technology, and Mass Media of Russia.
The subscription index of *Pressa Rossii*: **36924**

Тонкие химические технологии = Fine Chemical Technologies 2023, том 18, № 5

Научно-технический рецензируемый журнал «Тонкие химические технологии» освещает современные достижения фундаментальных и прикладных исследований в области тонких химических технологий, включая теоретические основы химической технологии, химию и технологию лекарственных препаратов и биологически активных соединений, органических веществ и неорганических материалов, биохимию и биотехнологию, синтез и переработку полимеров и композитов на их основе, аналитические и математические методы и информационные системы в химии и химической технологии.

Учредитель и издатель

федеральное государственное бюджетное
образовательное учреждение высшего образования
«МИРЭА – Российский технологический университет»
119454, РФ, Москва, пр-т Вернадского, д. 78.
Периодичность: один раз в два месяца.
Журнал основан в 2006 году. До 2015 года издавался под названием «Вестник МИТХТ» (ISSN 1819-1487).

Журнал входит в Перечень ведущих рецензируемых научных журналов ВАК РФ.
Индексируется:
SCOPUS, DOAJ, Chemical Abstracts, РИНЦ (Science Index), RSCI, Ulrich's International Periodicals Directory

119571, Москва, пр. Вернадского, 86, оф. Л-119.
Тел.: +7 (499) 600-80-80 (#31288)
E-mail: *seredina@mirea.ru*

Регистрационный номер и дата принятия решения о регистрации СМИ: ПИ № ФС 77-74580 от 14.12.2018 г. СМИ зарегистрировано Федеральной службой по надзору в сфере связи, информационных технологий и массовых коммуникаций (Роскомнадзор).
Индекс по Объединенному каталогу «Пресса России»: **36924**

Ivan A. Novakov – Academician at the RAS, Dr. Sci. (Chem.), Professor, President of the Volgograd State Technical University, Volgograd, Russian Federation.
Scopus Author ID 7003436556, ResearcherID I-4668-2015, http://orcid.org/0000-0002-0980-6591, *president@vstu.ru.*

Alexander N. Ozerin – Corresponding Member of the RAS, Dr. Sci. (Chem.), Professor, Enikolopov Institute of Synthetic Polymeric Materials of the RAS, Moscow, Russian Federation.
Scopus Author ID 7006188944, ResearcherID J-1866-2018, https://orcid.org/0000-0001-7505-6090, *ozerin@ispm.ru.*

Tapani A. Pakkanen – PhD, Professor, Department of Chemistry, University of Eastern Finland, Joensuu, Finland.
Scopus Author ID 7102310323, *tapani.pakkanen@uef.fi.*

Armando J.L. Pombeiro – Academician at the Academy of Sciences of Lisbon, PhD, Professor, President of the Center for Structural Chemistry of the Higher Technical Institute of the University of Lisbon, Lisbon, Portugal.
Scopus Author ID 7006067269, ResearcherID I-5945-2012, https://orcid.org/0000-0001-8323-888X, *pombeiro@ist.utl.pt.*

Dmitrii V. Pyshnyi – Corresponding Member of the RAS, Dr. Sci. (Chem.), Professor, Institute of Chemical Biologyand Fundamental Medicine, Siberian Branch of the RAS, Novosibirsk, Russian Federation.
Scopus Author ID 7006677629, ResearcherID F-4729-2013, https://orcid.org/0000-0002-2587-3719, *pyshnyi@niboch.nsc.ru.*

Alexander S. Sigov – Academician at the RAS, Dr. Sci. (Phys. and Math.), Professor, President of MIREA – Russian Technological University, Moscow, Russian Federation.
Scopus Author ID 35557510600, ResearcherID L-4103-2017, *sigov@mirea.ru.*

Alexander M. Toikka – Dr. Sci. (Chem.), Professor, Institute of Chemistry, Saint Petersburg State University, St. Petersburg, Russian Federation.
Scopus Author ID 6603464176, ResearcherI D A-5698-2010, http://orcid.org/0000-0002-1863-5528, *a.toikka@spbu.ru.*

Andrzej W. Trochimczuk – Dr. Sci. (Chem.), Professor, Faculty of Chemistry, Wrocław University of Science and Technology, Wrocław, Poland.
Scopus Author ID 7003604847, *andrzej.trochimczuk@pwr.edu.pl.*

Aslan Yu. Tsivadze – Academician at the RAS, Dr. Sci. (Chem.), Professor, A.N. Frumkin Institute of Physical Chemistry and Electrochemistry of the RAS, Moscow, Russian Federation.
Scopus Author ID 7004245066, ResearcherID G-7422-2014, *tsiv@phyche.ac.ru.*

Новаков Иван Александрович – академик РАН, д.х.н., профессор, президент Волгоградского государственного технического университета, Волгоград, Российская Федерация.
Scopus Author ID 7003436556, ResearcherID I-4668-2015, http://orcid.org/0000-0002-0980-6591, *president@vstu.ru.*

Озерин Александр Никифорович – член-корр. РАН, д.х.н., профессор, Институт синтетических полимерных материалов им. Н.С. Ениколопова РАН, Москва, Российская Федерация.
Scopus Author ID 7006188944, ResearcherID J-1866-2018, https://orcid.org/0000-0001-7505-6090, *ozerin@ispm.ru.*

Пакканен Тапани – PhD, профессор, Департамент химии, Университет Восточной Финляндии, Йоенсуу, Финляндия.
Scopus Author ID 7102310323, *tapani.pakkanen@uef.fi.*

Помбейро Армандо – академик Академии наук Лиссабона, PhD, профессор, президент Центра структурной химии Высшего технического института Университета Лиссабона, Португалия.
Scopus Author ID 7006067269, ResearcherID I-5945-2012, https://orcid.org/0000-0001-8323-888X, *pombeiro@ist.utl.pt.*

Пышный Дмитрий Владимирович – член-корр.РАН, д.х.н., профессор, Институт химической биологии и фундаментальной медицины Сибирского отделения РАН, Новосибирск, Российская Федерация.
Scopus Author ID 7006677629, ResearcherID F-4729-2013, https://orcid.org/0000-0002-2587-3719, *pyshnyi@niboch.nsc.ru.*

Сигов Александр Сергеевич – академик РАН, д.ф.-м.н., профессор, президент МИРЭА – Российского технологического университета, Москва, Российская Федерация.
Scopus Author ID 35557510600, ResearcherID L-4103-2017, *sigov@mirea.ru.*

Тойкка Александр Матвеевич – д.х.н., профессор, Институт химии, Санкт-Петербургский государственный университет, Санкт-Петербург, Российская Федерация.
Scopus Author ID 6603464176, Researcher ID A-5698-2010, http://orcid.org/0000-0002-1863-5528, *a.toikka@spbu.ru.*

Трохимчук Анджей – д.х.н., профессор, Химический факультет Вроцлавского политехнического университета, Вроцлав, Польша.
Scopus Author ID 7003604847, *andrzej.trochimczuk@pwr.edu.pl.*

Цивадзе Аслан Юсупович – академик РАН, д.х.н., профессор, Институт физической химии и электрохимии им. А.Н. Фрумкина РАН, Москва, Российская Федерация.
Scopus Author ID 7004245066, ResearcherID G-7422-2014, *tsiv@phyche.ac.ru.*

ТОНКИЕ ХИМИЧЕСКИЕ ТЕХНОЛОГИИ
Fine Chemical Technologies

18(5)
2023

CONTENTS

СОДЕРЖАНИЕ

THEORETICAL BASES OF CHEMICAL TECHNOLOGY

ТЕОРЕТИЧЕСКИЕ ОСНОВЫ ХИМИЧЕСКОЙ ТЕХНОЛОГИИ

ISSN 2686-7575 (Online)

https://doi.org/10.32362/2410-6593-2023-18-5-415-425

UDC 66.048:541.1

RESEARCH ARTICLE

Flowsheets for hydroxyacetone–phenol binary mixture separation: The use of special distillation methods

Ivan S. Gaganov, Elena V. Rytova✉, Alla K. Frolkova

MIREA – Russian Technological University, Moscow, 119454 Russia
✉Corresponding author, e-mail: erytova@gmail.com

Abstract

Objectives. *To study the possibility of hydroxyacetone–phenol binary mixture (a constituent of a mixture of phenol production by the cumene method) separation in flowsheets based on the use of distillation special methods. This is the addition of separating agents to increase the relative volatility of the components of the original mixture, and the variation of pressure in the columns.*
Methods. *A computational simulation in Aspen Plus® was used as the research method. Mathematical modeling of the vapor–liquid equilibrium was carried out using a local compositions model Non-Random Two Liquid. The viability of the latter was confirmed by comparing experimental and calculated on phase equilibrium data, and azeotropic data. The average relative error does not exceed 3%.*
Results. *The dependence of the composition and boiling point of the hydroxyacetone–phenol azeotrope on pressure was determined in a computational experiment (as the pressure increases, the azeotrope is enriched with phenol). The possibility of using a complex of columns operating under different pressures to separate the mixture was shown (the shift of the azeotrope*

is about 9%). The change in the relative volatility of components of the original mixture in the presence of a high- (diethylene glycol) and a low-boiling (acetone) separating agent was investigated. Both solvents are selective agents used in extractive and re-extractive distillation processes. Three technological separation flowsheets containing two distillation columns were proposed.

Conclusions. *The study established the operation parameters of the columns (number of theoretical stages, feed stages of the original mixture and separating agent, and reflux ratio) and energy consumption (total heat supplied to the columns boiler) of three separation flowsheets ensuring the production of products of a given quality (not less than 0.99 mol fractions). The flowsheet with diethylene glycol is characterized by the lowest energy consumption. It is recommended that complexes of extractive and re-extractive distillation be further optimized. This enables the second product of cumulus production—acetone—to be involved in the technological cycle.*

Keywords: *phenol, hydroxyacetone, vapor–liquid equilibrium, extractive distillation, re-extractive distillation, pressure-swing distillation complexes*

For citation: Gaganov I.S., Rytova E.V., Frolkova A.K. Flowsheets for hydroxyacetone–phenol binary mixture separation: The use of special distillation methods. Тонкие химические технологии. *Tonk. Khim. Tekhnol. = Fine Chem. Technol.* 2023;18(5):415–425. https://doi.org/10.32362/2410-6593-2023-18-5-415-425

НАУЧНАЯ СТАТЬЯ

Схемы разделения бинарной смеси гидроксиацетон–фенол с использованием специальных методов ректификации

И.С. Гаганов, Е.В. Рытова✉, А.К. Фролкова

МИРЭА – Российский технологический университет, Москва, 119454 Россия
✉Автор для переписки, e-mail: erytova@gmail.com

Аннотация

Цели. *Исследовать возможность разделения смеси гидроксиацетон-фенол (составляющей смеси производства фенола кумольным методом) в схемах, базирующихся на использовании специальных приемов ректификации: добавлении разделяющих агентов, повышающих относительную летучесть компонентов исходной смеси, и варьировании давления в колоннах.*

Методы. *В качестве метода исследования применялся вычислительный эксперимент в среде программного комплекса Aspen Plus®. Математическое моделирование равновесия жидкость-пар проводилось с использованием модели локальных составов Non-Random Two Liquid. Адекватность последнего подтверждена сравнением экспериментальных и расчетных данных о фазовом равновесии, данных об азеотропии; средняя относительная ошибка не превышала 3%.*

Результаты. *В вычислительном эксперименте определена зависимость состава и температуры кипения азеотропа гидроксиацетон-фенол от давления (при увеличении давления азеотроп обогащается фенолом), показана возможность использования комплекса колонн, работающих под разным давлением, для разделения смеси (сдвиг азеотропа составляет порядка 9%). Исследовано изменение относительной летучести пары компонентов исходной смеси в присутствии тяжело- (диэтиленгликоль)*

и легкокипящего (ацетон) разделяющего агента. Оба растворителя являются селективными агентами для процессов экстрактивной и реэкстрактивной ректификации. Предложены три принципиальные технологические схемы разделения, содержащие две ректификационные колонны.

Выводы. *Определены статические параметры работы колонн (число теоретических тарелок, номера тарелок подачи исходной смеси и разделяющего агента, флегмовое число) и энергозатраты (суммарные нагрузки на кипятильники колонн) трех схем разделения, обеспечивающие получение продуктов заданного качества (не ниже 0.99 мол. долей). Наименьшими энергозатратами характеризуется схема с диэтиленгликолем. Для дальнейшей оптимизации рекомендованы комплексы экстрактивной и реэкстрактивной ректификации. Последняя позволяет вовлечь в технологический цикл второй продукт кумольного производства – ацетон.*

Ключевые слова: *фенол, гидроксиацетон, парожидкостное равновесие, экстрактивная, реэкстрактивная ректификация, комплексы с варьированием давления в колоннах*

Для цитирования: Гаганов И.С., Рытова Е.В., Фролкова А.К. Схемы разделения бинарной смеси гидроксиацетон-фенол с использованием специальных методов ректификации. *Тонкие химические технологии*. 2023;18(5):415–425. https://doi.org/10.32362/2410-6593-2023-18-5-415-425

INTRODUCTION

Phenol is a large-scale product of industrial organic synthesis, the main amount of which is obtained by the cumene method [1–4]. The combination of an aromatic ring in the phenol molecule, which ensures a fairly high thermal stability of the compound, and a hydroxy group, which has increased polarity compared to the alcohol hydroxyl and is one of the strongest *ortho-para*-orienting substituents, creates favorable conditions for the versatile use of phenolic products [5].

Wide application of phenol in various industries[1,2] constantly tightens the requirements for the purity of the target product[3]. By-products formed at the stage of chemical transformations are dimethylbenzyl alcohol and acetophenone. In addition to these high-boiling substances, other components, such as hydroxyacetone (HA), 2-methylbenzofuran (2-MBF) and mesityl oxide, are also formed in small quantities [6–11]. The negative effect of HA on the quality of phenol is manifested in the fact that in distillation columns, as well as at the stage of catalytic purification of raw phenol from impurities using heterogeneous catalysts at high temperatures, a condensation reaction of HA with phenol occurs to form 2-MBF. This heterocyclic compound is colorless, but during storage it easily forms colored resinous products, which deteriorates the color of the phenol. Eliminating the formation of HA and completely removing it from products using

[1] Chemie Mania: World consumption of phenol. URL: http://www.chemiemania.ru/chemies-8878-1.html. Accessed April 13, 2023.

[2] Analytical portal of the chemical industry: Global phenol market: installed capacity and demand forecast. URL: https://www.newchemistry.ru/printletter.php?n_id=4044. Accessed April 13, 2023.

[3] GOST 23519-93. Interstate Standard. Technical synthetic phenol. Specifications. Moscow: IPK Izdatelstvo standartov; 1996.

conventional distillation is a technically intractable task due to the presence of limitations imposed by vapor–liquid equilibrium (VLE) [6]. Previously, a method was proposed for producing high-quality phenol by reducing the content of 2-MBP at the stage of catalytic purification of phenol and changing the technology of distillation of the separated products. To achieve conditions that meet the requirements for phenol of the highest quality category, it was necessary to significantly complicate the traditional distillation flowsheet by introducing additional azeotropic-extractive distillation columns and installing more efficient trays in a number of columns. These measures, although not radically, solved the problem of purification from HA and 2-MBP: phenol of the required quality is produced at most plants, but it is too expensive, and any failures in the composition of the initial mixture entering the separation result in a decrease in quality [7].

Despite the proposed chemical and technological solutions, the task of improving the quality of phenol remains relevant and requires an assessment of the prospects and conditions for the use of special separation techniques in order to achieve the required purity of the target product (phenol). In this regard, the aim of this work is to find alternative options for separating a HA–phenol mixture, allowing reducing the HA content in the products of phenol synthesis using the cumene method.

OBJECTS AND METHODS OF RESEARCH

The binary component of the industrial mixture: HA–phenol was chosen as the object of study. Some physicochemical characteristics of the components at atmospheric pressure are presented in Table 1.

In order to evaluate options for the separation of a mixture of a specific composition, information is needed on the VLE under various conditions, in particular, when varying pressure and when additional substances are added to the system. To obtain the required data and further calculate the distillation process, the method of mathematical modeling of VLE in the Aspen Plus® V. 10.0 software package[4] (*AspenTech*, USA) using the Non-Random Two Liquid (NRTL) equation was used. The binary interaction parameters of the NRTL equation (Table 2) were taken from [7] and used to calculate the VLE at a pressure of 0.2 atm (Table 3).

The choice of reduced pressure is due to the fact that at atmospheric pressure there is a high probability of HA decomposition at temperatures above 145°C. At a pressure of 0.2 atm the temperature of the mixture does not exceed 135°C.

As follows from the data presented, the description of the VLE of the HA–phenol binary system at a pressure of 0.2 atm is generally satisfactory.

Table 1. Physicochemical characteristics of phenol and HA at a pressure of 1 atm [7]

Name	Gross formula	*M*, g/mol	$T_{b.p.}$, °C	n_D^{20}	d_4^{20}, g/cm^3
Phenol	C_6H_6O	94.11	181.8	1.5426	1.063
HA	$C_3H_6O_2$	74.08	145.5	1.4295	1.082

Note: M is the molar mass, g/mol; $T_{b.p.}$ is the boiling point, °C; n_D^{20} is the refractive index; d_4^{20} is density, g/cm^3.

Table 2. Binary interaction parameters for the NRTL equation [7]

Component *i*	Component *j*	a_{ij}	a_{ji}	b_{ij}	b_{ji}	c_{ij}
HA	Phenol	−0.798	−0.291	1.341	1.113	0.3

Note: a_{ij}, a_{ji}, b_{ij}, b_{ji} are parameters taking into account the binary interaction of components *i-j*, *j-i*; c_{ij} is the parameter taking into account the non-ideality of the mixture.

[4] Aspen Plus® is a powerful software designed for modeling processes in the chemical, petroleum, energy, and many other industries. The model obtained in a computational environment allows engineers and researchers to design and optimize various chemical processes and systems.

Table 3. Comparison of experimental [7] and calculated data on the VLE of the HA (1)–phenol (2) system at a pressure of 0.2 atm

x_{HA}, mol fract.	y_{HA}, mol fact.		Uncertainty errors y_{HA}		T, °C		Uncertainty errors T	
	exp.	calc.	abs., mol fract.	rel., %	exp.	calc.	abs., °C	rel., %
0.000	0.000	0.000	0.000	0.00	131.84	131.65	0.19	0.14
0.044	0.044	0.041	0.003	6.82	133.00	131.71	1.29	0.97
0.100	0.119	0.117	0.002	1.59	132.80	131.53	1.27	0.96
0.200	0.290	0.285	0.005	1.69	131.20	130.18	1.02	0.78
0.400	0.700	0.649	0.051	7.26	125.00	123.17	1.83	1.47
0.500	0.818	0.784	0.034	4.18	120.00	118.32	1.68	1.40
0.600	0.890	0.876	0.014	1.61	115.00	113.38	1.62	1.41
0.700	0.937	0.934	0.003	0.33	110.50	108.79	1.71	1.55
0.800	0.970	0.968	0.002	0.19	105.05	104.78	0.27	0.25
0.900	0.989	0.990	−0.001	0.08	101.13	101.44	−0.31	0.31
1.000	1.000	1.000	0.000	0.000	98.45	98.78	−0.33	0.34
			Average	2.637			Average	0.87

Note: x_{HA}, y_{HA} are the HA concentrations in liquid and vapor phases, respectively, mol fract.; T is the boiling point of the mixture. (1) A component of the mixture with a lower boiling point (in this case, HA), (2) A component of the mixture with a higher boiling point (phenol).

Therefore, the parameters of the binary interaction of the NRTL equation (Table 2) can be used in the future to calculate the distillation process.

RESULTS OF COMPUTATIONAL EXPERIMENT

The HA–phenol system is characterized by the presence of an azeotrope with a maximum boiling point (at constant pressure), which indicates significant negative deviations of the system from ideal behavior and, accordingly, the predominance of strong interactions of opposite molecules. The latter imposes thermodynamic restrictions on the process of conventional distillation and requires the use of special distillation techniques based on the principle of redistribution of concentration fields [12] between separation areas with different sets of final products. The method of extractive distillation (ED) [13, 14], which has proven itself to be an energy-efficient separation process, including mixtures containing phenol, has been widely used for the separation of mixtures of various natures [15–17].

To assess the possibility of using and operating conditions for separation complexes for a HA–phenol mixture, additional information was obtained on the effect of pressure on the composition of the binary azeotrope and potential separating agents (SA) (high-boiling diethylene glycol (DEG) and low-boiling acetone) on the relative volatility of the starting components. Table 4 shows the characteristics of a binary azeotrope at different pressures, which indicate the presence of a noticeable azeotropic shift in the considered pressure range.

Table 4. Calculated characteristics of azeotropes at different pressures

Pressure, atm	x_{HA}, mol fract.	T, °C
0.1	0.990	114.07
0.2	0.959	131.71
1.0	0.902	182.45

Note: x_{HA} is the concentration of HA in azeotropic mixture; T is the azeotropic mixture boiling point.

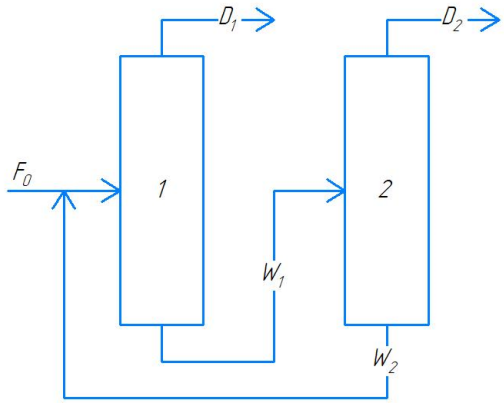

Fig. 1. Flowsheet I of separation of a mixture of HA (1)–phenol (2) at a pressure of 0.1 atm and 1.0 atm in columns *1* and *2*, respectively. F_0 is the amount of initial mixture, kmol/h; D is the distillate flow, kmol/h; W is the bottom flow, kmol/h.

Figure 1 shows a schematic diagram of separation (I), representing a complex of two columns operating at different pressures.

The calculation of the distillation process was carried out at 100 kmol/h of the initial mixture (feed to column *1*). The HA content (x_{HA}) in the initial mixture was 0.7 mol fract. (model composition). The initial mixture was fed into the column at a temperature T close to the boiling point of the mixture. Requirements for the quality of the resulting products: HA content x_{HA} = 0.995 mol fract., phenol content x_F = 0.999 mol fract. When calculating the distillation process, optimization of parameters: overall efficiency of the column N (number of theoretical stages, NTS), numbers of feed stages for the feed mixture streams (N_F) and SA (N_{SA}), as well as the reflux ratio R was carried out using the Sensitivity Analysis module. The model composition of the initial mixture was chosen to establish the general principles of separation of the HA–phenol mixture of the final composition (to exclude the situation of dilution of the mixture with the target product).

Table 5 shows the material balance and operating parameters of the columns of Flowsheet I, which represents a complex of two columns operating under a pressure of 0.1 and 1.0 atm, respectively.

The course of the lines of constant relative volatility of the HA–phenol pair in the presence of DEG (Fig. 2) and acetone (Fig. 3) shows that DEG (high-boiling SA, $T_{b.p.}$ = 244.8°C) and acetone (low-boiling SA, $T_{b.p.}$ = 56.0°C) increase the volatility of HA relative to phenol in mixtures with a high phenol content. For a model composition containing 0.7 mol fract. HA, in the presence of DEG, the relative volatility of HA decreases slightly, but remains high enough to realize the extractive effect.

Thus, in the first case, it is possible to organize the ED process [13–14], and in the second case, the process of re-extractive distillation (RED) [15].

Figure 4 shows the structures of the ED (Flowsheet II) and RED (Flowsheet III) complexes.

Flowsheets II and III are antipodean flowsheets and differ in the recovery of final products: in the first case (Fig. 4a) HA and phenol are recovered as the distillate flows; in the second (Fig. 4b)—as the bottom flows. An essential requirement for the functioning of the first column of both flowsheets is the organization of a counterflow of the initial mixture (F_0) and SA.

The calculation of the ED and RED process was carried out using the binary interaction parameters of the NRTL equation taken from [7], the NIST database[5], or modeled using the UNIFAC equation. The quantity and composition of the initial mixture, as well as the quality requirements for HA and phenol, correspond to Flowsheet I; purity of SA x_{SA} = 0.999 mol fract.

[5] Aspen Plus® V. 10.0 database. NIST Chemistry WebBook URL: https://webbook.nist.gov/. Accessed April 22, 2023.

Table 5. Material balance and operating parameters of distillation columns at different pressures

Col. No.	*P*, atm	*N*, NTS	N_F	*R*	Distillate (*D*)	Bottom flow (*W*)	Q_{boil}, kW
					Flow rate / x_{HA} (*T*, °C)	Flow rate / x_{HA} (*T*, °C)	
1	0.1	60	3	3	70 / 0.995 (82.11)	33.41 / 0.021 (97.77)	3575.6
2	1.0	70	17	2	30 / 0.001 (165.15)	3.41 / 0.098 (182.45)	1287.8
						Total energy consumption	4863.3

Note: Flow rate is the number of flows, kmol/h; x_{HA} is the concentration of HA in the flow, mol fract.; *T* is the flow temperature (distillate/still), corresponds to the boiling temperature at a given composition of the distillate/still, °C. The plates are numbered from the top of the column. Q_{boil} is the energy consumption of the boiler, kW.

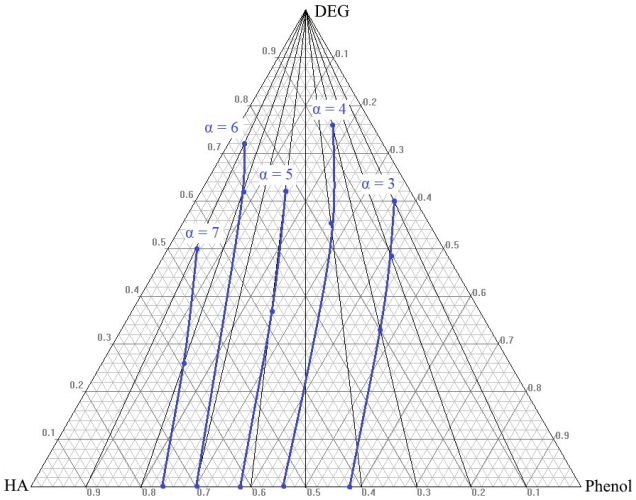

Fig. 2. Isoline diagram of the relative volatility of the HA–phenol binary system in the presence of DEG (SA) at a pressure of 0.2 atm, α is the relative volatility of the components.

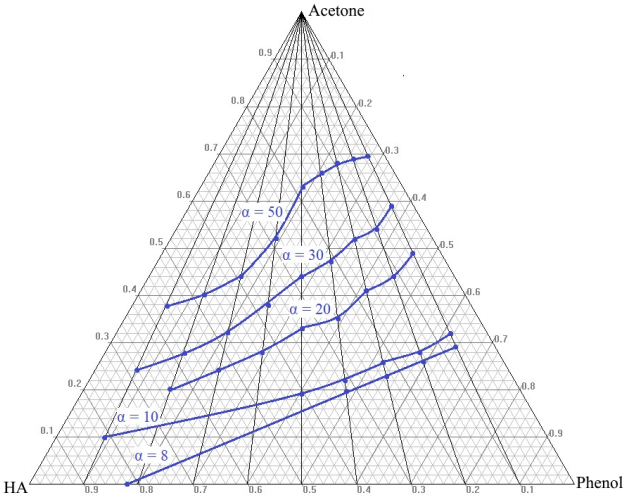

Fig. 3. Isoline diagram of the relative volatility of the HA–phenol binary system in the presence of acetone (SA) at a pressure of 0.2 atm, α is the relative volatility of the components.

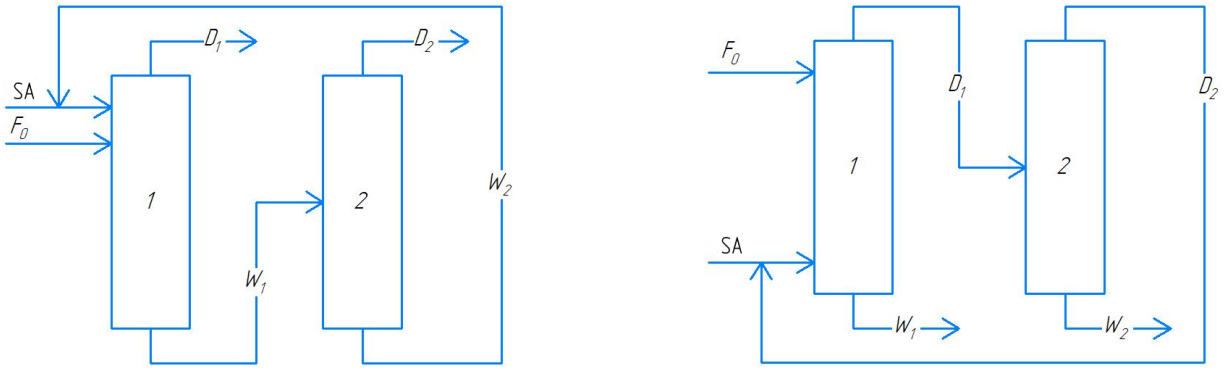

Fig. 4. Structures of the ED (Flowsheet II, a) and RED (Flowsheet III, b) complexes. F_0 is the flow of the initial mixture, kmol/h; *D* is the distillate flow, kmol/h; *W* is the bottom flow, kmol/h.

An important indicator of the ED and RED processes is the SA consumption, which ensures its selective action. Therefore, at the first stage of optimization of the parameters of the corresponding columns of Flowsheet II and III, a "manual" selection of the SA flow rates and pressure in the column necessary to achieve the specified purity of the product streams was carried out, and in most cases the quality of the products exceeded the specified one. Next, the Design Specs and Sensitivity Analysis modules were used.

The calculation results for the ED and RED processes are presented in Table 6.

DISCUSSION OF RESULTS

The data from the computational experiment showed that in all three options the required quality of product flows was achieved. The most efficient option for separating an HA–phenol mixture is the ED process with high-boiling SA (DEG). As one would expect, the RED mode with low-boiling SA (acetone) requires the highest (almost twice as much as in ED) energy consumption, which is due, among other things, to the higher ratio of SA (2.0 compared to 1.2 in ED), which it is necessary to evaporate twice to isolate acetone in the distillates of both columns of the RED complex. Flowsheets I and III differ slightly in energy consumption (8.6%).

A comparison of the ED and RED modes shows a significant reduction in the total energy consumption in the first column of the ED complex, which is associated with the additional ease of isolating HA as a product with a minimum boiling point in the distillation region, which belongs to the mixture of F_0 + SA gross composition. In this case, at close levels of supply of the initial mixture and SA, we can talk about the process of conventional distillation of a ternary mixture of HA–phenol–DEG. A feature of this mode is the production in the cube of a column of a composition belonging to a separatrix [14], which, due to curvature, touches the side of the DEG–phenol triangle in the DEG concentration range of 0.65–1.0 mol fract. (Fig. 5). The latter leads to a decrease in the content of HA impurities in the bottom product of the ED column, which otherwise would be about 1.0–1.5%.

Despite the high energy consumption of the RED complex, its main advantage is the involvement of acetone in the technological process—the second target product of the cumene method

Table 6. Material balance and operating parameters of distillation columns of the ED and RED complexes

Col. No.	*P*, atm	*N*, NTS	N_F / N_{SA}	*R*	Distillate (*D*)	Bottom flow (*W*)	Q_{boil}, kW
					Flow rate / x_{HA} / x_F (*T*, °C)	Flow rate / x_{HA} / x_F (*T*, °C)	
ED complex (SA/mixture ratio = 120 : 100)							
1	0.2	16	9 / 6	0.67	70 / 0.996 / 0.004 (98.88)	150 / 0.002 / 0.198 (172.69)	1602.0
2	0.2	20	6 / –	1.45	30 / 0.001 / 0.999 (131.69)	120 / 0.000 / 0.008 (190.91)	1111.0
						Total energy consumption	2713.0
RED complex (PA/mixture ratio = 200 : 100)							
1	0.35	60	7 / 53	0.15	270 / 0.259 / 0.000 (34.24)	30 / 0.001 / 0.999 (147.44)	3050.0
2	1.0	11	7 / –	0.08	200 / 0.002 / 0.000 (56.18)	70 / 0.999 / 0.000 (143.61)	2230.0
						Total energy consumption	5280.0

Note: Flow rate is the number of flows, kmol/h; x_{HA} and x_F are concentrations of HA and phenol in the flow, respectively, mol fract.; *T* is the flow temperature (distillate/still), corresponds to the boiling temperature at a given composition of the distillate/still, °C. The plates are numbered from the top of the column. Q_{boil} is the energy consumption of the boiler, kW.

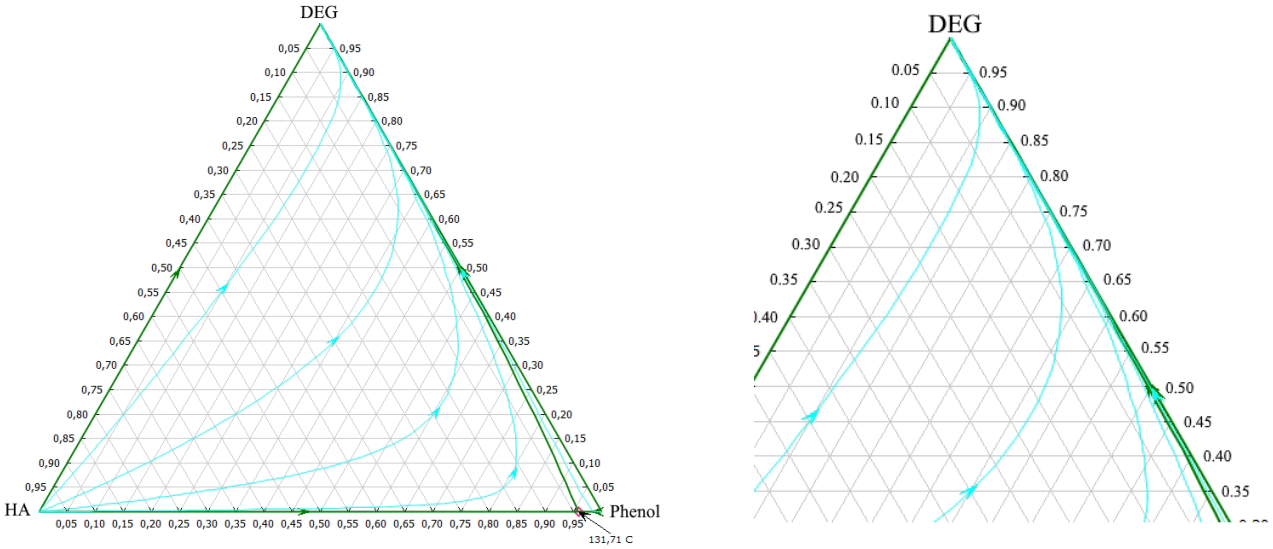

(a) (b)

Fig. 5. Distillation lines in the concentration triangle of the HA–phenol–DEG system (a) and a fragment of the diagram (b), reflecting the features of the location of the separatrix in the vicinity of the DEG–phenol side at a pressure of 0.2 atm.

for the production of phenol, which is not in full demand today. This circumstance undoubtedly increases the prospects for further optimization of the RED process and its use in industry.

CONCLUSIONS

New physicochemical information was obtained on the phase behavior of binary and ternary systems by using mathematical modeling of the VLE of the HA–phenol system at three pressures and in the presence of potential SAs (DEG, acetone). This formed the basis for the development of variant flowsheets based on the use of special techniques, and explanation of the separation results from the perspective of thermodynamic-geometric analysis of the phase diagram.

The conditions for the distillation process and the static parameters of the operation of columns of three flowsheets, based on varying the pressure in the columns and the use of ED and RED, were determined in a computational experiment using the Aspen Plus® software package. RED was proposed as an alternative separation option, taking into account the possibility of involving the second product of cumene production—acetone—into technological circulation.

Acknowledgments

The work was financially supported by the Russian Science Foundation, grant No. 19-19-00620-P.

Authors' contribution

All authors equally contributed to the research work.

The authors declare no conflicts of interest.

REFERENCES

1. Kharlampovich G.D., Churkin Yu.V. *Fenoly* (*Phenols*). Moscow: Khimiya; 1974. 376 p. (in Russ.).

2. Kruzhalov B.D., Golovanenko B.I. *Sovmestnoe poluchenie fenola i atsetona* (*Joint Production of Phenol and Acetone*). Moscow: Goskhimizdat; 1963 p. (in Russ.).

3. Timofeev V.S., Serafimov L.A, Timoshenko A.V. *Printsipy tekhnologii osnovnogo organicheskogo i neftekhimicheskogo sinteza* (*Principles of basic organic and petrochemical synthesis technology*). Moscow: Vysshaya shkola; 2010. 408 p. (in Russ.). ISBN 978-5-06-006067-6

СПИСОК ЛИТЕРАТУРЫ

1. Харлампович Г.Д., Чуркин Ю.В. *Фенолы*. М.: Химия; 1974. 376 с.

2. Кружалов Б.Д., Голованенко Б.И. *Совместное получение фенола и ацетона*. М.: Госхимиздат; 1963. 200 с.

3. Тимофеев В.С., Серафимов Л.А, Тимошенко А.В. *Принципы технологии основного органического и нефтехимического синтеза*. М.: Высшая школа; 2010. 408 с. ISBN 978-5-06-006067-6

4. Закошанский В.М. *Фенол и ацетон: анализ технологий, кинетики и механизма основных реакций*. СПб.: Химиздат; 2009. 608 с. ISBN 978-5-93808-168-0

4. Zakoshanskii V.M. *Fenol i atseton: Analiz tekhnologii, kinetiki i mekhanizma osnovnykh reaktsii* (*Phenol and acetone: Analysis of Technologies, Kinetics and Mechanism of the Main Reactions*). St. Petersburg: Khimizdat; 2009. 608 p. (in Russ.). ISBN 978-5-93808-168-0

5. Zakoshansky V.M. The cumene process for phenol–acetone production. *Pet. Chem*. 2007;47(4):273–284307. https://doi.org/10.1134/S096554410704007X

[Original Russian Text: Zakoshanskii V.M. The cumene process for phenol–acetone production. *Neftekhimiya*. 2007;47(4):301–313 (in Russ.).]

6. Weber M., Weber M., Shnurr O. *Method of producing phenol*: RF Pat. RU2430082C2. Publ. 09.27.2011 (in Russ.).

7. Vasil'eva I.I., Tyvina T.N., Dmitrieva I.V. Purification of phenol from hydroxyacetone and 2-methylbenzofuran by rectification. *Ros. Khim. Zh*. 2008;52(4):117–124 (in Russ.).

8. Zakoshanskii V.M. Problems of separation and purification of products in the industrial production of phenol. *Ros. Khim. Zh*. 2008;52(4):103–111 (in Russ.).

9. Vasil'eva I.I., Tyvina T.N. Dmitrieva I.V. *Method for purification of phenol from hydroxyacetone*: RF Pat. RU2323202C1. Publ. 04.27.2008 (in Russ.).

10. Vasil'eva I.I., Zakoshanskii V.M., Koshelev Yu.N., Chulkov V.P. Pathways of Acetol Formation in the Course of Production of Phenol and Acetone by Cleavage of Cumyl Hydroperoxide. *Russ. J. Appl. Chem*. 2001;74(1):111–113. https://doi.org/10.1023/A:1012712420588

[Original Russian Text: Vasil'eva I.I., Zakoshanskii V.M., Koshelev Yu.N., Chulkov V.P. Pathways of Acetol Formation in the Course of Production of Phenol and Acetone by Cleavage of Cumyl Hydroperoxide. *Zhurnal prikladnoi khimii*. 2001;74(1):107–110 (in Russ.).]

11. Koshelev Yu.N., Zakoshanskii V.M., Vasil'eva I.I., Malov Yu.I. *Method for treatment phenol from impurities*: RF Pat. RU2266275C1. Publ. 20.12.2005 (in Russ.).

12. Serafimov L.A., Frolkova A.K. Fundamental principle of concentration-field redistribution between separation regions as a basis for the design of technological systems. *Theor. Found. Chem. Eng*. 1997;31(2):159–166.

[Original Russian Text: Serafimov L.A., Frolkova A.K. Fundamental principle of concentration-field redistribution between separation regions as a basis for the design of technological systems. *Teor. osnovy khim. tekhnologii*. 1997;31(2):193–201 (in Russ.).]

13. Anokhina E.A. Energy saving in extractive distillation. *Fine Chem. Technol*. 2013;8(5):3–19 (in Russ.).

14. Frolkova A.K. *Razdelenie azeotropnykh smesei. Fiziko-khimicheskie osnovy i tekhnologicheskie priemy* (*Separation of Azeotropic Mixtures. Physico-Chemical Basics and Technological Methods*). Moscow: VLADOS; 2010. 192 p. (in Russ.).

15. Gaganov I.S. Optimization of phenol extraction technology by extractive distillation. In: *Proceedings of The 30th Mendeleev Conference of Young Scientists*. Moscow. 2020. P. 51. URL: http://www.chem.msu.su/rus/events/mendeleev-2020/theses.pdf

16. Gaganov I., Frolkova A., Frolkova A. Process for the recovery of phenol from a reaction mixture obtained by cumene method. In: *Proceedings of The 47th International Conference of SSCHE* – online conference. Bratislava, Slovakia: 2021.

17. Gaganov I.S., Fertikova V.G., Frolkova A.V., Frolkova A.K. Purification of phenol and chloroform from impurity components by extractive rectification. *Khimicheskaya tekhnologiya*. 2022;23(3):138–144 (in Russ.).

5. Закошанский В.М. Кумольный процесс получения фенола – ацетона. *Нефтехимия*. 2007;47(4):301–313.

6. Вебер М., Вебер М., Шнурр О. *Способ получения фенола*: пат. 2430082 С2 РФ. Заявка № 2008145110/04; заявл. 27.05.2010; опубл. 27.09.2011.

7. Васильева И.И., Тывина Т.Н., Дмитриева И.В. Очистка фенола от гидроксиацетона и 2-метилбензофурана методом ректификации. *Рос. хим. ж*. (*Ж. Рос. хим. об-ва*). 2008;52(4):117–124.

8. Закошанский В.М. Проблемы разделения и очистки продуктов при промышленном получении фенола. *Рос. хим. ж*. (*Ж. Рос. хим. об-ва*). 2008;52(4):103–111.

9. Васильева И.И., Тывина Т.Н. Дмитриева И.В. Способ очистки фенола от гидроксиацетона: пат. 2323202 С1 РФ. Заявка № 2006127521/04; заявл. 28.07.2006; опубл. 27.04.2008.

10. Васильева И.И., Закошанский В.М., Кошелев Ю.Н., Чулков В.П. Пути образования ацетола в процессе производства фенола и ацетона кумольным способом. *Журн. прикладной химии*. 2001;74(1):107–110.

11. Кошелев Ю.Н., Закошанский В.М., Васильева И.И., Малов Ю.И. *Способ очистки фенола от примесей*: пат. 2266275 С1 РФ. Заявка № 2004111561/04; заявл. 16.04.2004: опубл. 20.12.2005.

12. Серафимов Л.А., Фролкова А.К. Фундаментальный принцип перераспределения полей концентраций между областями разделения как основа создания технологических комплексов. *Теор. основы хим. технологии*. 1997;31(2):193–201.

13. Анохина Е.А. Энергосбережение в процессах экстрактивной ректификации. *Тонкие химические технологии* (*Вестник МИТХТ им. МВ Ломоносова*). 2013;8(5):3–19.

14. Фролкова А.К. Р*азделение азеотропных смесей. Физико-химические основы и технологические приемы*: монография. М.: Гуманитар. изд. центр ВЛАДОС; 2010. 192 с.

15. Гаганов И.С. Оптимизация технологии выделения фенола экстрактивной ректификацией. В сб. тезисов: *XXX Менделеевская конференция молодых ученых*. М. 2020. С. 51. URL: http://www.chem.msu.su/rus/events/mendeleev-2020/theses.pdf

16. Gaganov I., Frolkova A., Frolkova A. Process for the recovery of phenol from a reaction mixture obtained by cumene method. In: *Proceedings of 47th International Conference of SSCHE* – online conference. Bratislava, Slovakia: 2021.

17. Гаганов И.С., Фертикова В.Г., Фролкова А.В., Фролкова А.К. Очистка фенола и хлороформа от примесных компонентов экстрактивной ректификацией. *Химическая технология*. 2022;23(3):138–144.

About the authors:

Ivan S. Gaganov, Postgraduate Student, Department of Chemistry and Technology of Basic Organic Synthesis, M.V. Lomonosov Institute of Fine Chemical Technologies, MIREA – Russian Technological University (86, Vernadskogo pr., Moscow, 119571, Russia). E-mail: ivan.gaganov@yandex.ru. Scopus Author ID 57224575918, https://orcid.org/0000-0003-4837-2332

Elena V. Rytova, Cand. Sci. (Eng.), Senior Lecturer, Department of Chemistry and Technology of Basic Organic Synthesis, M.V. Lomonosov Institute of Fine Chemical Technologies, MIREA – Russian Technological University (86, Vernadskogo pr., Moscow, 119571, Russia). E-mail: erytova@gmail.com. Scopus Author ID 57196147610, RSCI SPIN-code 7130-6919, https://orcid.org/0000-0002-9244-5319

Alla K. Frolkova, Dr. Sci. (Eng.), Professor, Head of the Department of Chemistry and Technology of Basic Organic Synthesis, M.V. Lomonosov Institute of Fine Chemical Technologies, MIREA – Russian Technological University (86, Vernadskogo pr., Moscow, 119571, Russia). E-mail: frolkova@gmail.com. Scopus Author ID 35617659200, ResearcherID G-7001-2018, RSCI SPIN-code 4116-3223, https://orcid.org/0000-0002-9763-4717

Об авторах:

Гаганов Иван Сергеевич, аспирант кафедры химии и технологии основного органического синтеза Института тонких химических технологий им. М.В. Ломоносова ФГБОУ ВО «МИРЭА – Российский технологический университет» (119571, Россия, Москва, пр-т Вернадского, д. 86). E-mail: ivan.gaganov@yandex.ru. Scopus Author ID 57224575918, https://orcid.org/0000-0003-4837-2332

Рытова Елена Вячеславовна, к.т.н., старший преподаватель кафедры химии и технологии основного органического синтеза Института тонких химических технологий им. М.В. Ломоносова ФГБОУ ВО «МИРЭА – Российский технологический университет» (119571, Россия, Москва, пр-т Вернадского, д. 86). E-mail: erytova@gmail.com. Scopus Author ID 57196147610, SPIN-код РИНЦ 7130-6919, https://orcid.org/0000-0002-9244-5319

Фролкова Алла Константиновна, д.т.н., профессор, заведующий кафедрой химии и технологии основного органического синтеза Института тонких химических технологий им. М.В. Ломоносова ФГБОУ ВО «МИРЭА – Российский технологический университет» (119571, Россия, Москва, пр-т Вернадского, д. 86). E-mail: frolkova@gmail.com. Scopus Author ID 35617659200, ResearcherID G-7001-2018, SPIN-код РИНЦ 4116-3223, https://orcid.org/0000-0002-9763-4717

The article was submitted: December 21, 2022; approved after reviewing: March 28, 2023; accepted for publication: October 17, 2023.

Translated from Russian into English by H. Moshkov
Edited for English language and spelling by Dr. David Mossop

THEORETICAL BASES OF CHEMICAL TECHNOLOGY

ТЕОРЕТИЧЕСКИЕ ОСНОВЫ ХИМИЧЕСКОЙ ТЕХНОЛОГИИ

ISSN 2686-7575 (Online)

https://doi.org/10.32362/2410-6593-2023-18-5-426-445

UDC 53.091+53.092+53.096+66.084.8

REVIEW ARTICLE

The effects of physical treatment on physicochemical and biological properties of water and aqueous solutions

Elena S. Don[1,✉], German O. Stepanov[1], Sergey A. Tarasov[1,2]

[1]*Materia Medica Holding, Moscow, 129272 Russia*
[2]*Institute of General Pathology and Pathophysiology, Moscow, 125315 Russia*
[✉]*Corresponding author, e-mail: physactive@yandex.ru*

Abstract

Objectives. *Changes to the properties of water caused by factors such as pressure or temperature, can only be explained by its structural changes. Scientists study changes to the properties of water due to various physical stimuli only without the addition of any substances. Examples of stimuli are acoustic exposure, thermal exposure, pressure variation, shaking, intensive vibration treatment followed by dilutions, vortexing, bubble generation, inter alia. The aim of the present review article is to summarize the available data on how the above processes affect the physicochemical and biological properties of water and aqueous solutions.*

Results. *It has been shown that heating makes water less compressible and decreases air solubility in water, while cooling enhances its viscosity. Acoustic exposure makes the structure of water become coarse-grained, followed by an increase the number of large clusters, pH and temperature inside a cavitation bubble. High pressure enhances the viscosity, self-diffusion, and compressibility of water. For bubble processed water, there are changes in the spin-spin and spin-lattice relaxation times. Reactive oxygen species are formed, as well as increased solubility of gases in liquids and reduced friction. Vortex process technology causes an increase of electrical conductivity of water and reduced viscosity. Intensive vibration treatment and dilution processes result in changes in electrical conductivity of water, dissolved gas*

concentration, ultrasonic wave velocity, pH, surface tension, dielectric constant, and spectral response. There is also data to support the biological effects of different types of physical treatment of solutions.

Conclusions. *This review shows that physical treatment of water can induce changes both in physicochemical and biological properties of water and aqueous solutions.*

Keywords: *water technology, water properties, mechanical treatment, aqueous solution*

For citation: Don E.S., Stepanov G.O., Tarasov S.A. The effects of physical treatment on physicochemical and biological properties of water and aqueous solutions. *Tonk. Khim. Tekhnol. = Fine Chem. Technol.* 2023;18(5):426–445. https://doi.org/10.32362/2410-6593-2023-18-5-426-445

ОБЗОРНАЯ СТАТЬЯ

Влияние физической обработки на физико-химические и биологические свойства воды и водных растворов

Е.С. Дон[1,✉], Г.О. Степанов[1], С.А. Тарасов[1,2]

[1]НПФ «МАТЕРИА МЕДИКА ХОЛДИНГ», Москва, 129272 Россия
[2]Научно-исследовательский институт общей патологии и патофизиологии, Москва, 125315 Россия
[✉]Автор для переписки, e-mail: physactive@yandex.ru

Аннотация

Цели. *Изменения свойств воды, вызванные различными факторами, такими как давление или температура, могут объясняться только структурными изменениями воды. Ученые исследуют изменения свойств воды, происходящие исключительно из-за различных физических раздражителей и без добавления каких-либо веществ. Примерами таких раздражителей являются акустическое и тепловое воздействие, изменение давления, встряхивание, интенсивная вибрационная обработка с последующим разведением, вихревое перемешивание, образование пузырьков и т.д. Целью данного обзора является обобщение имеющихся данных о том, как вышеуказанные процессы влияют на физико-химические и биологические свойства воды и водных растворов.*

Результаты. *Показано, что нагрев делает воду менее сжимаемой и снижает растворимость воздуха в воде, а охлаждение повышает ее вязкость. Акустическое воздействие приводит к тому, что структура воды становится крупнозернистой, что сопровождается увеличением количества крупных кластеров, pH и температуры внутри кавитационного пузыря. Высокое давление способствует увеличению таких физических свойств воды, как вязкость, самодиффузия и сжимаемость. Для воды, обработанной пузырьками, происходят изменения времен спин-спиновой и спин-решеточной релаксации, образуются активные формы кислорода, а также наблюдается повышенная растворимость газов в жидкостях наряду со снижением вязкости. Вихревой технологический процесс приводит к увеличению электропроводности воды и снижению*

вязкости. Интенсивная вибрационная обработка и процессы разбавления приводят к изменению некоторых характеристик воды, таких как электропроводность, концентрация растворенного газа, скорость ультразвуковой волны, pH, поверхностное натяжение, диэлектрическая проницаемость и спектральный отклик. В работе также представлены данные, подтверждающие биологические эффекты различных типов упомянутой физической обработки растворов.

Выводы. *Данный обзор показывает, что физическая обработка воды может вызывать изменения как физико-химических, так и биологических свойств воды и водных растворов.*

Ключевые слова: *физическая обработка, свойства воды, свойства водных растворов*

Для цитирования: Дон Е.С., Степанов Г.О., Тарасов С.А. Влияние физической обработки на физико-химические и биологические свойства воды и водных растворов. *Тонкие химические технологии*. 2023;18(5):426–445. https://doi.org/10.32362/2410-6593-2023-18-5-426-445

INTRODUCTION

Water is a unique chemical compound which has no analogue in nature. Many of its properties are considered anomalous from the perspective of theoretical science. In a stationary state water is an open non-equilibrium system capable of accumulating additional free energy [1]. It has been demonstrated that external influence (optical, plasma, mechanical, etc.) can radically change the macroscopic properties of liquid solutions [2–10]. Many papers describing the unique properties and features of the structure of water have been published [11–16], so we would like to focus more on data supporting the emergence of new properties of water and aqueous solutions after their exposure to mechanical actions. The influence of mechanical treatment on the chemical properties of compounds has been studied for a long period of time and is currently undergoing a boom [17–20]. Nevertheless, scientists in the field of mechanochemistry mainly focus on changes in the structure of solid chemical compounds rather than the structure of water which is usually viewed, if at all, as a nominal solvent. However, when liquid water is affected by certain factors, such as pressure or temperature, changes in some of its properties can only be explained by structural changes of water [21].

With regard to the mechanical treatment of aqueous solutions, scientists and primarily physicists are thoroughly investigating the acquisition of new properties by water which can arise without the addition of any chemicals. They are exclusively due to various mechanical stimuli such as: acoustic exposure; thermal exposure; pressure variation; shaking, intensive vibration treatment followed by a dilution step; vortexing; bubble generation, etc. The aim of this review is not only to describe the available data on how the above processes affect the physicochemical properties of water, but also to assess influence on the biological effects of such aqueous solutions. We are also interested in topics concerning exposure of water and aqueous solutions to other physical stimuli, for example, exposure to electromagnetic fields. However, we intentionally omit them in this review as they are much more investigated to date [22–25].

FEATURES OF THE STRUCTURE OF WATER

Before discussing the properties of water which can be modified following mechanical treatment, it is important to gain an understanding of the special properties of initial untreated water. For this, the features of its structure need to be analyzed. Bernal's basic work [26] and further development of its ideas resulted in the creation of the so-called standard model for water representing the structure of water as a hydrogen-bonded network: loose but tight at the same time. These asymmetric properties were established by Bernal and Fowler after comparing the radius of a water molecule with its expected density, found to be markedly lower than the calculated value (1.0 instead of 1.8 g/cm^3). These results were confirmed by Meyer, Steward, and Amaldi using X-ray diffraction measurements of water [27–29].

At the present time, the current model of water can be described as follows:

1. The tetrahedral geometry of water molecules might be responsible for water's unusual properties [26]. Two hydrogen atoms form hydrogen bonds with oxygen responsible for water's unique properties [30–34]. However, the manifestation of the unique properties of water is explained by the formation of two additional acceptor hydrogen bonds. As a result, water has strong orientational interactions in addition to van der Waals attractions and repulsions.

2. This leads to cage-like structuring, not only in the solid phases (ices) but also even in liquid water. Liquid water is a mixture of two fluids: a low-density one and a high-density one [35].

3. Liquid water is a mixture of types of structure. It is the structure of water that gives water its macroscopic properties [36–40].

4. Liquid water tends to be more cohesive than other simple liquids. Owing to their structural arrangement, water molecules spontaneously associate with each other into a tetramer through hydrogen bonds. Although hydrogen bonds are much weaker than covalent bonds (they have energies of 4–13 kJ mol compared to approximately 418 kJ mol for a carbon-hydrogen covalent bond [41]), they contribute to the overall molecular energy due to their high number and fast formation [42].

The above model is rarely disputed nowadays, but there are still a few questions to be asked. Moreover, the growing number of new experimental facts raises even more questions. One of these questions concerns the stability of density inhomogeneities in water. The existence of density inhomogeneities (so called water structures and clusters) in liquid water is a well-recognized fact [43–45]. However, some specialists think that water structures may be long-lived [14, 43], while other scientists consider that the life time of water structures is determined by the hydrogen-bond jump time. This does not exceed a few picoseconds, or longer times, but comparable to the hydrogen-bond jump time [31, 46].

The jump time of hydrogen bonds and, therefore, individual water structural elements can indeed be several picoseconds. However, replacing one structural element with another one does not lead to the destruction of the whole structure, making it dynamic and long-lived at the same time. The existence of a dynamic self-replicating network of water molecules in liquid water was proposed in 1998 [47]. It was then independently confirmed by an X-ray diffraction study of water nanodroplets [48, 49].

Different cluster sizes have been experimentally studied and theoretically described to date: small clusters (dimers to decamers) and clusters formed by several dozen [45, 50, 51], or even hundreds of water molecules [52]. The existence of water octamer, a formation previously regarded as thermodynamically unstable, has been confirmed. The ^{1}H nuclear magnetic resonance (NMR) spectroscopy demonstrated that dynamic hydrogen bonding in the size-specific cluster (n = 8) is one of the features of the thermodynamically metastable water cluster formed in hydrophobic solvents [53]. However, even highly purified water can contain impurities or ions that form stable water structures around themselves [54, 55]. The structures generated can be transformed into low-density to high-density forms, bending but not damaging some of the hydrogen bonds. The sizes of these structures depend on the concentration of impurities, medium temperature and pH, etc. [56–59].

PHYSICOCHEMICAL PROPERTIES OF WATER

The model of water described in the previous section is characterized by properties well known in the scientific literature. Being loose but tight, water has relatively high values of surface tension, melting point, and boiling point. Water has density anomalies which are manifested in various ways. For example, ice floats on liquid water. In most other materials, the solid sinks in the liquid. This density anomaly is due to the fact that applying pressure melts solid water into a liquid, whereas applying pressure drives most liquids to freeze into a solid [60].

Polymorphism of a crystal structure is a well-known phenomenon. More than five such structures can be counted for carbon (diamond, graphite, graphene, fullerene, etc.). Most substances are characterized by only one or two solid phases, water has more than a dozen phases of its solid, ice [11]. Water is

a polar molecule, so its liquid can dissolve polar and ionic solutes. Its thermodynamic signatures for dissolving non-polar molecules are different from those of most other solvents. In order to signify that difference, it has been given its own name: the hydrophobic effect. Nevertheless, water has a number of properties which are beyond any doubt. For instance, water changes its phase into a solid at low temperatures. When heat is added to solid water (ice), it melts to become a liquid. Further heating results in boiling: a phase transition from the liquid phase to the gas phase. Therefore, at this level, the pressure-temperature (*pT*) phase diagram of water, which shows these features, is similar to the phase diagrams of other materials. The main physicochemical properties of water are presented in Table.

Experiments have demonstrated that exposure of water to mechanical stress may change some of the properties listed in the table. Since the structure of water is responsible for its properties, most types of exposure are directed at the clustering of this structure (formation, destruction, and association), changing intermolecular distance and the nature of hydrogen bonding, as well as the formation and collapsing of bubbles, which may change some of the properties (for example, heat capacity, molar volume, coefficient of thermal expansion, coefficient of isothermal compressibility, air solubility in water, water expansion with increasing temperature, viscosity with decreasing temperature, etc.). Each type of exposure will be detailed in the next sections.

ACOUSTIC EXPOSURE

The ultrasound beam originates from mechanical oscillations with frequencies ranging from 15 kHz to 10 MHz, above the range of normal human hearing. Since the speed of sound in water is about 1500 $m \cdot s^{-1}$, the corresponding wavelengths of acoustic waves are within the range of 10 to ~0.01 cm, which usually exceeds the sizes of atoms or chemical bonds to a significant level. As an ultrasound wave travels through a liquid, local pressure fluctuations, variable in space and time, induce acoustic cavitation. The effects of ultrasound result from acoustic cavitation, associated with the formation, growth and collapse of bubbles in liquids. In these processes, the low energy density of the sound field is converted into high energy density inside and outside the collapsing bubble [61]. The energy accumulated during the growth of a bubble in the expansion phase is released as acoustic noise, shock waves, chemical reactions, or as light emission when the bubble collapses abruptly during the contraction phase [62]. Didenko's work shows that ultrasound causes the temperature inside a

Table. The main physicochemical properties of water (at 25 °C and 101.325 kPa, where applicable)

Characteristic	Value
Density	997.047013 $kg \cdot m^{-3}$
Dielectric constant	78.375218
Magnetic susceptibility	$-1.64 \cdot 10^{-10}$ $m^3 \cdot mol^{-1}$
Electric conductivity	0.05501 $\mu S \cdot cm^{-1}$
Limiting ionic conductivity	
H^+	349.19 $S \cdot cm^2 \cdot mol^{-1}$
OH^-	199.24 $S \cdot cm^2 \cdot mol^{-1}$
Ionic mobility	
H^+	3.623 Å ~ 10^{-7} $m^2 \cdot V^{-1} \cdot s^{-1}$
OH^-	2.064 Å ~ 10^{-7} $m^2 \cdot V^{-1} \cdot s^{-1}$

Table. Continued

Characteristic	Value
Thermal conductivity	0.610 $W \cdot m^{-1} \cdot K^{-1}$
Speed of sound	1496.69922 $m \cdot s^{-1}$
Refractive index	1.33286 (λ = 589.26 nm)
pH	6.9976
pK_w	13.995
Surface tension	0.07198 $N \cdot m^{-1}$
Kinematic viscosity	$0.8935 \cdot 10^{-6}$ $m^2 \cdot s^{-1}$
Dynamic viscosity	0.8909 mPa·s
Bulk viscosity	2.47 mPa·s
Diffusion coefficient	0.2299 $Å^2 \cdot ps^{-1}$
Dipole moment	2.95 D (at 27°C)
Adiabatic compressibility	0.4477 GPa^{-1}
Isothermal compressibility	0.4599 GPa^{-1}
Expansion coefficient	0.000253 $°C^{-1}$
Adiabatic elasticity	2.44 GPa
Joule–Thomson coefficient	0.214 $K \cdot MPa^{-1}$
Vapor pressure	3.165 kPa
Cryoscopic constant	1.8597 $K \cdot kg \cdot mol^{-1}$
Ebullioscopic constant	0.5129 $K \cdot kg \cdot mol^{-1}$
Polarizability	$1.636 \cdot 10^{-40}$ $F \cdot m^2$

Note: Data collected from Chaplin M. *Water Structure and Science;* 2016. http://www1.lsbu.ac.uk/water/ (accessed June 29, 2020).

bubble to increase dramatically. The effective emission temperature during cavitation in water was measured to be 4027 ± 73°C (4300 ± 200 K) [62]. Ultrasound waves move through the solution as a result of several physical phenomena, such as micro-turbulence, micro-streaming, micro-jets and sound (or shock) waves. In this way they enhance the contact area and mass transfer between both media through cavitation process [63]. Therefore, ultrasonic irradiation may improve water purification. For example, an ultrasonic-assisted method was found to have advantages over shaking in terms of Pb^{2+} extraction from water. The extraction recovery of Pb^{2+} was enhanced by ≥2%, with a 7.5-fold shorter extraction time achieved, when compared to a thermostatic electrical shaker [64].

Kovalenko *et al*. [65] demonstrated that sound waves influenced the structural properties of water using a light-scattering method. It was shown that infrasonic waves of certain frequencies (5 and 10 Hz) destroyed clusters of less than 1.6 μm considerably. On the other hand, normal sound and ultrasound waves decreased the concentration of medium and small clusters with a radius of less than 0.9 μm and promoted the formation of extremely large clusters (≥3 μm). Thus, exposure to acoustic waves makes the structure of water coarse-grained. The increasing intensity of the affecting wave enhances damaging effects. As predicted by the authors, the number of extremely large clusters may also grow. This is due to the increased probability that the spatial relationship of clusters of various sizes will become optimal for the multiple occurrences of hydrogen bonds between them [65].

When water is exposed to long sound waves at the operating frequencies of the cavitator, the distance between clusters exceeds the acceptable limits at a certain moment. As a result, the interaction forces diminish and the liquid 'breaks'. Later, the broken clusters will form clusters again, but with a different structure. There are several possible outcomes for this process:

1) a cluster may dissociate either into several fragments or into molecules;

2) the initial cluster may transform into another cluster and completely change its structure and shape (plane or spatial);

3) the structure of a cluster may be partially changed, with defects in configuration observed (for example, only from rigid deformation induced by the shock-wave front);

4) combinations of water molecules may appear due to hydrogen bonding with other molecules of the oxide group, with similar structures forming, but with a different composition, i.e., they are composed of the molecules of substances resulting from the destructive action of cavitation of solids;

5) water clusters may also be filled with molecules or fragments of other substances. It can have either more atomized or more integrated fragments. Clearly, changes to the shape and position of clusters can lead to changes in the properties of water when exposed to sound waves [66].

Thus, from the physical perspective, ultrasonic treatment increases the number of large clusters in water and the pH level. Intensive exposure to ultrasound causes cavitation that results in the formation of various free radicals and a temperature rise inside a cavitation bubble. This effect may be used for removing metal ions from water.

Water with changed properties can exert new effects on biological systems due to the transformation of its initial structure. Exposure of water to cavitation has been shown to enhance the germination capacity of seeds soaked in the exposed water when compared to untreated water [66]. Nevertheless, when biological systems themselves are exposed to ultrasound in an aqueous medium, this results in DNA damage, inhibition of enzyme activity, membrane damage, and cell death. This effect is caused by the generation of free radicals induced by ultrasound [61].

HEATING/COOLING

The presence of clusters in water can also be explained by temperature-dependent changes in its properties. When the temperature of distilled water and salt solutions rises to 40°C, clusters of 2 to 40 μm are destroyed, and energy absorption observed [57]. Water possesses characteristics of temperature dependence, such as heat capacity, molar volume, thermal expansion coefficient, isothermal compressibility coefficient, etc.

The heat capacity of water is relatively large, since water stores energy in both its van der Waals and hydrogen bonds. Water has a minimum volume at a temperature of maximum density, 4°C, whereas the volumes of simpler liquids increase monotonically. Cold water has a negative thermal expansion coefficient between 0 and 4°C; heating shrinks it. Further heating to 46°C makes water less compressible; while above 46°C water exhibits normal liquid behavior, in that as it heats up the compressibility increases [67].

The lifetime of molecular vibrations in excitation is expected to decrease with increasing temperature, while energy and the probability of

interaction with other molecules also increase. For example, the lifetime of excited liquid HCl stretch vibrations decreases from 2.1 ns at −100°C to 1.0 ns at −25°C [68]. Excited OH-stretch vibrations in liquid water have a lifetime of 0.26 ps at 25°C, increasing to 0.32 ps at 85°C [69]. The increase in lifetime with temperature can be explained by the effects of the hydrogen bond network. OH-stretch vibrations usually become weaker through energy transfer to the overtone of the H–O–H bending mode. However, water hydrogen bonds are weakened with increasing temperature, resulting in high-frequency stretch vibrations and low-frequency bending vibrations. This increase in temperature gives rise to a shift of the overtone of the bending mode beyond the resonance with the stretching mode, making energy transfer less probable [69].

The solubility of air in water decreases as temperature increases: water contains less air at high temperature. For example, at 1 bar at 10°C city water will hold approximately 2.3% air by volume. If the water is heated to 91°C at the same pressure of 1 bar, it can only hold about 0.3% air by volume.[1]

When water is rapidly heated using a pulsed infrared laser to temperatures well below boiling point, the initial expansion is followed by an apparent contraction and then a re-expansion. The first expansion phase occurs more slowly than the timescale for bulk H-bond re-structuring of the water, as determined from vibrational bands in the Raman spectra. The second phase of the expansion is caused by hydrodynamic effects and is accompanied by morphological changes resulting in light scattering, as well as droplet spallation [70].

As the temperature decreases, an increase in viscosity is observed, which is especially noticeable in supercooled water. The cooperative formation of an open hydrogen-bonded network is observed as temperature decreases. This structure is formed by stronger hydrogen bonding, giving rise to larger clusters and reducing easy traveling (increased viscosity) [165].

The effects of heat treatment on the biological properties of water strongly depend on the object exposed. Fenkes *et al*. have discovered that an upward thermal shift from cold acclimation (8°C) to 13°C reduces salmonid sperm swimming speed, while an increased activation temperature also lowers the proportion of motile cells [71]. The authors consider such effects to be caused by changes in the number of thermosensitive ion channels. Many publications indicate that the soaking of seeds in hot water at 80–90°C with shaking followed by dipping in chilled water results in effective seed decontamination from *Escherichia coli* and *Salmonella* [72, 73].

However, certain pathogens, such as *Legionella pneumophila* and *Mycobacteria avium*, tend to be detected at greater frequencies in hot water systems than in cold water [74]. There is strong evidence of elevated hydrogen metabolism in hot water microbes. Hot waters in electric water heaters can contain as much as three orders of magnitude more H_2 than influent cold water due to metal corrosion [75, 76]. Such elevated H_2 levels enhance the growth of hydrogen oxidizing bacteria and hydrogen metabolism [76]. Moreover, the elevated proportions of hydrogenase genes, as well as chaperon genes for the correct folding and functioning of hydrogenase in *Legionella pneumophila* provided strong evidence of stimulated hydrogen metabolism in hot water.

ELEVATED PRESSURE

In the same way that a high-density crystalline phase is formed, liquid water also undergoes significant structural changes at high pressure. The viscosity, self-diffusion and compressibility of water contribute to achieving approximately 200 MPa pressure. At higher temperatures, these changes are induced at higher pressure values (for example, at 127°C, a pressure of 600 MPa is required, and at 177°C, changes will be achieved at 1 GPa [77].

Viscosity is one of the properties of water, the change of which will have a stronger effect on biological systems. The diffusion velocities of reactants and products strongly depend on the medium viscosity which determines the liquid-phase reaction rate. Water viscosity, which rapidly increases at low temperatures, in contrast to expectations does not increase with growing pressure, as common for other liquids. Water shows anomalous behavior at 30°C and low pressure: while the pressure in this case increases, water's viscosity unexpectedly decreases, not increases [78]. The weakening of hydrogen bonds caused by the reduction in intermolecular distance allows freer displacement of water molecules. The viscosity decrease appears to be minimal at around 150 MPa, increasing thereafter to follow the classical behavior for higher pressures [79].[2] At sufficiently high

[1] Watreco. VPT – Vortex Process Technology. URL: https://www.watreco.com/technology. Accessed August 31, 2021.

[2] Revised Release on the IAPS Formulation 1985 for the Viscosity of Ordinary Water Substance. Erlangen, Germany: The International Association for the Properties of Water and Steam; 1997. 15 p. https://doc.modelica.org/Modelica%204.0.0/Resources/Documentation/Media/Water/IF97documentation/visc.pdf. Accecced May 24, 2023.

pressure (above 200 mPa), water viscosity increases significantly compared to that at the atmospheric pressure. The specific volume and heat capacity of water both decrease monotonously with pressure as a result of the weakened hydrogen bonds that are its energy storage.

The dielectric constant increases with pressure. This, in association with the increase in density, manifests itself as a reduction in the strength of electrostatic interactions [80]. Density increases with pressure [81], while the fundamental tetrahedral H-bonding pattern is preserved at up to about 1 GPa: the stability limit of liquid water at 27°C [82]. A study of the densities of trimethylamine *N*-oxide aqueous solutions measured at pressures of 0.1 to 100 MPa demonstrates that the concentration dependence of densities is minimal at pressures of 75 MPa and higher. The apparent molar volumes of trimethylamine *N*-oxide in aqueous solution increased as the pressure grew, if temperature and concentration were not too high. Considering these thermodynamic criteria, it can be concluded that such hydrophobic substances act as structure-forming agents in water [83].

As an explanation for all these effects, there appears to be an increase in interpenetration of hydrogen bonded networks at about 200 MPa (at 17°C). Interpenetration of hydrogen bonded clusters is preferred over more extreme bending or breaking of the hydrogen bonds. This structural arrangement of liquid water at high pressures corresponds to that detected at neutron scattering [84], suggesting that the structuring of liquid water at high pressure is similar to the structure of ice phases obtained at high pressure [85].

Study of the high-pressure effects on the properties of solutions are essential in understanding the functioning of microorganisms living in the ocean under pressures of up to 100 MPa. Such pressure can affect the structure and density of aqueous solutions of osmolytes that influence the osmotic pressure inside organisms and the stability of their enzymes [81].

BUBBLE GENERATION AND BUBBLING

Micro- and nanobubbles (MNBs) have been a subject of intensive research over the past decade.

Gas particles exist with sizes ranging about several hundreds of nanometers and with number volume density in the range of approximately from 1 to 5 (up to 12) 106 cm^{-3} [86]. The characteristics of MNBs include the increased solubility of gases in liquids, reduced friction, either negative or positive zeta potentials and the generation of free radicals [87–89]. Some authors indicate an abrupt increase in the electrical conductivity of MNB water [90], while others provide evidence of reduced conductivity compared to purified water [91]. It is evident that air bubbles in water cannot be viewed as neutral and that ions are closely involved in the generation mechanism of these bubbles, thus influencing the properties of a solution. Furthermore, the selective adsorption of dissolved anions at nanobubble (NB) interface contributes to their stabilization [86]. The pH value of the solution may be observed to either increase or decrease, which also supports this hypothesis [92]. Electric fields emerging around bubbles due to their polarization affect one another. Based on NMR results, the number of NBs is positively correlated with the relaxation time, T2, of the water. The increase in T2 with the generation of NBs indicates that the mobility of the water molecules increases [93].

In addition, ultra-fine hydrogen-bubbled water has been shown to obtain properties different from those of reductive hydrogen water and tap water. The authors proved that the pH and oxidation-reduction potential were changed by 0.6 and almost 1000 mV, respectively, when compared to tap water [94]. It was also found that, as in the case of shaking, reactive oxygen species (ROS) are produced by NB water. The fluorescent response to ROS was found to be maintained within 2 days, and the number of ROS has a positive correlation with the NB number density in the water [95]. The positive and negative biological effects of NBs depend on the size of the organism and its susceptibility to ROS, NB size and amounts, temperature, flow rate and nature of the liquid. NBs have been reported to produce negative effects on bacteria and positive effects on yeast [96].

Recently, there has been considerable focus on the application of MNB technology in biological processes. Water containing MNBs has been reported to accelerate the growth of plants and shellfish, and has also been used in the aerobic cultivation of yeast [97]. Ebina *et al*. showed that oxygen-NB water promoted the growth of plants, fish, and mice [98]. Kurata *et al.*, who applied oxygen micro-bubbles in an osteoblast cell-culture system, reported greater alkaline phosphatase activity, related to increased osteoblastic cell activity [99]. Park *et al*. found that the fresh weights of micro-bubble treated lettuces were 2.1 times greater than those of the macro-bubble treated lettuces, when grown under the same conditions [100]. Ushikubo *et al*. showed that when barley coleoptile cells were floated in water after the generation of oxygen MNBs, cytoplasmic streaming rates inside the cells were

accelerated [101]. Moreover, NBs may provide a transport mechanism for gas delivery to a membrane or cell and thus alter the cell function [102, 103]. Liu *et al*. also demonstrated that the germination rates of barley seeds dipped in water containing MNBs were 15–25% greater than those of the seed dipped in distilled water. Tap water containing NBs reduces bacterial diversities and decreases the deposition of mineral precipitation [104]. The germination rates of seeds dipped in water containing NBs are 15–25% higher and are characterized by greater spin-lattice relaxation times and spin-spin relaxation times measured by the NMR method [93].

VORTEXING, SHAKING, AND INTENSIVE VIBRATION TREATMENT FOLLOWED BY DILUTION STEP

One of the most common mechanical effects on water is vigorous shaking. This technology implies using a vortex mixer, magnetic stirrer and other similar devices, as well as ordinary shaking. It has been shown that the vortex-processed water has a higher electrical conductivity than non-treated water (2.8–2.9 dS/m *vs* 2.5 dS/m), as well as reduced viscosity (by 3–17%, depending on water quality) and increased heat capacity (by 3%).[3] Mechanically treated aqueous solutions also produce biological effects. A study examining the effects of vortex-processed water further used on tomato plants demonstrated that the stem height and width of the plants were significantly greater, regardless of their culture. Both higher electrical conductivity and higher availability of nutrients in the vortex-processed water might have given the tomato plants a slight advantage [105].

Some simple organisms are sensitive to mechanically treated water. Dinoflagellates enhance their bioluminescence in response to a medium (seawater with salts) exposed to shaking. This effect is observed in 10 min after mechanical exposure [106]. RNS60, a physiologic saline solution containing oxygen NBs, generated by subjecting normal saline to Taylor–Couette–Poiseuille (TCP) flow under elevated oxygen pressure, has been shown to inhibit the expression of proinflammatory molecules in glial cells via phosphatidylinositol-3-kinase (PI3K)-mediated upregulation of IκBα. Thus, RNS60 treatment decreases the activation of astrocytes and microglia and reduces neuronal a poptosis in the brain of mice after traumatic brain injury [107]. RNS60 solution also exhibits immunomodulatory effects [108]. Long-lived luminescence in the blue region was found to occur in deionized water saturated with atmospheric gases following mechanical shaking.

Effects of intensive vibration treatment combined with serial dilution steps on the properties of solutions have been studied to a much greater extent. This technology is often used to prepare ultra-dilutions or high dilutions (UHDs) which refer to extremely low molarity (frequently above the number of Avogadro) preparations of biologically active substances [109]. Due to a combination of various physical influences (like pressure, temperature, NB formation, etc.), this technology should, therefore, be considered a complex physical process that changes the properties of water [3, 110–112]. The properties of UHDs prepared using this technology (for example, electrical conductivity, dissolved gas concentration, ultrasonic wave velocity, pH, surface tension, dielectric constant, and spectral response) are quite different from those of the initial substance solution and the solvent (water), and can be explained by the formation of nanoassociates [111–119]. Another example of anomalous properties of such an UHD is the fact that oxygen molecules in aqueous solutions subjected to external physical action transition from the triplet to the singlet state. This may indicate the possibility of overcoming or bypassing the quantum exclusion principle [3, 120]. Furthermore, for dilutions saturated with NBs generated by turbulent flow mixing, it has been shown that the H_2O_2 concentration in the solution increases with each successive dilution step. This suggests that the generation of free radicals may also alter the concentration of hydrogen peroxide obtained from water molecules, while atmospheric oxygen increases in the process of vigorous shaking [4]. The ROS generation rate has been found to increase exponentially with an increase in the frequency of mechanical action. The major pathways for hydrogen peroxide generation are probably associated with the formation of singlet oxygen and its further reduction. The alternative pathway is the formation of hydrogen peroxide as a result of hydroxyl radical recombination [121]. The pH of water tends to increase immediately after mechanical exposure. The droplet evaporation method shows that succussion of pharmaceutical preparations obtained as described (compared to gently mixed samples) induces the formation of structures characterized by a greater disorder (parameter entropy), increased gaps between the structure elements (parameter lacunarity), and smaller complexity (parameter local connected fractal dimension) [122]. According

[3] Watreco. VPT – Vortex Process Technology. URL: https://www.watreco.com/technology. Accessed August 31, 2021.

to the literature, the addition of substances in ultra-low concentrations leads to a change in the structure of water, i.e., to a change in its hydrogen bonds [123–125]. It has been demonstrated that near-ultraviolet scattering spectra of water change significantly following intensive vibration treatment combined with serial dilution step, with the changes persisting for several hours after exposure [126]. Subsonic-frequency mechanical oscillations have been shown to increase the redox potential of water, which is also maintained for a considerable period of time [127].

There is also data to indicate that molecules of the original substance are preserved in UHDs [4, 118, 128, 129], while common vigorous shaking (using a vortex mixer or similar devices) removes bubbles from the solution, including those with adsorbed impurities. Multiple serial dilutions preserve the molecules of the initial substance. These may become nucleation sites for forming stable [130–133] NB structures generated during the vigorous mechanical process (like preparation of UHDs) and highly-organized water around them [134]. The possibility of the presence of initial substance molecules, even in the high dilutions, can also be explained by the froth flotation. This does not mean, however, that these residual molecules are responsible for the high dilution unique properties [2, 4, 10, 118, 129, 135, 136]. The spontaneously formed nanoassociates may represent the carrier of activity that determines the special physical, chemical, and biological properties of UHDs [113, 119].

Long-lived nano and micro entities of an unknown nature are also detected experimentally in UHD substances [118, 134, 137–139]. The stability of these clusters may be achieved via the presence of deuterium [123, 140] in water, residual amounts of the initial substance [118, 129], or impurities (ions, silicates) released from the surfaces of the containers used for serial dilutions combined with intensive vibration treatment [141]. It has been shown experimentally that nanosilica can self-assemble into trimeric structures [142–147]. Adsorption of ions (from glass or water) or hydrophobic molecules on the surface of heterophase elements makes them more stable. The longevity of NBs and its correlation with the material of the bottle may be associated with the negative charge of the NBs. The glass surface becomes negatively charged due to silica hydrolysis and SiOH dissociation into SiO^- and H^+. Therefore, the charged NBs support the stabilizing electrical interaction [148, 149].

Individual density inhomogeneities are believed to be organized into giant heterostructures, the topology of which depends on the primer, i.e., the residual initial substance [140]. These nanostructures can be maintained through the dilution process due to their drive for hydrophobic surfaces (a plastic pipette tip) or electrostatic interactions, in a case with a glass pipette/glass chip or a glass container surrounded by an electric field, forming new clusters in each dilution [150].

It may be concluded that a serial dilution process combined with intensive vibration treatment is a good technique for producing stabilized water structures in water solutions. The special biological properties of aqueous solutions exposed to the serial dilution process combined with intensive vibration treatment are also determined by the specificity of the initial substance. They offer new opportunities for treating various diseases, as has been demonstrated in a number of studies [151–159]. This also can be useful in the technology where the treatment of piezoelectric ceramics by the corresponding UHDs during the hot pressing caused changes to the physical features of the resultant ceramic samples [160]. Thus, in spite of high-temperature processing, the activity of UHDs is retained. Serial dilutions of a solvent containing no initial substance (control) followed by intensive vibration treatment also result in the formation of nanostructures different from those in water. However, their properties (activity) will lack specificity [161].

Agricultural studies have demonstrated that adding extremely diluted substances results in increased chlorophyll production, significantly changes the amino acid profile and amino acid production as well as photosynthesis, germination rates and metabolism. The ability of highly diluted formaldehyde to affect the rate of demethylation/re-methylation of veratric acid by the *Rhodococcus erythropolis* bacteria was shown using electrophoretic and microscopic techniques [162]. Also, the germination rates of wheat seeds treated with UHDs increase significantly when the number of strokes is increased during the dilution process [163, 164]. All of these (and many other) physicochemical reactions, as well as effects on living systems exposed to the water and aqueous solutions obtained during the intensive vibration treatment and dilution process, stress the importance of this approach in many disciplines.

CONCLUSIONS

This review shows that physical treatment of water can induce changes both in physicochemical and biological properties of water and aqueous solutions. Many of the properties listed in the table may change in response to certain exposure.

As the structure of water is responsible for its properties, most types of exposure are directed at the clustering of water molecules (formation, destruction, and association), changing intermolecular distance and the nature of hydrogen bonding, as well as the formation and collapsing of bubbles.

These structural modifications may change the main properties of water, such as: heat capacity; molar volume; thermal expansion coefficient; isothermal compressibility coefficient; air solubility in water; water expansion with increasing temperature; and viscosity with decreasing temperature. It has been experimentally demonstrated that heating makes water less compressible and decreases air solubility in water, and cooling enhances its viscosity, while changes in the molar volume and expansion rate have a non-monotonic nature.

Acoustic exposure also results in significant changes. This type of exposure makes the structure of water coarse-grained, i.e., it increases the number of large clusters, increases pH and temperature inside a cavitation bubble and leads to the formation of various free radicals.

High pressure enhances the physical properties of water such as viscosity, self-diffusion, and compressibility. Water viscosity increases considerably at quite high pressure. However, water shows anomalous behavior at 30°C. Water viscosity decreases with increasing pressure and can drop to 150 MPa, increasing thereafter to follow the classical behavior. It has also been shown that the specific volume and heat capacity of water both decrease monotonously with increasing pressure, while dielectric constant and density tend to increase.

Some researchers indicate an abrupt increase in the electrical conductivity of micro-nano bubbled water, whereas others report reduced conductivity when compared to purified water. It has been proved that the pH and oxidation-reduction potential are changed by 0.6 and 1000 mV, respectively, when compared to the initial water. For NB processed water, there are changes in the spin-spin and spin-lattice relaxation times, ROS are formed as well as the increased solubility of gases in liquids and reduced friction are observed.

Vortex process technology results in the increased electrical conductivity of water and reduced viscosity as undissolved gases are removed. However, there is an increase by 3% in electrical conductivity after vortex process technology treatment. Intensive vibration treatment and dilution processes also exert pronounced effects on water. When treated by this method, water can change some of its characteristics, such as: electrical conductivity; dissolved gas concentration; ultrasonic wave velocity; pH, surface tension; dielectric constant; and spectral response. The vigorous mixing of the solution results in the increased generation rate of ROS with an increase in the frequency of mechanical action, increased pH, altered near-ultraviolet scattering spectra of the water, as well as enhanced oxidation-reduction potential. Nanoassociates formation is one of the possible explanations of this phenomena.

With regard to the effects on living systems, treatment of water using various methods, such as ultrasonic exposure, bubble generation, intensive vibration treatment, or vigorous mixing, including that with serial dilution process, changes the biological properties of water. Many authors report improvement in the growth and development of organisms and plants soaked in the processed water. Water exposed to various types of mechanical stress produces positive effects on the germination rates of seeds, plant weight and stem width, and the growth of fish and mice. From the practical point of view one of the most important abilities of mechanically-treated dilutions is the ability to exert influence on the initial substance. This is useful for improving the material features, and for medicines with the physical mechanism of action affecting the target molecules. Most data on the biological effects of processed aqueous solutions were experimentally obtained for solutions exposed to mixing combined with serial dilution steps. Other test factors have been barely studied, so further investigations are required to develop this topic.

Acknowledgments

The study was supported by Materia Medica Holding, Moscow, Russia.

Authors' contributions

E.S. Don – conceptualization, data search, writing the original draft;

G.O. Stepanov – conceptualization, review and editing the text of the manuscript;

S.A. Tarasov – supervision, review and editing the text of the manuscript.

Conflicts of interest

The authors declared the following potential conflicts of interest with respect to the research, authorship, and/or publication of this article: E.S. Don, G.O. Stepanov, and S.A. Tarasov are employees of *Materia Medica Holding* (fully or partly). Employees of *Materia Medica Holding* made a decision to publish the work and took part in the manuscript writing. *Materia Medica Holding* produces the drugs based on the technology of serial dilution process combined with external treatment.

REFERENCES

1. Bruskov V.I., Chernikov A.V., Ivanov V.E., Karmanova E.E., Gudkov C.V. Formation of the Reactive Species of Oxygen, Nitrogen, and Carbon Dioxide in Aqueous Solutions under Physical Impacts. *Phys. Wave Phen*. 2020;28(2):103–106. https://doi.org/10.3103/S1541308X2002003X

2. Shcherbakov I. Specific features of the concentration dependences of impurities in condensed media. *Phys. Wave Phen.* 2020;28(2):83–87. http://doi.org/10.3103/S1541308X20020156

3. Gudkov S.V., Penkov N.V., Baimler I.V., Lyakhov G.A., Pustovoy V.I., Simakin A.V., Sarimov R.M., Scherbakov I.A. Effect of Mechanical Shaking on the Physicochemical Properties of Aqueous Solutions. *Int. J. Mol. Sci.* 2020;21(21):8033. https://doi.org/10.3390/ijms21218033

4. Gudkov S.V., Lyakhov G.A., Pustovoy V.I., Shcherbakov I.A. Influence of Mechanical Effects on the Hydrogen Peroxide Concentration in Aqueous Solutions. *Phys. Wave. Phen.* 2019;27(2):141–144. http://doi.org/10.3103/S1541308X19020092

5. Baymler I.V., Gudkov S.V., Sarimov R.M., Simakina A.V., Shcherbakov I.A. Concentration Dependences of Molecular Oxygen and Hydrogen in Aqueous Solutions. *Dokl. Phys.* 2020;65(1):5–7. https://doi.org/10.1134/S1028335820010085

6. Lauterborn W. High-speed photography of laser-induced breakdown in liquids. *Appl. Phys. Lett.* 1972;21(1):27–29. https://doi.org/10.1063/1.1654204

7. Bunkin N.F., Bunkin F.V. The new concepts in the optical breakdown of transparent liquids. *Laser Physics*.1993;3(1):63–78. URL: https://www.researchgate.net/publication/298926340_The_New_Concepts_in_the_Optical_Breakdown_of_Transparent_Liquids

8. Mai-Prochnow A., Zhou R., Zhang T., Ostrikov K.K., Mugunthan S., Rice S.A., Cullen P.J. Interactions of plasma-activated water with biofilms: inactivation, dispersal effects and mechanisms of action. NPJ Biofilms *Microbiomes*. 2021;7(1):11. https://doi.org/10.1038/s41522-020-00180-6

9. Zhao Y.M., Patange A., Sun D.W., Tiwari B. Plasma-activated water: Physicochemical properties, microbial inactivation mechanisms, factors influencing antimicrobial effectiveness, and applications in the food industry. *Compr. Rev. Food Sci. Food Saf*. 2020;19(6):3951–3979. https://doi.org/10.1111/1541-4337.12644

10. Shcherbakov I. Influence of External Impacts on the Properties of Aqueous Solutions. *Phys. Wave Phen*. 2021;29(2):89–93. http://doi.org/10.3103/S1541308X21020114

11. Brini E., Fennell C.J., Fernandez-Serra M., Hribar-Lee B., Lukšič M., Dill K.A. How Water's Properties Are Encoded in Its Molecular Structure and Energies. *Chem. Rev*. 2017;117(19):12385–12414. https://doi.org/10.1021/acs.chemrev.7b00259

12. Geesink G.J.H., Jerman I., Meijer D.K.F. Water, The Cradle of Life via its Coherent Quantum Frequencies. *Water.* 2020;11:78–108. http://dx.doi.org/10.14294/WATER.2020.1

13. Wang L.P., Head-Gordon T., Ponder J.W., Ren P., Chodera J.D., Eastman P.K., Pande V.S. Systematic Improvement of a Classical Molecular Model of Water. *J. Phys. Chem. B*. 2013; 117:9956–9972. https://doi.org/10.1021/jp403802c

14. Plumridge T.H., Waigh R.D. Water structure theory and some implications for drug design. *J. Pharm. Pharmacol*. 2002;54(9):1155–1179. https://doi.org/10.1211/002235702320402008

15. Cisneros G.A., Wikfeldt K.T., Ojamäe L., Lu J., Xu Y., Torabifard H., Bartók A.P., Csányi G., Molinero V., Paesani F. Modeling Molecular Interactions in Water: From Pairwise to Many-Body Potential Energy Functions. *Chem. Rev.* 2016;116(3):7501–7528. https://doi.org/10.1021/acs.chemrev.5b00644

16. Bellissent-funel M-C., Hassanali A., Havenith M., Henchman R., Pohl P., Sterpone F., Van Der Spoel D., Xu Y., Garcia A.E. Water Determines the Structure and Dynamics of Proteins. *Chem. Rev*. 2016;116(13):7673–7697. https://doi.org/10.1021/acs.chemrev.5b00664

17. Tan D., Garcia F. Main group mechanochemistry: from curiosity to established protocols. *Chem. Soc. Rev.* 2019;48(8):2274–2292. https://doi.org/10.1039/c7cs00813a

18. Howard J.L., Cao Q., Browne D.L. Mechanochemistry as an emerging tool for molecular synthesis: what can it offer? *Chem. Sci.* 2018;9(12):3080–3094. https://doi.org/10.1039/c7sc05371a

19. Do J.L., Fris T. Mechanochemistry: A Force of Synthesis. *ACS Cent. Sci*. 2017;3(1):13–19. https://doi.org/10.1021/acscentsci.6b00277

20. Andersen J., Mack J. Mechanochemistry and organic synthesis: from mystical to practical. *Green Chem*. 2018;20(7):1435–1443. http://doi.org/10.1039/C7GC03797J

21. Roy R., Tiller W.A., Bell I., Hoover M.R. The Structure Of Liquid Water; Novel Insights From Materials Research; Potential Relevance To Homeopathy. *Materials Research Innovations*. 2005;9(4):98–103. https://doi.org/10.1080/14328917.2005.11784911

22. Wu T., Brant J.A. Magnetic Field Effects on pH and Electrical Conductivity: Implications for Water and Wastewater Treatment. *Environmental Engineering Science*. 2020;37(11):717–727. https://doi.org/10.1089/ees.2020.0182

23. Wang Y., Wei H., Li Z. Effect of magnetic field on the physical properties of water. *Results in Physics*. 2018;8:261–267. https://doi.org/10.1016/j.rinp.2017.12.022

24. Chibowski E., Szcześ A., Hołysz L. Influence of Magnetic Field on Evaporation Rate and Surface Tension of Water. *Colloids and Interfaces*. 2018;2(4):68. https://doi.org/10.3390/colloids2040068

25. Sronsri C., U-yen K., Sittipol W. Analyses of vibrational spectroscopy, thermal property and salt solubility of magnetized water. *J. Mol. Liquids*. 2021;323:114613. https://doi.org/10.1016/j.molliq.2020.114613

26. Bernal J.D., Fowler R.H. A Theory of Water and Ionic Solution, with Particular Reference to Hydrogen and Hydroxyl Ions. *J. Chem. Phys*. 1933;1:515–548. https://doi.org/10.1063/1.1749327

27. Meyer H.H. Über den Einfluß der Temperatur und gelöster Elektrolyte auf das monochromatische Debye-Scherrer-Diagramm des Wassers. *Ann. Phys*. 1930;397(6):701–734. https://doi.org/10.1002/andp.19303970603

28. Stewart G.W. The Cybotactic (Molecular Group) Condition in Liquids; the Nature of the Association of Octyl Alcohol Molecules. *Phys. Rev*. 1930;35(7):726–732. https://doi.org/10.1103/physrev.35.726

29. Amaldi E. Über den Ramaneffekt des CO. *Zeitschrift für Physik*. 1932;79(7–8):492–494. https://doi.org/10.1007/BF01342171

30. Omta A.W., Kropman M.F., Woutersen S., Bakker H.J. Negligible effect of ions on the hydrogen-bond structure in liquid water. *Science*. 2003;301(5631):347–349. https://doi.org/10.1126/science.1084801

31. Fecko C.J., Eaves J.D., Loparo J.J., Tokmakoff A., Geissler P.L. Ultrafast hydrogen-bond dynamics in the infrared spectroscopy of water. *Science*. 2003;301(5640):1698–1702. http://doi.org/10.1126/science.1087251

32. Smith J.D., Smith J.D., Cappa C.D., Wilson K.R., Messer B.M., Cohen R.C., Saykally R.J. Energetics of hydrogen bond network rearrangements in liquid water. *Science*. 2004;306:851–853. https://doi.org/10.1126/science.1102560

33. Stiopkin I.V., Weeraman C., Pieniazek P.A., Shalhout F.Y., Skinner J.L., Benderskii A.V.: Hydrogen bonding at the water surface revealed by isotopic dilution spectroscopy. *Nature*. 2011;474(7350):192–195. https://doi.org/10.1038/nature10173

34. Richardson J.O., Pérez C., Lobsiger S., Reid A.A., Temelso B., Shields G.C., Kisiel Z., Wales D.J., Pate B.H., Althorpe S.C. Concerted hydrogen-bond breaking by quantum tunneling in the water hexamer prism. *Science*. 2016;351(62–79):1310–1313. https://doi.org/10.1126/science.aae0012

35. Röntgen W.C. Ueber die Constitution des flüssigen Wassers. *Ann. Phys*. 1892;281(1):91–97. https://doi.org/10.1002/andp.18922810108

36. Pauling L. *The Nature of the Chemical Bond*. 2nd ed. Ithaca, NY: Cornell University Press; 1939. 663 p.

37. Samoilov O.Y. *Structure of Aqueous Solutions of Electrolytes and Hydration of Ions*. NY: Consultants Bureau; 1965. 185 p.

38. Bushuev Y.G. Properties of the network of the hydrogen bonds of water. *Russ. Chem. Bull.* 1997;46(5):888–891. https://doi.org/10.1007/BF02496112

39. Bushuev Y.G., Lyashchenko A.K. Structural Characteristics of H-Bond Networks in Water: 3D Model. *Russ. J. Phys. Chem*. 1995;69(1):33–38.

40. Malenkov G. Liquid water and ices: understanding the structure and physical properties. *J. Phys. Condens. Matter*. 2009;21(28):283101. https://doi.org/10.1088/0953-8984/21/28/283101

41. Berg J.M., Tymoczko J.L., Stryer L. Chemical Bonds in Biochemistry. In: *Biochemistry*. 5th edition. NY: W.H. Freeman and Company; 2010. P. 42–51.

42. Suresh S.J., Naik V.M. Hydrogen bond thermodynamic properties of water from dielectric constant data. *J. Chem. Phys.* 2000;113(21):9727–9732. http://doi.org/10.1063/1.1320822

43. Oka K., Shibue T., Sugimura N., Watabe Y., Winther-Jensen B., Nishide H. Long-lived water clusters in hydrophobic solvents investigated by standard NMR techniques. *Sci. Rep.* 2019;9(1):223. https://doi.org/10.1038/s41598-018-36787-1

44. Lobyshev V.I., Solovei A.B., Bulienkov N.A. Computer modular design of parametric structures of water. *Biophysics*. 2003;48(6):932–941. https://doi.org/10.1016/S0167-7322(03)00115-6

45. Maheshwary S., Patel N., Sathyamurthy N., Kulkarni A.D., Gadre S.R. Structure and Stability of Water Clusters $(H_2O)_n$, n = 8−20: An Ab Initio Investigation. *Phys. Chem. A*. 2001; 105(46):10525–10537. https://doi.org/10.1021/jp013141b

46. Elsaesser T. Ultrafast memory loss and relaxation processes in hydrogen-bonded systems. *Biol. Chem.* 2009;390(11):1125–1132. https://doi.org/10.1515/bc.2009.126

47. Chaplin M.F. A proposal for the structuring of water. *Biophys. Chem*. 200;83(3):211–221. https://doi.org/10.1016/s0301-4622(99)00142-8

48. Müller A., Bögge H., Diemann E. Structure of a cavity-encapsulated nanodrop of water. *Inorg. Chem. Commun*. 2003;6(1):52–53. https://doi.org/10.1016/S1387-7003(02)00679-2

49. Garcia-Ratés M., Miró P., Poblet J.M., Bo C., Avalo J.B. Dynamics of encapsulated water inside Mo132 cavities. *Phys. Chem. B*. 2011;115(19):5980–5992. https://doi.org/10.1021/jp110328z

50. Fujii A., Mizuse K. Infrared spectroscopic studies on hydrogen-bonded water networks in gas phase clusters. *Int. Rev. Phys. Chem*. 2012;32(2):266–307. https://doi.org/10.1080/0144235X.2012.760836

51. Lenz A., Ojamäea L. A theoretical study of water equilibria: the cluster distribution versus temperature and pressure for $(H_2O)_n$, n=1–60, and ice. *J. Chem. Phys.* 2009;131(13):134302. https://doi.org/10.1063/1.3239474

52. Buck U., Pradzynski C., Zeuch T., Dieterich J., Hartke B. A size resolved investigation of large water clusters. *Phys. Chem. Chem*. Phys. 21014;16(15):6859–6871. https://doi.org/10.1039/c3cp55185g

53. Cole W.T.S., Farrell J.D., Wales D.J., Saykally R.J. Structure and torsional dynamics of the water octamer from THz laser spectroscopy near 215 μm. *Science*. 2016;352(6290):1194–1197. https://doi.org/10.1126/science.aad8625

54. Marcus Y. Effect of ions on the structure of water: structure making and breaking. *Chem. Rev*. 2009;109(3):1346–1370. https://doi.org/10.1021/cr8003828

55. Shu L., Jegatheesan L., Jegatheesan V., Li, C-Q. The structure of water. *Fluid Phase Equilibria*. 2020;511:112514. https://doi.org/10.1016/j.fluid.2020.112514

56. Goncharuk V.V., Orekhova E.A., Malyarenko V.V. Influence of temperature on water clusters. *J. Water Chem. Technol.* 2008;30(2):80–84. https://doi.org/10.3103/S1063455X08020033

57. Baranov A.V., Petrov V.I., Fedorov A.V., Chernyakov G.M. Effect of microscopic NACL impurities on clustering dynamics in liquid water: low-frequency Raman spectroscopy. *J. Exper. Theor. Phys. Lett*. (*JETP Letters*). 1993;57(6):371–375.

58. Farashchuk N.F., Telenkova O.G., Mikhailova R.I. Recovery of water structure after boiling. *Water Purification. Water Treatment*. *Water Supply*. 2008; 6(6):20–21 (in Russ.).

59. Syroeshkin A.V., Smirnov A.N., Goncharuk V.V., *et al.* Water as heterogeneous structure. *INVESTIGATED in RUSSIA*. 2006;9:843–854 (in Russ.).

60. Sotthewes K., Bampoulis P., Zandvliet H.J.W., Lohse D., Poelsema B. Pressure-Induced Melting of Confined Ice. *ACS Nano*. 2017;11(12):12723–12731. https://doi.org/10.1021/acsnano.7b07472

61. Riesz P., Kondo T. Free radical formation induced by ultrasound and its biological implications. *Free Radic. Biol. Med*. 1992;13(3):247–270. https://doi.org/10.1016/0891-5849(92)90021-8

62. Didenko Y., McNamara W., Suslick S. Hot Spot Conditions during Cavitation in Water. *J. Am. Chem. Soc*. 1999;121(24):5817–5818. https://doi.org/10.1021/ja9844635

63. Yusof N.S., Babgi B., Alghamdi Y., Aksu M., Madhavan J., Ashokkumar M. Physical and chemical effects of acoustic cavitation in selected ultrasonic cleaning applications. *Ultrason. Sonochem*. 2016;29:568–576. https://doi.org/10.1016/j.ultsonch.2015.06.013

64. Nizamani S., Kazi T.G., Afridi H.I. Ultrasonic-energy enhance the ionic liquid-based dual microextraction to preconcentrate the lead in ground and stored rain water samples as compared to conventional shaking method. *Ultrason. Sonochem*. 2018;40(Part A):265–270. https://doi.org/10.1016/j.ultsonch.2017.07.024

65. Kovalenko V.F., Glazkova V.V. The influence of acoustic waves on water structure properties. *Biomed. Eng. Electron*. 2013;(1):2–14 (in Russ.). URL: https://www.elibrary.ru/item.asp?id=19825530

66. Ivanov E.G., Kokorin N.V., Chevachina E.E. The activation of water informational qualities by method of acoustic cavitation. *Bulletin NGIEI*. 2017;4(71):16–27 (in Russ.). URL: https://cyberleninka.ru/article/n/aktivizatsiya-informatsionnyh-kachestv-vody-sposobom-akusticheskoy-kavitatsii

67. Skinner L.B., Benmore C.J., Neuefeind J.C., Parise J.B. The structure of water around the compressibility minimum. *J. Chem. Phys.* 2014;141(12):214507. https://doi.org/10.1063/1.4902412

68. Chesnoy J. Ricard D. Experimental study of vibrational relaxation in liquid hydrogen chloride. *Chem. Phys. Lett*. 1980;73(3):433–437. https://doi.org/10.1016/0009-2614(80)80689-0

69. Lock J., Bakker H.J. Temperature dependence of vibrational relaxation in liquid H_2O. *J. Chem. Phys*. 2002;117:1708–1713. https://doi.org/10.1063/1.1485966

70. Hobley J., Kuge Y., Gorelik S., Kasuya M., Hatanaka K., Kajimoto S., Fukumura H. Water expansion dynamics after pulsed IR laser heating. *Phys. Chem. Chem. Phys*. 2008;10(34):5256–5263. https://doi.org/10.1039/b805838e

71. Fenkes M., Fitzpatrick J.L., Ozolina K., Shiels H.A., Nudds R.L. Sperm in hot water: direct and indirect thermal challenges interact to impact on brown trout sperm quality. *J. Exp. Biol*. 2017;220(Part 14):2513–2520. https://doi.org/10.1242/jeb.156018

72. Bari M.L., Inatsu Y., Isobe S., Kawamoto S. Hot water treatments to inactivate *Escherichia coli* O157:H7 and Salmonella in mung bean seeds. *J. Food. Prot.* 2008;71(4):830–834. https://doi.org/10.4315/0362-028x-71.4.830

73. Bari M.L., Sugiyama J., Kawamoto S. Repeated quick hot-and-chilling treatments for the inactivation of *Escherichia coli* O157:H7 in mung bean and radish seeds. *Foodborne Pathog. Dis*. 2009;6(1):137–143. https://doi.org/10.1089/fpd.2008.0143

74. Dai D., Rhoads W.J., Edwards M.A., Pruden A. Shotgun Metagenomics Reveals Taxonomic and Functional Shifts in Hot Water Microbiome Due to Temperature Setting and Stagnation. *Front. Microbiol*. 2018;9:2695. https://doi.org/10.3389/fmicb.2018.02695

75. Brazeau R.H., Edwards M.A. Role of Hot Water System Design on Factors Influential to Pathogen Regrowth: Temperature, Chlorine Residual, Hydrogen Evolution, and Sediment. *Environ. Eng. Sci*. 2013;30(10):617–627. https://doi.org/10.1089/ees.2012.0514

76. Dai D.J., Proctor C.R., Williams K., Edwards M.A., Pruden A. Mediation of effects of biofiltration on bacterial regrowth, Legionella pneumophila, and the microbial community structure under hot water plumbing conditions. *Environ. Sci.: Water Res. Technol*. 2018;4(2):183–194. https://doi.org/10.1039/C7EW00301C

77. Ranieri U., Giura P., Gorelli F.A., Santoro M., Klotz S., Gillet P., Paolasini L., Koza M.M., Bove L.E. Dynamical crossover in hot dense water: The hydrogen bond role. *J. Phys. Chem. B*. 2016;120(34):9051–9059. https://doi.org/10.1021/acs.jpcb.6b04142

78. Bridgman P.W. The viscosity of liquids under pressure. *Proc. Nat. Acad. Sci. USA*. 1925;11(10):603–606. https://doi.org/10.1073/pnas.11.10.603

79. Lodemann H.D. Water and its solutions at high pressures and low temperatures. *Polish J. Chem.* 1994;68(1):1–22.

80. Molina-García A.D. The Effect of Hydrostatic Pressure on Biological Systems. *Biotechnol. Genet. Eng Rev.* 2002;19:3–54. https://doi.org/10.1080/02648725.2002.10648021

81. Knierbein M., Venhuis M., Held C., Sadowski G. Thermodynamic properties of aqueous osmolyte solutions at high-pressure conditions. *Biophys. Chem*. 2019;253:106211. https://doi.org/10.1016/j.bpc.2019.106211

82. Imoto S., Marx D. Pressure response of the THz spectrum of bulk liquid water revealed by intermolecular instantaneous normal mode analysis. *J. Chem. Phys.* 2019;150(8):084502. https://doi.org/10.1063/1.5080381

83. Makarov D.M., Egorov G.I., Kolker A.M. Density and Volumetric Properties of Aqueous Solutions of Trimethylamine *N*-Oxide in the Temperature Range from (278.15 to 323.15) K and at Pressures up to 100 MPa. *J. Chem. Eng. Data*. 2015;60(5):1291–1299. http://doi.org/10.1021/je500977g

84. Strässle T., Saitta A.M., Godec Y.L., Hamel G., Klotz S., Loveday J.S., Nelmes R.J. Structure of dense liquid water by neutron scattering to 6.5 GPa and 670 K. *Phys. Rev. Lett*. 2006;96(6):067801. https://doi.org/10.1103/physrevlett.96.067801

85. Koga Y., Westh P., Yoshida K., Inaba A., Nakazawa Y. Gradual crossover in molecular organization of stable liquid H_2O at moderately high pressure and temperature. *AIP Advances*. 2014;4(9):097116. http://doi.org/10.1063/1.4895536

86. Yurchenko S.O., Shkirin A.V., Ninham B.W., Sychev A.A., Babenko V.A., Penkov N.V., Kryuchkov N.P., Bunkin N.F. Ion-specific and thermal effects in the stabilization of the gas nanobubble phase in bulk aqueous electrolyte solutions. *Langmuir*. 2016;32(43):11245–11255. http://doi.org/10.1021/acs.langmuir.6b01644

87. Takahashi M., Kawamura T., Yamamoto Y., Ohnari H., Himuro S., Shakutsui H. Effect of Shrinking Microbubble on Gas Hydrate Formation. *J. Phys. Chem. B*. 2003;107(10):2171–2173. https://doi.org/10.1021/jp022210z

88. Chu X., Agmo A. Sexual incentive motivation in old male rats: the effects of sildenafil and a compound (Impaza) stimulating endothelial NO synthase. *Pharmacol. Biochem. Behav*. 2008;89(2):209–217. https://doi.org/10.1016/j.pbb.2007.12.012

89. Serizawa A., Inui T., Yahiro T., Kawara Z. Pseudo-Laminarization of Micro-Bubble Containing Milky Bubbly Flow in a Pipe. *Multiphase Sci. Technol*. 2005;17(1–2):79–101. http://doi.org/10.1615/.v17.i1-2.50

90. Kumykov T.C., Jekamukhov M.K., Karov B.G. The bubbles influences on the water conductivity. Bulleten of Higher Education Institutes. *North Caucasus Region Natural Sciences*. 2009;2:42–43 (in Russ.). URL: https://cyberleninka.ru/article/n/o-vliyanii-puzyrkov-na-provodimost-vody/viewer

91. Ueda Y., Tokuda Y., Nihei N., Sugiyama A., Ogawa Y., Shiraga K. Electric and Electrochemical Properties of Fine Bubble Water and Analysis of the Correlation with Applied Research. *Japanese J. Multiphase Flow*. 2015;28(5):555–561. https://doi.org/10.3811/jjmf.28.555

92. Kushnir S.V., Kost' M.V., Seniv O.R. Influence of Bubbling of "Passive" Gases on the Properties of Water and Aqueous Solutions of Sodium Chloride. *Mater. Sci*. 2016;51:734–740. https://doi.org/10.1007/s11003-016-9897-1

93. Liu S., Kawagoe Y., Makino Y., Oshita S. Effects of nanobubbles on the physicochemical properties of water: The basis for peculiar properties of water containing nanobubbles. *Chem. Eng. Sci*. 2013;93:250–256. http://doi.org/10.1016/j.ces.2013.02.004

94. Kamimura Ch., Kamimura T. *Metod for manufacturing ultra-fine bubbles having oxidizing radical or reducing radicl by resonance foaming and vacuum cavitation, and ultra-fine bubble water manufacturing device*: US Patent Application 20200094205. Publ. 26.03.2020. http://www.freepatentsonline.com/y2020/0094205.html. Accessed August 31, 2021.

95. Liu Q., Zhou Y.H., Ye F., Yang Z.Q. Antivirals for Respiratory Viral Infections: Problems and Prospects. *Semin. Respir. Crit. Care. Med*. 2016;37(4):640–646. https://doi.org/10.1055/s-0036-1584803

96. Marui T. An Introduction to Micro/Nano-Bubbles and their Applications. *Systemics, Cybernetics and Informatics.* 2013;11(4):68–73. URL: https://www.hidronano.com.br/wp-content/uploads/2018/10/An-Introduction-to-Micro-ano-Bubbles-and-their-Applications.pdf

97. Ohnari H. Fisheries experiments of cultivated shells using micro-bubbles techniques. *J. Heat. Transfer. Soc. Japan*. 2001;40(160):2–7. URL: Fisheries experiments of cultivated shells using micro-bubbles technique | CiNii Research

98. Ebina K., Shi K., Hirao M., Hashimoto J., Kawato Y., Kaneshiro S., Morimoto,T., Koizumi K., Yoshikawa H. Oxygen and Air Nanobubble Water Solution Promote the Growth of Plants, Fishes, and Mice. *PLoS One.* 2013;8(6):e65339. https://doi.org/10.1371/journal.pone.0065339

99. Kurata K., Taniguchi T., Fukunaga T., Matsuda J., Higaki H. Development of a compact microbubble generator and its usefulness for three-dimensional osteoblastic cell culture. *J. Biomechan. Sci. Eng*. 2008;2(4):166–177. http://doi.org/10.1299/jbse.2.166

100. Park J., Kurata K. Application of microbubble to hydroponics solution promotes lettuce growth. *Horttechnology*. 2009;19(1):212–215. http://doi.org/10.21273/HORTSCI.19.1.212

101. Ushikubo F.Y., Oshita S., Furukawa T., Makino Y., Kawagoe Y., Shiina T. A study of water containing micro and nano-bubbles and its possible effect on physiological activity. In: *Proceedings of the CIGR International Conference of Agricultural Engineering*. 2008.

102. Dzubiella J. Explicit and implicit modeling of nanobubbles in hydrophobic confinement. *An. Braz. Acad. Sci*. 2010;82(1):3–12. http://doi.org/10.1590/S0001-37652010000100002

103. Seddon J.R.T., Lohse D., Ducker W.A., Craig V.S.J. A deliberation on nanobubbles at surfaces and in bulk. *Chem. Phys. Chem*. 2012;13(8):2179–2187. https://doi.org/10.1002/cphc.201100900

104. Xiao Y., Jiang S.C., Wang X., Muhammad T., Song P., Zhou B., Zhou Y., Li Y. Mitigation of biofouling in agricultural water distribution systems with nanobubbles. *Environ. Int*. 2020;141:105787. https://doi.org/10.1016/j.envint.2020.105787

105. Vagnell M. Effect of Vortex-processed Water on Tomato (Solanum lycopersicum) Plants. *Swedich University of Agrocultural Sciences*. 2012. 21 p. URL: https://stud.epsilon.slu.se/5243/1/vagnell_m_130130.pdf

106. Tschulakow A.V., Yan Y., Klimek W. A new approach to the memory of water. *Homeopathy*. 2005;94(4):241–247. https://doi.org/10.1016/j.homp.2005.07.003

107. Rangasamy S.B., Ghosh S., Pahan K. RNS60, a physically-modified saline, inhibits glial activation, suppresses neuronal apoptosis and protects memory in a mouse model of traumatic brain injury. *Exp. Neurol*. 2020;328:113279. https://doi.org/10.1016/j.expneurol.2020.113279

108. Mondal S., Martinson J.A., Ghosh S., Watson R., Pahan K. Protection of Tregs, suppression of Th1 and Th17 cells, and amelioration of experimental allergic encephalomyelitis by a physically-modified saline. *PLoS ONE*. 2012;7(12):1–18. https://doi.org/10.1371/journal.pone.0051869

109. Bonamin L. *Signals and Images. Contributions and Contradictions about High Dilution Research*. Springer Netherlands; 2008. 222 p. http://doi.org/10.1007/978-1-4020-8535-2

110. Penkov N.V. Temporal dynamics of the scattering properties of deionized water. *Phys. Wave Phe*n. 2020;28(2):135–139. http://doi.org/10.3103/S1541308X20020132

111. Slatinskaya O.V., Pyrkov Y.N., Filatova S.A., Guryev D.A., Penkov N.V. Study of the Effect of Europium Acetate on the Intermolecular Properties of Water. *Front. Phys*. 2021;(9):641110. https://doi.org/10.3389/fphy.2021.641110

112. Lobyshev V.I. Evolution of High-Frequency Conductivity of Pure Water Samples Subjected to Mechanical Action: Effect of a Hypomagnetic Filed. *Phys. Wave Phen*. 2021;(29):98–101. https://doi.org/10.3103/S1541308X21020084

113. Ryzhkina I.S., Murtazina L.I., Kiseleva Y.V., Konovalov A.I. Self-Organization and Physicochemical Properties of Aqueous Solutions of the Antibodies to Interferon Gamma at Ultrahigh Dilution. *Dokl. Phys. Chem*. 2015;462(1):110–114. http://doi.org/10.1134/S0012501615050048

114. Petrov S.I., Epstein O.I. Effect of potentiated solutions on mercury(II) signal in inversion voltammetry. *Bull. Exp. Biol. Med*. 2003;135(Suppl. 7):99–101. https://doi.org/10.1023/a:1024707519510

115. Elia V., Niccoli M. New Physico-Chemical Properties of Extremely Diluted Aqueous Solutions. *J. Thermal Analys. Calorimetry*. 2004;75(3):815–836. http://doi.org/10.1023/B:JTAN.0000027178.11665.8f

116. Murtazina L.I., Ryzhkina I.S., Mishina O.A., Andrianov V.V., Bogodvid T., Gainutdinov Kh.L., Muranova L.N., Konovalov A.I. Aqueous and salt solutions of quinine of low concentrations: self-organization, physicochemical properties and actions on the electrical characteristics of neurons. *Biofizika*. 2014;59(4):717–722 (in Russ.).

117. Lobyshev V.I. Dielectric characteristics of highly diluted aqueous diclofenac solutions in the frequency range of 20 Hz to 10MHz. *Phys. Wave. Phen*. 2019;27(2):119–127. http://doi.org/10.3103/S1541308X19020067

118. Bunkin N.F., Shkirin A.V., Penkov N.V., Chirikov S.N., Ignatiev P.S., Kozlov V.A. The Physical Nature of Mesoscopic Inhomogeneities in Highly Diluted Aqueous Suspensions of Protein Particles. *Phys. Wave. Phen*. 2019;27(2):102–112. https://doi.org/10.3103/S1541308X19020043

119. Lyakhov G., Shcherbakov I. Approaches to the physical mechanisms and theories of low-concentration effects in aqueous solutions. *Phys. Wave Phen*. 2019;27(2):79–86. http://doi.org/10.3103/S1541308X19020018

120. Gudkov S.V., Lyakhov G.A., Pustovoy V.I., Shcherbakov I.A. Vibration–vortex mechanism of radical-reaction activation in an aqueous solution: Physical analogies. *Phys. Wave Phen*. 2021;29(2):108–113. http://doi.org/10.3103/S1541308X21020060

121. Gudkov S.V., Baimler I.V., Uvarov O.V., Smirnova V.V., Volkov M.Y., Semenova A.A., Lisitsyn A.B. Influence of the Concentration of Fe and Cu Nanoparticles on the Dynamics of the Size Distribution of Nanoparticles. *Front. Phys.* 2020;8(11):622551. http://doi.org/10.3389/fphy.2020.622551

122. Kokornaczyk M.O., Würtenberger S., Baumgartner S. Impact of succussion on pharmaceutical preparations analyzed by means of patterns from evaporated droplets. *Sci. Rep.* 2020;10(1):570. https://doi.org/10.1038/s41598-019-57009-2

123. Goncharuk V.V., Syroeshkin A.V., Pleteneva T.V., Uspenskaya E.V., Levitskaya O.V., Tverdislov V.A. On the Possibility of Chiral Structure-Density Submillimeter Inhomogeneities Existing in Water. *J. Water Chem.* Technol. 2017;39(6):319–324. http://doi.org/10.3103/S1063455X17060029

124. Konovalov A.I., Ryzhkina I.S. Formation of nanoassociates as a key to understanding of physicochemical and biological properties of highly dilute aqueous solutions. *Russ. Chem. Bull.* 2014;63(1):1–14. https://doi.org/10.1007/s11172-014-0388-y

125. Rubtsova E.V., Soloveĭ A.B., Lobyshev V.I. Distribution of internal parameters of protein hydration shell structure. *Biofizika*. 2014;59(6):1071–1078 (in Russ.).

126. Belovolova L.V., Glushkov M.V., Vinogradov E.A., Babintsev V.A., Golovanov V.I. Ultraviolet Fluorescence of Water and Highly Diluted Aqueous Media. *Phys. Wave. Phen*. 2009;17(1):21–31. http://doi.org/10.3103/S1541308X0901004X

127. Styrkas A.D., Nikishina N.G. Mechanochemical processes in water. *High Energy Chemistry*. 2007;41(6):396–402. https://doi.org/10.1134/S0018143907060021

128. Ashmarin I.P., Karazeeva E.P., Lelekova T.V. Effectiveness of ultrasmall doses of endogenous bioregulators and immunoactive compounds. *Zh. Mikrobiol. Epidemiol. Immunobiol*. 2005;(3):109–116 (in Russ.).

129. Chikramane P.S., Kalita D., Suresh A.K., Kane S.G., Bellare J.R. Why extreme dilutions reach non-zero asymptotes: a nanoparticulate hypothesis based on froth flotation. *Langmuir*. 2012;28(45):15864–15875. https://doi.org/10.1021/la303477s

130. Nirmalkar N., Pacek A.W., Barigou M. Bulk Nanobubbles from Acoustically Cavitated Aqueous Organic Solvent Mixtures. *Langmuir*. 2019;35(6):2188–2195. https://doi.org/10.1021/acs.langmuir.8b03113

131. Meegoda J.N., Hewage S.A., Batagoda J.H. Stability of Nanobubbles. *Environmen. Eng. Sci*. 2018;35(11):1216–1227. http://doi.org/10.1089/ees.2018.0203

132. Bunkin N.F., Lyakhov G.A., Shkirin A.V., Kobelev A.V., Penkov N.V., Ugraitskaya S.V., Fesenko E.E. Study of the submicron heterogeneity of aqueous solutions of hydrogen-bond acceptor molecules by laser diagnostics methods. *Phys. Wave. Phen*. 2015;23(4):241–254. https://doi.org/10.3103/S1541308X15040019

133. Ushikubo F.Y., Furukawa T., Nakagawa R., Enari M., Makino Y., Kawagoe Y., Shiina T., Oshita S. Evidence of the existence and the stability of nano-bubbles in water. *Colloids and Surfaces A: Physicochem. Eng. Asp.* 2010;361(1–3):31–37. https://doi.org/10.1016/j.colsurfa.2010.03.005

134. Demangeat J.L. NMR water proton relaxation in unheated and heated ultrahigh aqueous dilutions of histamine: evidence for an air-dependent supramolecular organization of water. *J. Mol. Liq*. 2009;144:32–39. http://doi.org/10.1016/j.molliq.2008.07.013

135. Betti L., Trebbi G., Kokornaczyk M.O., Nani D., Peruzzi M., Dinelli G., Bellavite P., Brizzi M. Number of succussion strokes affects effectiveness of ultra-high-diluted arsenic on in vitro wheat germination and polycrystalline structures obtained by droplet evaporation method. *Homeopathy*. 2017;106(1):47–54. https://doi.org/10.1016/j.homp.2016.12.001

136. Sundqvist C. Plants are responding to homeopathy. 2020. URL: https://www.researchgate.net/publication/341432748_PLANTS_ARE_RESPONDING_TO_HOMEOPATHY

137. Elia V., Ausanio G., Gentile F., Germano R., Napoli E., Niccoli M. Experimental evidence of stable water nanostructures in extremely dilute solutions, at standard pressure and temperature. *Homeopathy*. 2014;103(1):44–50. https://doi.org/10.1016/j.homp.2013.08.004

138. Konovalov A.I., Ryzhkina I.S. Highly diluted aqueous solutions: Formation of nano-sized molecular assemblies (nanoassociates). *Geochem. Int*. 2014;52(13):1207–1226. http://doi.org/10.1134/S0016702914130072

139. Pershin S.M., Bunkin A.F., Grishin M.Y., Davydov M.A., Lednev V.N., Fedorov A.N., Palmina N.P. Correlation of optical activity and light scattering in ultra-low-concentrated phenosan-potassium aqueous solutions. *Doklady Akademii Nauk*. 2015;461(2):160–163 (in Russ.). https://doi.org/10.7868/S0869565215080113

140. Syroeshkin A.V., Nikiforova M.V., Koldina A.M., Gornak A.A., Tarabrina I.V. Drugs based on release-active antibodies. *Handbook for Practitioners Doctors*. 2018;3:25–30 (in Russ.).

141. Anick D.J., Ives J.A. The silica hypothesis for homeopathy: physical chemistry. *Homeopathy*. 2007;96(3):189–195. https://doi.org/10.1016/j.homp.2007.03.005

142. Perry C.C., Keeling-Tucker T. Crystalline silica prepared at room temperature from aqueous solution in the presence of intrasilica bioextracts. *Chem. Commun.* 1998;9(23):2587–2588. https://doi.org/10.1039/A807404F

143. Perry C.C., Keeling-Tucker T. Model studies of colloidal silica precipitation using biosilica extracts from Equisetum telmateia. *Colloid Polym. Sci*. 2003;281:652–664. https://doi.org/10.1007/s00396-002-0816-7

144. Khripin C.Y., Pristinski D., Dunphy D.R., Brinker C.J., Kaehr B. Protein-directed assembly of arbitrary three-dimensional nanoporous silica architectures. *ACS Nano*. 2011;5(2):1401–1409. https://doi.org/10.1021/nn1031774

145. Wang D.C., Chen G.Y., Chen K.Y., Tsai C.H. DNA as a template in self-assembly of Au nano-structure. *IET Nanobiotechnol*. 2011;5(4):132–135. https://doi.org/10.1049/iet-nbt.2011.0013

146. Baca H.K., Carnes E.C., Ashley C.E., Lopez D.M., Douthit C., Karlin S., Brinker C.J. Cell-directed-assembly: directing the formation of nano/bio interfaces and architectures with living cells. *Biochim. Biophys. Acta*. 2011;1810(3):259–267. https://doi.org/10.1016/j.bbagen.2010.09.005

147. Neville F., Broderick M.J., Gibson T., Millner P.A. Fabrication and activity of silicate nanoparticles and nanosilicate-entrapped enzymes using polyethyleneimine as a biomimetic polymer. *Langmuir.* 2011;27(1):279–285. https://doi.org/10.1021/la1033492

148. Duval E., Adichtchev S., Sirotkin S., Mermeta A. Long-lived submicrometric bubbles in very diluted alkali halide water solutions. *Phys. Chem. Chem. Phys*. 2012;14(12):4125–4132. https://doi.org/10.1039/c2cp22858k

149. Demangeat J.L. Nanobulles et superstructures nanométriques dans les hautes dilutions homéopathiques: le rôle crucial de la dynamisation et hypothèse de transfert de l'information. *La Revue d'Homéopathie*. 2015;6(4):125–139. https://doi.org/10.1016/j.revhom.2015.10.002

150. Demangeat J.L. Towards a Rational Insight into the Paradox of Homeopathy. *Adv. Complement. Alt. Med*. 2018;2(2):121–133. http://doi.org/10.31031/ACAM.2018.02.000534

151. Castagne,V., Lemaire M., Kheyfets I., Dugina J.L., Sergeeva S.A., Epstein O.I. Antibodies to S100 proteins have anxiolytic-like activity at ultra-low doses in the adult rat. *J. Pharm. Pharmacol.* 2008;60(3):309–316. https://doi.org/10.1211/jpp.60.3.0005

152. Epstein O. The Spatial Homeostasis Hypothesis. *Symmetry*. 2018;10(4):103. http://doi.org/10.3390/sym10040103

153. Rafalsky V., Averyanov A., Bart B., Minina E., Putilovskiy M., Andrianova E., Epstein O. Efficacy and safety of Ergoferon versus oseltamivir in adult outpatients with seasonal influenza virus infection: a multicenter, open-label, randomized trial. *Int. J. Infect. Dis*. 2016;51:47–55. https://doi.org/10.1016/j.ijid.2016.09.002

154. Carello R., Ricottini L., Miranda V., Panei P., Rocchi L., Arcieri R., Galli E. Long-term treatment with low-dose medicine in chronic childhood eczema: a double-blind two-stage randomized control trial. *Ital. J. Pediatr.* 2017;43(1):78. https://doi.org/10.1186/s13052-017-0393-5

155. Mkrtumyan A., Romantsova T., Vorobiev S., Volkova A., Vorokhobina N., Tarasov S., Putilovskiy M., Andrianova E., Epstein O. Efficacy and safety of Subetta add-on therapy in type 1 diabetes mellitus: The results of a multicenter, double-blind, placebo-controlled, randomized clinical trial. *Diabetes Res. Clini. Pract*. 2018;142:1–9. https://doi.org/10.1016/j.diabres.2018.04.044

156. Martin-Martin L.S., Giovannangeli F., Bizzi E., Massafra U., Ballanti E., Cassol M., Migliore A. An open randomized active-controlled clinical trial with low-dose SKA cytokines versus DMARDs evaluating low disease activity maintenance in patients with rheumatoid arthritis. *Drug Des. Devel. Ther*. 2017;11:985–994. https://doi.org/10.2147/dddt.s118298

157. Pushkar D., Vinarov A., Spivak L., Kolontarev K., Putilovskiy M., Andrianova E., Epstein O. Efficacy and safety of Afalaza in men with symptomatic benign prostatic hyperplasia at risk of progression: a multicenter, double-blind, placebo-controlled, randomized clinical trial. *Cent. European J. Urol.* 2018;71(4)427–435. https://doi.org/10.5173/ceju.2018.1803

158. Uberti F., Morsanuto V., Ghirlanda S., Ruga S., Clemente N., Boieri C., Boldorini R., Molinari C. Highly Diluted Acetylcholine Promotes Wound Repair in an *In Vivo* Model. *Adv. Wound Care* (*New Rochelle*). 2018;7(4):121–133. https://doi.org/10.1089/wound.2017.0766

159. Ivashkin V.T., Poluektova E.A., Glazunov A.B., Putilovskiy M.A., Epstein O.I. Pathogenetic approach to the treatment of functional disorders of the gastrointestinal tract and their intersection: results of the Russian observation retrospective program COMFORT. *BMC Gastroenterol.* 2020:20(1):2–10. https://doi.org/10.1186/s12876-019-1143-5

160. Spitsin A., Bush A., Kamentsev K. Piezoelectric and dielectric properties of Bi_3TiNbO_9 prepared by hot pressing from powders activated using the serial dilution method. *Sci. Rep*. 2020;10(1):22198. https://doi.org/10.1038/s41598-020-78826-w

161. Penkov N.V. Peculiarities of the perturbation of water structure by ions with various hydration in concentrated solutions of $CaCl_2$, CsCl, KBr, and KI. *Phys. Wave Phenom*. 2019;27(2):128–134. http://doi.org/10.3103/S1541308X19020079

162. Malarczyk E., Pazdzioch-Czochra M., Grąz M., Kochmańska-Rdest J., Jarosz-Wilkołazka A. Nonlinear changes in the activity of the oxygen-dependent demethylase system in Rhodococcus erythropolis cells in the presence of low and very low doses of formaldehyde. *Nonlinear Biomed. Phys.* 2011;5(1):9. http://doi.org/10.1186/1753-4631-5-9

163. Bunkin N.F., *et al*. Shaking-induced aggregation and flotation in immunoglobulin dispersions: Differences between water and water–ethanol mixtures. *ACS Omega.* 2020;5(24):14689–14701. https://doi.org/10.1021/acsomega.0c01444

164. Bell I.R., Schwartz G.E. Adaptive network nanomedicine: an integrated model for homeopathic medicine. *Front. Biosci.* (*Schol. Ed.*). 2013;5(2):685–708. https://doi.org/10.2741/s400

165. Dehaoui A., Issenmann B., Caupin F. Viscosity of deeply supercooled water and its coupling to molecular diffusion. *PNAS*. 2015;112(39):12020–12025. https://doi.org/10.1073/pnas.1508996112

About the authors:

Elena S. Don, Cand. Sci. (Biol.), Senior Researcher, Laboratory of Physiologically Active Substances, Institute of General Pathology and Pathophysiology (8, Baltiyskaya ul., Moscow 125315, Russia); Scientific Project Manager, Materia Medica Holding (47-1, Trifonovskaya ul., Moscow, 129272, Russia). E-mail: physactive@yandex.ru. Scopus Author ID 57070128700, ResearcherID L-6765-2018, RSCI SPIN-code 2226-9051, https://orcid.org/0000-0001-8219-0482

German O. Stepanov, Cand. Sci. (Biol.), Senior Researcher, Materia Medica Holding (47-1, Trifonovskaya ul., Moscow, 129272, Russia). E-mail: stepanovgo@materiamedica.ru. Scopus Author ID 15046034100, https://orcid.org/0000-0002-8576-9745

Sergey A. Tarasov, Dr. Sci. (Medicine), Leading Researcher, Laboratory of Physiologically Active Substances, Institute of General Pathology and Pathophysiology (8, Baltiyskaya ul., Moscow,125315, Russia); Director of Research & Development Department, Materia Medica Holding (47-1, Trifonovskaya ul., Moscow, 129272, Russia). E-mail: TarasovSA@materiamedica.ru. Scopus Author ID 7005125924, ResearcherID X-2509-2018, RSCI SPIN-code 9448-8529, https://orcid.org/0000-0002-6650-6958

Об авторах:

Дон Елена Сергеевна, к.б.н., старший научный сотрудник лаборатории физиологически активных веществ, ФГБНУ ««Научно-исследовательский институт общей патологии и патофизиологии» (125315, Россия, Москва, ул. Балтийская, д. 8); руководитель научных проектов, ООО «НПФ «МАТЕРИА МЕДИКА ХОЛДИНГ» (129272, Россия, Москва, ул. Трифоновская, д. 47, стр. 1). E-mail: physactive@yandex.ru. Scopus Author ID 57070128700, ResearcherID L-6765-2018, SPIN-код РИНЦ 2226-9051, https://orcid.org/0000-0001-8219-0482

Степанов Герман Олегович, к.б.н., старший научный сотрудник, ООО «НПФ «МАТЕРИА МЕДИКА ХОЛДИНГ» (129272, Россия, Москва, ул. Трифоновская, д. 47, стр. 1). E-mail: stepanovgo@materiamedica.ru. Scopus Author ID 15046034100, https://orcid.org/0000-0002-8576-9745

Тарасов Сергей Александрович, д.м.н., ведущий научный сотрудник лаборатории физиологически активных веществ, ФГБНУ «Научно-исследовательский институт общей патологии и патофизиологии» (125315, Россия, Москва, ул. Балтийская, д. 8); директор департамента научных исследований и разработок, ООО «НПФ «МАТЕРИА МЕДИКА ХОЛДИНГ» (129272, Россия, Москва, ул. Трифоновская, д. 47, стр. 1). E-mail: TarasovSA@materiamedica.ru. Scopus Author ID 7005125924, ResearcherID X-2509-2018, SPIN-код РИНЦ 9448-8529, https://orcid.org/0000-0002-6650-6958

The article was submitted: January 31, 2023; approved after reviewing: March 29, 2023; accepted for publication: October 06, 2023.

The text was submitted by the authors in English
Edited for English language and spelling by Dr. David Mossop

CHEMISTRY AND TECHNOLOGY OF ORGANIC SUBSTANCES

ХИМИЯ И ТЕХНОЛОГИЯ ОРГАНИЧЕСКИХ ВЕЩЕСТВ

ISSN 2686-7575 (Online)
https://doi.org/10.32362/2410-6593-2023-18-5-446-460
UDC 544.723.21

RESEARCH ARTICLE

Environmentally safe sorbent from ash-and-slag waste of heat power engineering

Svyatoslav A. Bushumov, Tatyana G. Korotkova✉

Kuban State Technological University, Krasnodar, 350072 Russia
✉*Corresponding author, e-mail: korotkova1964@mail.ru*

Abstract

Objectives. *To determine the physical and chemical properties (bulk density, ash content, total pore volume, abrasion, humidity, sorption capacity) of sorbent based on ash-and-slag waste from heat power engineering, calcined and modified with a Tiprom K organosilicon water repellent.*
Methods. *The physicochemical properties of the modified sorbent were determined using an experimental method according to the methods of regulatory documents on equipment verified and certified in the prescribed manner.*
Results. *Ash and slag taken from the ash dump of the Novocherkasskaya GRES power station were dried, then calcined at a temperature of 600°C for 30 min and modified with a Silor hydrophobizing silicon-containing liquid (HSL). The modifier/ash ratios (by weight) were 1:20, 1:10, 1:5, 1:3, and 1:2. The optimal ratio was 1:5 at a sorption capacity with respect to hexane of 0.86 g/g. The modification temperature was optimized in the temperature range of 110–200°C. The optimal approach it to dry samples at 160°C to constant weight. At a temperature of 200°C, sintering of the material was observed. The analysis of HSL modifiers was carried out in terms of the price/sorption properties ratio. The following were considered as HSL: Silor, HSL-11BSP, HSL 136-157M, PROFILUX, Tiprom K, Tiprom U. The optimal modifier Tiprom K was selected. The physicochemical properties of the modified sorbent obtained at a ratio of 1:5 (by weight) and dried at 160°C were experimentally determined. The sorption properties were studied on the water surface with respect to various oil products: fuel oil, kerosene, AI-92 gasoline, nefras, oil sludge, and n-hexane. The smallest sorption capacity was obtained with respect to n-hexane, amounting to 0.86 g/g. During the experiment, it was found that half of the sorption capacity*

was filled with oil in the first minutes of contact. Complete sorption time was 30–40 min for relatively light hydrocarbons (n-hexane, AI-92 gasoline, kerosene, nefras), 40–60 min for oil sludge, and more than 60 min for fuel oil. Experiments established that the sorption process does not depend on the matrix (salinity) of water. A visual assessment of the color intensity of the residual spot of oil sludge allowed a conclusion to be made about a significant content of oil products in the case of sorption of oil sludge by quartz sand based on the residual yellow layer of oil sludge. In the case of sorption of oil sludge by calcined and modified sorbents, the residual oil products were insignificant. A comparative analysis of data on the effectiveness of the developed sorbent and currently available analogues based on sludge and slag is presented.

Conclusions. *The next physicochemical properties of the sorbent modified with HSL Tiprom K were determined: bulk density was 0.621 g/mL, ash content was 97.1%, total pore volume by water was less than 0.05 mL/g, attrition was 8.8%, humidity was less than 0.5%; sorption capacity, in g/g: for n-hexane, 0.86; for AI-92 gasoline, 0.89; for nefras, 0.93; for kerosene, 0.99; for oil sludge, 1.18; for fuel oil, 1.46. The efficiency of cleaning a solid surface from oil sludge with a calcined sorbent was 97%, and with a modified sorbent 95%. The modified sorbent has high buoyancy when saturated with oil products and the ability to retain them for a long time.*

Keywords: *sorbent, ash-and-slag waste, thermal power engineering, oil products, water-repellent silicon-containing liquids*

For citation: Bushumov S.A., Korotkova T.G. Environmentally safe sorbent from ash-and-slag waste of heat power engineering. *Tonk. Khim. Tekhnol. = Fine Chem. Technol*. 2023;18(5):446–460. https://doi.org/10.32362/2410-6593-2023-18-5-446-460

НАУЧНАЯ СТАТЬЯ

Экологически безопасный сорбент из золошлаковых отходов теплоэнергетики

С.А. Бушумов, Т.Г. Короткова✉

Кубанский государственный технологический университет, Краснодар, 350072 Россия
✉*Автор для переписки, e-mail: korotkova1964@mail.ru*

Аннотация

Цели. *Определение физико-химических свойств (насыпной плотности, зольности, суммарного объема пор, истираемости, влажности, сорбционной емкости) сорбента на основе золошлаковых отходов теплоэнергетики, прокаленного и модифицированного кремнийорганическим гидрофобизатором Типром К.*

Методы. *Физико-химические свойства модифицированного сорбента определены экспериментальным методом по методикам нормативных документов на оборудовании, поверенном и аттестованном в установленном порядке.*

Результаты. *Золошлак, отобранный на золоотвале Новочеркасской ГРЭС, высушен, прокален при температуре 600°С в течение 30 мин и модифицирован гидрофобизирующей кремнийсодержащей жидкостью (ГКЖ) марки Силор. Исследованы соотношения*

модификант/зола (по массе) 1:20, 1:10, 1:5, 1:3, 1:2. Оптимальным принято соотношение 1:5 при сорбционной емкости по отношению к н-гексану 0.86 г/г. Проведена оптимизация температуры модификации в интервале температур 110–200°С. Наиболее оптимальным является высушивание образцов при 160°С до постоянной массы. При температуре 200°С наблюдалось спекание материала. Выполнен анализ модификаторов ГКЖ по соотношению цена/сорбционные свойства. В качестве ГКЖ рассмотрены марки: Силор, ГКЖ-11БСП, ГКЖ 136-157М, PROFILUX, Типром К, Типром У. Выбран оптимальный модификатор марки Типром К. Экспериментально определены физико-химические свойства модифицированного сорбента, полученного при соотношении 1:5 (по массе) и высушенного при 160°С. Изучены его сорбционные свойства на водной поверхности по отношению к различным нефтепродуктам: мазуту, керосину, бензину марки АИ-92, нефрасу, нефтешламу и н-гексану. Наименьшая сорбционная емкость получена по отношению к н-гексану, которая составила 0.86 г/г. В ходе эксперимента установлено, что половина величины сорбционной емкости заполнена нефтепродуктом в первые минуты контакта. Время полной сорбции составило 30–40 мин для относительно легких углеводородов (н-гексан, бензин АИ-92, керосин, нефрас), 40–60 мин для нефтешлама и более 60 мин для мазута. Экспериментально выявлено, что процесс сорбции не зависит от матрицы (солености) воды. При визуальной оценке по интенсивности окраски остаточного пятна нефтешлама сделан вывод о значительном содержании нефтепродуктов в случае сорбции нефтешлама кварцевым песком на основе остаточного желтого слоя нефтешлама. В случае сорбции нефтешлама прокаленным и модифицированным сорбентами остаточные нефтепродукты незначительны. Приведен сравнительный анализ данных по эффективности разработанного сорбента и имеющихся в настоящее время аналогов на основе шламов и шлаков.

Выводы. *Определены физико-химические свойства сорбента, модифицированного ГКЖ Типром К: насыпная плотность 0.621 г/см^3, зольность 97.1%, суммарный объем пор по воде менее 0.05 см^3/г, истираемость 8.8%, влажность менее 0.5%; сорбционная емкость, в г/г: по н-гексану 0.86, по бензину АИ-92 0.89, по нефрасу 0.93, по керосину 0.99, по нефтешламу 1.18, по мазуту 1.46. Эффективность очистки твердой поверхности от нефтешлама прокаленным сорбентом составила 97%, а модифицированным – 95%. Модифицированный сорбент обладает высокой плавучестью при насыщении нефтепродуктами и способностью их длительного удержания.*

Ключевые слова: *сорбент, золошлаковые отходы, теплоэнергетика, нефтепродукты, гидрофобизирующие кремнийсодержащие жидкости*

Для цитирования: Бушумов С.А., Короткова Т.Г. Экологически безопасный сорбент из золошлаковых отходов теплоэнергетики. *Тонкие химические технологии*. 2023;18(5):446–460. https://doi.org/10.32362/2410-6593-2023-18-5-446-460

INTRODUCTION

Ash and slag (ash residue) is formed by mixing water with captured fly ash and solid slag waste generated by the combustion of coal in the furnaces of power plants. It is sent for storage in the form of a pulp outside the territory of the thermal power station (TPS) to an ash dump, also called a hydroash dump.

Currently, the quantity of accumulated ash-and-slag waste (ASW) amounts to billions of tons. The area occupied by them is thousands of hectares of land. Seepage into the soil and dusting of ASWs have a negative impact on the environment and the health of people living in urban areas near TPSs, combined heat and power stations (TETS in Russian abbreviation), and state district power stations (GRES in Russian abbreviation) [1, 2]. Recycling of ASWs in Russia is no more than 8% [1].

This waste is cheap, accessible, non-explosive and non-flammable.

The review [2] analyzed research by scientists on the impact of ASWs on the environment. The results of the analysis are summarized in a table which

shows that the storage of ash waste leads to dust from the surface of the ash dump, migration of pollutants along the soil profile and alienation of the territory. The first two factors contribute to the deposition of pollutants on the surface, pollution of atmospheric air, surface, ground and underground waters. Data from the literature regarding the content of isotopes in the ash of thermal power plants enabled a conclusion to be made about the danger to public health and the threat to flora and fauna due to the leaching of radionuclides and heavy metals into the soil and groundwater. The following areas for processing and disposal of ASWs were identified: use in agriculture; extraction of metals; rare and valuable components; firefighting; alumina production; as well as wastewater treatment and isolation of various wastes. The analysis of the chemical composition of the ashes of the *Khabarovskaya TETS-3* power station showed that the waste is classified as a technogenic mineral raw material which accumulates over time.

Many research and review works have been devoted to the areas of recycling of ASWs [3–6]. In [3], the composition of ASWs of the *Kazanskaya TETS-2* power station was studied. It can be concluded that the main promising areas for the utilization of ASWs, in addition to the construction industry, can be the extraction of titanium from them, the synthesis of zeolites from the aluminosilicate components of ash and slag. In order to maximize the level of ASW recycling, it is recommended that the ASW removal system be switched to the dry method [4]. In order to reduce the negative impact of ASWs on the environment and involve them in economic turnover, the issue of regulating this problem is proposed to be returned to the legislative level [6].

ASWs from the combustion of coal from TPS is generally considered to be non-hazardous to the environment. In [7] the chemical composition of the ASWs of the *Khabarovskaya TETS-3* is given. Based on the calculation method and the phytotesting method, the waste is classified as hazard class V.

Our quantitative chemical [8] and toxicological (biotesting) analyzes of the ashes of the *Novocherkasskaya GRES* power station showed that the dry ash-and-slag mixture collected by an electric precipitator, cyclone and bag filter belongs to hazard class IV [9], while the ash-and-slag mixture accumulated at the ash dump according to the hydraulic ash removal scheme, belongs to hazard class V [10].

Every year, the pollution of water bodies with oil products (OPs) increases as a result of the discharge of partially treated or untreated wastewater into them. This in the future may lead to an environmental disaster. Research by scientists confirms the presence of adsorption properties of ASWs. The paper [11] proposes the use of waste water from an energy generating enterprise (Russia) as a sorbent (filter media) to clean the drainage of a storm drainage system. The characteristics of the proposed ash-and-slag sorbent (Russia) are given. A device for drainage of storm and snowmelt runoff, including a filter media, has been developed. It is recommended that purified water be used for household needs (irrigation, construction activities, etc.) in order to save drinking water.

In [12], the authors used fly ash from coal-fired power plants (India) as a sorbent for the treatment of domestic wastewater. Waste water was purified after preliminary settling for 24 h to precipitate coarse mechanical impurities. Wash water samples were placed in flasks with a capacity of 250 mL, a weighed portion of the adsorbent was added and kept in a thermostat with a shaker at a temperature of 25°C for 7 h. No significant adsorption was observed. Next, the effect of ash/wastewater ratio on the removal efficiency of pH, surfactants, and suspended solids was studied. As a result, it was proposed that the sorbent be used for the treatment of household wastewater at a dosage of 40 g of sorbent per 1 L of treated water for 6 h.

In [13], the ash and slag of the *Taichung Power Plant* (Taiwan) was studied from the point of view of its use as a sorbent for the purification of synthetic (model) wastewater. Based on chemical oxygen demand (COD), it was found that model wastewater contains copper in a quantity from 10 to 40 mg/L and potassium hydrophthalate in a quantity from 250 to 1000 mg/L. Wastewater (leachate) from the Taichung City landfill with known contents of ammonium nitrogen, total nitrogen, iron, phosphates, zinc, and manganese was also tested. Sorption conditions were optimized, such as solution pH, temperature, sorbent dosage (sorbent/purified water ratio). When using ash and slag as a sorbent, the purification efficiency for COD was 47.0%, for ammonium nitrogen, 39.4%; for total nitrogen, 31.1%; for zinc, 82.2%; for manganese, 94.3%; for iron, 96.5%; for phosphates, 92.9%.

Indian scientists have conducted studies on the treatment of wastewater with fly ash from phosphates and fluorides [14], suspended solids, COD and biochemical oxygen demand (BOD) [15], heavy metals and organic substances [16].

Wastewater with a volume of 1.0 L was filtered through a layer of sorbent (dynamic sorption) 10 cm thick. The free filtration process took about 1.3 h. As a result, the degree of purification of the wastewater sample in terms of suspended solids was 69.02%, in terms of BOD—71.48% and in terms of COD—66.59% [15].

In [16], fly ash was used as a sorbent, in order to purify wastewater from a number of heavy metals: nickel, zinc, lead, iron, manganese, and aluminum. The purification efficiency of the wastewater sample was more than 80% for all metals except manganese. Its cleaning efficiency was in the range of 70–80%.

In [17], fly ash was used as a sorbent to purify water from 2,4-dimethyl phenol. The sorption properties of the material were studied in model aqueous solutions containing 2,4-dimethylphenol, depending on the temperature of the solutions, the dose of the sorbent, and the initial content of 2,4-dimethylphenol. The authors managed to achieve a degree of extraction of 2,4-dimethylphenol from an aqueous solution at a level of about 90%. In addition, a method was proposed for regenerating the sorbent with a 2% aqueous solution of hydrogen peroxide.

In [18], fly ash was used as a sorbent for the removal of 2-chlorophenol (2-CP) and 2,4-dichlorophenol (2,4-DCP) from aqueous solutions. The effect of pH solution on the removal process was studied (the pH value is lower than the pK_a value of 2-CP and 2,4-DCP). An experimental setup was assembled with a filter filled in layers from the edges with quartz sand and in the middle layer with fly ash. Sorption was mobile in nature of the solution being purified (dynamic sorption). The sorption capacity of fly ash reached its maximum stable value already at a passing time of about 60 min and was about 2.0 g/g and 1.3 g/g for 2,4-DCP and 2-CP, respectively. The mutual influence of 2,4-DCP and 2-CP on the sorption process was studied.

This paper presents the results of studies of an environmentally friendly sorbent based on ASW thermal power engineering, calcined and modified with the Tiprom K organosilicon water-repellent agent. It has a high buoyancy when saturated with OPs and the ability to retain them for a long time. The modified sorbent was studied on model mixtures containing fuel oil, kerosene, AI-92 gasoline, nefras, oil sludge and *n*-hexane and is intended for cleaning wastewater from free-floating and emulsified petroleum products. The sorption of oil sludge on a water surface was carried out under laboratory conditions. A real sample of sea water (the Black Sea) was studied as a water body.

METHODS

The physicochemical properties of the modified sorbent are determined according to Russian regulatory documents: bulk density according to GOST R 51641-2000[1], ash content according to PND F 16.2.2:2.3:3.32-02[2], total pore volume according to GOST 17219-71[3], abrasion strength according to GOST R 51641-2000, mass concentration of OPs according to PND F 14.1:2:4.5-95[4], humidity according to GOST 5180-2015[5]. The sorption capacity of the modified sorbent in relation to OPs was determined experimentally, as described in this article.

To calcinate the samples, a LM-312.11 laboratory electric furnace (*VEB ELEKTRO BAD FRANKENHAU-ZEN*, 1990, German Democratic Republic) was used, maintaining a temperature range from +50 to +1200°C. The study of the OP content in the samples was carried out using a KN-3 concentration meter (*SIBEK-OPRIBOR*, 2018, Russia). To dry reagents and samples and prepare laboratory glassware, a drying cabinet of the LOIP LF-60/350-GG1 series (*Laboratornoe Oborudovanie i Pribory*, 2012, Russia) was used, maintaining a temperature range from +50 to +350°C. To weigh the samples, Adventurer electronic laboratory scales of AR214 modification (*OHAUS Europe*, 2004, Switzerland) were used. Extraction of solutions was carried out on an ES-8000 rotary extraction unit (*Ekokhim*, 2015, Russia), extraction of solid samples was conducted on a universal laboratory shaker of WU-4 type (*PREMED*, 1985, Poland). Abrasion tests of materials were carried out using a KP-131 set of sieves (*Meridian*, 2015, Russia) with a lid and tray. All measuring instruments are included in the Russian State Registry of Measuring Instruments[6] and verified in accordance with the procedure established by the legislation of the Russian Federation. When conducting laboratory

[1] GOST R 51641-2000. State Standard of the Russian Federation. Filtering granular materials. General specifications. Moscow: Gosstandart Rossii; 2000.

[2] PND F 16.2.2:2.3:3.32-02. Measurement procedure of the content of dry and calcined residue in solid and liquid waste of production and consumption, sediments, sludge, activated sludge, bottom sediments by gravimetric method. Moscow: NTF “Khromos”; 2002 (publ. 2017).

[3] GOST 17219-71. State Standard of the USSR. Active carbons. Method for determination of summary pore volume by the moisture capacity test. Moscow: Ordena “Znak Pochyota” Izdatelstvo stantartov; republication October 1987.

[4] PND F 14.1:2:4.5-95. Quantitative chemical analysis of waters. Method of measuring the mass concentration of petroleum products in drinking, surface and wastewater by IR spectrometry. Moscow: FTsAO; 1995 (publ. 2011).

[5] GOST 5180-2015. Interstate Standard. Soils. Methods of laboratory determination of physical characteristics. Moscow: Standartinform; 2015.

[6] https://fgis.gost.ru/fundmetrology/registry. Accessed October 03, 2022.

studies, volumetric glassware was used: cylinders, burettes, volumetric flasks, and pipettes in accordance with GOST 29228-91[7].

RESULTS AND DISCUSSION

The object of the study is ASW taken from the 3rd section of the ash dump of the *Novocherkasskaya GRES* power station (Novocherkassk, Rostov oblast), which is a liquid-solid mass. A sample of ASW was homogenized and placed in a drying oven, where it was kept at 110°C for 30 min to remove free moisture. The dried ASW had a lumpy shape. As a result of calcination in a muffle furnace at 600°C and holding at this temperature for 30 min, a loose crumbly material was obtained, called calcined sorbent, the physicochemical properties of which were determined by us in [19] and amounted to: bulk density was 0.666 g/mL; ash content, 99.5%; total pore volume, 0.506 mL/g; abrasion, 8.5%; humidity, less than 1%. According to the results of granulometric analysis, 95.2% of the mass of the calcined sorbent falls in the fraction from 0.25 to 0.5 mm.

In order to impart buoyancy when saturated with OPs and ability to retain them for a long time on the water surface, the calcined sorbent is modified with an organosilicon water repellent (hydrophobizing silicon-containing liquid, HSL) and is called a modified sorbent.

At the first stage of research, the optimal mass ratio of HSL and prepared calcined sorbent was determined. Five samples were prepared based on Silor/ASW HSL in mass ratios of 1:20, 1:10, 1:5, 1:3, and 1:2. The samples were left open for a day at room temperature until completely dry. Next, the samples were ground in an agate mortar to break up the lumps formed during the process of wetting the ASW by HSL, and the sorption properties of the resulting samples with respect to *n*-hexane were studied.

Distilled water of 1.0 L was placed in an open cylindrical glass container with a capacity of about 3 L. An aliquot of 2.00 mL was placed into the same container using a microdispenser and, in a separate experiment, 4.00 mL of chemically pure (99.9% purity) *n*-hexane (density at 20°C is 0.6548 g/mL), which corresponds to 1308 mg and 2617 mg in terms of pure substance. *n*-Hexane was placed on the surface of the water in the region of the geometric center so that the *n*-hexane spot did not touch the walls of the container. Next, an accurate weighed portion of the prepared sample of the modified sorbent weighing about 1.0 g was selected (the mass value was recorded with an accuracy of 0.0001 g and was used in further calculations) and was scattered in a uniform thin layer on the surface of the *n*-hexane spot. The samples were left in this form for 30 min. After this, the sorbent was collected with ash-free blue ribbon filter paper, the sample with the filter paper was placed in a Petri dish and dried open in air for about a day to evaporate water and residual *n*-hexane. The air-dry sample together with filter paper was placed in a conical flask with a ground stopper with a capacity of 100 mL, 10 mL of carbon tetrachloride was added, the flask was closed with a lid and the sample was shaken vigorously on a universal laboratory shaker for 1 h. The resulting extract was filtered through an ash-free blue-ribbon filter, installed in a glass funnel, in a flask with a ground stopper with a capacity of 50 mL. Extraction of the sample followed by filtration was repeated 2 more times with new portions of carbon tetrachloride, 10 mL each. All extracts were combined in the same flask with a ground stopper with a capacity of 50 mL, into which the first portion of the extract was collected, and the contents of the flask were mixed with rotational movements.

The resulting combined extract was passed through a previously prepared chromatographic column, which was a cut burette with a capacity of 25 mL. A small piece of glass wool was placed in the lower part of the column, previously kept in a 1:1 solution of sulfuric acid for 12 h, washed with distilled water and, after drying, washed with carbon tetrachloride and dried in air. Then 6 g of aluminum oxide, activated by calcination in a muffle furnace at a temperature of 600°C for 4 h, was poured into the column, followed by the addition of distilled water with a volume of 15 mL per 500 g of calcined aluminum oxide, followed by stirring and holding for 24 h in a desiccator. The top layer of aluminum oxide was also fixed in the column with a small piece of glass wool. Then 8 mL of carbon tetrachloride was poured into the column for wetting. After absorbing a portion of carbon tetrachloride, the column tap was opened and the eluate passing through the column was collected into a measuring cylinder with a volume of 10 mL. As soon as the upper limit of carbon tetrachloride passed through the chromatographic column reached the top layer of glass wool, the column tap was closed and the first portion of the sample extract with a volume of about 10 mL was added to the column, after which the column tap was opened and the eluate continued to be collected into a measuring cylinder with a capacity of 10 mL. As soon

[7] GOST 29228-91. State Standard of the USSR. Laboratory glassware. Graduated pipettes. Part 2. Graduated pipettes without a set waiting time. Moscow: Standartinform; 1991.

as the quantity of eluate in the cylinder reached 8 mL, the column tap was closed and the collected eluate was discarded, then the column tap was opened and the eluate continued to be collected in a conical flask with a ground stopper with a capacity of 50 mL. In this way, the entire volume of the sample extract was passed through the sorption column and as soon as the top layer of the extract touched the top layer of glass wool, the column was closed and 5 mL of carbon tetrachloride was added, after which the stopcock was opened and the eluate continued to be collected in a conical flask until the liquid in the column sank to the level of the top layer of glass wool. The resulting eluate with a volume of 30 mL was thoroughly mixed in a flask by shaking, the eluate was successively diluted 1000 times, the diluted eluate was poured into a measuring cuvette, and the OP content was measured using a KN-3 concentrator previously prepared in accordance with the operational documentation. The OP content in samples X, g/g, was calculated using the expression

$$X = \frac{C_m \cdot B \cdot K}{M \cdot 1000} \quad (1)$$

where C_m is the measured quantity of OP in the extract, mg/L; B is the eluate volume, L (equal to 0.03 L); K is the eluate dilution factor (equal 1000); M is the sample weight, g.

The obtained values of OP content in the samples are expressed in g/g and are the values of the sorption capacity of the modified sorbent samples. The results are shown in Tables 1 and 2 and in Fig. 1.

Based on the analysis of the data obtained, it was concluded that the sorption capacity of the samples does not depend on the amount of *n*-hexane excess. The highest value of the sorption capacity of the studied samples was taken as the result. The optimal weight ratio of HSL to ASW was 1:5, while the sorption capacity with respect to *n*-hexane reached a maximum of 0.86 g/g.

At the second stage of the research, the optimal conditions for drying the samples were determined. The sample masses were subjected to forced drying in an oven at temperatures of 110–200°C to constant mass. At temperatures above 180°C, non-uniform drying of the sample, adhesion and enlargement of grains were observed, which in turn led to a decrease in porosity and a deterioration in sorption properties. At a temperature of 200°C, sintering of the material was observed. The most optimal method is to dry samples at 160°C. For samples weighing 1 g, the drying process took no more than 10 min. Optimization of modification temperature is given in Table 3.

At the third stage of research, the optimal HSL modifier was selected based on the price/sorption properties ratio. Silor, HSL-11BSP, HSL 136-157M, PROFILUX, Tiprom K, and Tiprom U modifiers were considered as HSL. The sorbents obtained on the basis of HSL 136-157M and Tiprom K have the highest oil capacity, but Tiprom K has the lowest price, due to than chosen as the optimal modifier. Figure 2 shows the values of sorption capacity (oil capacity), in g/g, in relation to *n*-hexane, indicating the price of HSL in RUR/kg. The price is shown in figures around HSL in 2021 prices.

Tiprom K HSL was accepted as optimal; its price was 420 RUR/kg, and the sorption capacity of the resulting modified sorbent is 0.86 g/g.

At the fourth stage, the physicochemical properties of the Tiprom K modified HSL sorbent

Table 1. Sorption capacity in relation to *n*-hexane of hydrophobizing silicon-containing liquid (HSL) samples of the Silor brand—calcined sorbent according to the measured content of OPs in the samples when interacting with 1308 mg of *n*-hexane

Modifier/ash ratio (by weight)	Sample weight, g	Measured content of OPs in the extract, mg/L	Eluate dilution factor	Sorption capacity in relation to *n*-hexane, g/g
1:20	1.0008	20.7	1000	0.62
1:10	1.0016	23.7	1000	0.71
1:5	0.9999	28.3	1000	0.85
1:3	0.9968	28.2	1000	0.85
1:2	0.9972	28.3	1000	0.85

Table 2. Sorption capacity in relation to *n*-hexane of HSL samples of the Silor brand—calcined sorbent according to the measured content of OPs in the samples when interacting with 2617 mg of *n*-hexane

Modifier/ash ratio (by weight)	Sample weight, g	Measured content of OPs in the extract, mg/L	Eluate dilution factor	Sorption capacity in relation to *n*-hexane, g/g
1:20	0.9972	21.3	1000	0.64
1:10	0.9976	23.9	1000	0.72
1:5	1.0022	28.7	1000	0.86
1:3	0.9981	28.6	1000	0.86
1:2	0.9974	28.6	1000	0.86

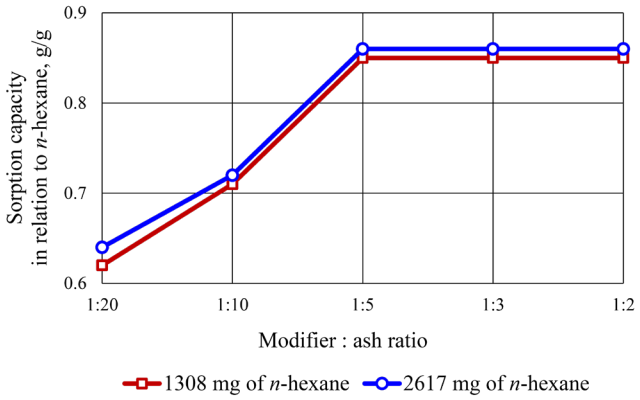

Fig. 1. Dependence of sorption capacity on the modifier/ash ratio (by weight).

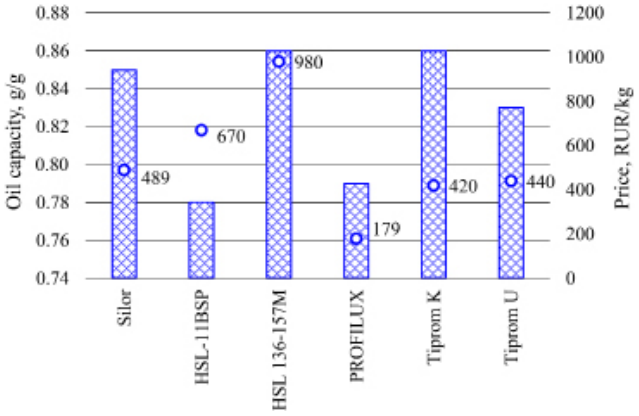

Fig. 2. Sorption capacity (oil capacity) in relation to *n*-hexane and price of HSL.

Table 3. Modification temperature optimization

Temperature °C	Sorption capacity in relation to *n*-hexane, g/g
110	0.72
120	0.75
130	0.78
140	0.81
150	0.85
160	0.86
170	0.84
180	0.78
200	0.60

were studied: bulk density, ash content, total pore volume, abrasion, humidity, and sorption capacity, which are given in Table 4. Methods for determining these indicators were described in detail by us in [19] when studying the properties of a calcined sorbent.

At the fifth stage, the sorption properties of the modified sorbent were studied in relation to various petroleum products, such as: fuel oil, kerosene, AI-92 gasoline, nefras, oil sludge, and *n*-hexane. OP samples were applied to the surface of distilled water at the rate of 2.00 g per 1 L of water, after which 1.00 g of sorbent was evenly scattered in a thin layer over the entire area of the OP spot. The time of interaction of the sorbent with the OPs was recorded. After a certain time, the samples were collected with blue ribbon filter paper, dried in Petri dishes in the open air for 24 h, and in the case of fuel oil and oil sludge, excess OPs were additionally blotted with filter paper and the sorption capacity of the samples was measured. The highest oil capacity was observed in the case of sorption of fuel oil, the lowest—with *n*-hexane. The increase in oil intensity can be explained by an increase in the density and molecular weight of the oil. The sorption time was optimized (Table 5).

For relatively light OPs, the optimal sorption time was at least 30–40 min, for heavy ones—at least 60 min. During the experiment, it was established that half the sorption capacity is filled with OPs

Table 4. Physical and chemical properties modified sorbent

Indicators	Units of measurement	Modified sorbent
Bulk density	g/mL	0.621
Ash content	%	97.1
Total pore volume	mL/g	Less than 0.050*
Abrasion	%	8.8
Humidity	%	Less than 0.5

*The total pore volume is determined by water; the resulting hydrophobized sorbent has hydrophobic properties.

Table 5. Optimization of sorption time

Sorption time, min	Fuel oil	Kerosene	AI-92 gasoline	Nefras	Oil sludge	*n*-Hexane
	Sorption capacity (oil capacity) g/g					
10	0.68	0.58	0.59	0.52	0.61	0.56
20	1.03	0.79	0.72	0.68	0.84	0.73
30	1.20	0.92	0.85	0.81	0.99	0.84
40	1.32	0.97	0.88	0.89	1.09	0.86
60	1.45	0.99	0.89	0.92	1.17	0.86
90	1.46	0.99	0.89	0.93	1.18	0.85

in the first minutes of contact. Conventionally, complete sorption can be considered 30–40 min for relatively light hydrocarbons (*n*-hexane, AI-92 gasoline, kerosene, and nefras), 40–60 min for oil sludge and more than 60 min for fuel oil (Fig. 3).

A laboratory study of the sorption of oil sludge on the water surface was carried out (Fig. 4). A real sample of sea water (the Black Sea) was studied as a water body.

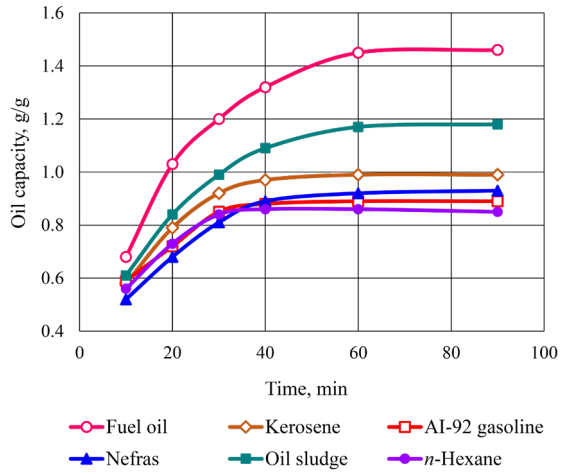

Fig. 3. Dependence of the oil capacity of OPs on the time of sorption.

(a)

(b)

Fig. 4. Sorption of oil sludge on the water surface: (a) applying oil sludge to the water surface with a microdoser; (b) sorption of oil sludge by a modified sorbent.

Oil sludge of 1.00 g was applied to the surface of water with a volume of 1 L using a microdoser. Then 1.00 g of sorbent was applied to the OP spot. After 30 min, the sorbent with oil sludge was removed and the water was analyzed for OP content using the infrared spectrometry.

The sea water sample was transferred to a separating funnel with a capacity of 2 L. 20 mL of a 1:9 sulfuric acid solution was added to the separating funnel with the water sample under study and mixed. Next, 20 mL of carbon tetrachloride was added to the funnel and the OPs were extracted with carbon tetrachloride by intensively mixing the contents of the funnel using a rotary extraction unit for 5 min. After extraction, the funnel with the sample was left alone for 10 min for phase separation. After phase separation, the lower organic phase was poured into a glass with a capacity of 50 mL. 10 mL of carbon tetrachloride was again added to the separating funnel with the sample and the OPs were re-extracted in the manner described above, and the lower organic layer was poured into the same beaker with a capacity of 50 mL that contained the first portion of the extract, thus combining the resulting extracts. Next, 5 g of sodium sulfate, previously dried in an oven at 110°C for 3 h, was added to the glass with the extract, the contents were thoroughly mixed with a glass rod and left for 30 min to completely dry the extract. After drying, the extract was passed through a pre-prepared chromatographic column, as described in the experiment to study the sorption capacity for *n*-hexane of Silor HSL samples.

The resulting eluate with a volume of 30 mL (0.03 L) was thoroughly mixed in a flask by shaking, the eluate was diluted 10 times, the diluted extract was poured into a measuring cuvette, and the OP content was measured using a KN-3 concentrator. The OP content in sea water sample X, mg/L, was calculated using the expression

$$X = \frac{C_m \cdot B \cdot K}{V} \quad (2)$$

where C_m is the measured quantity of OP in the extract, mg/L; B is the eluate volume, L (equal to 0.03 L); K is the eluate dilution factor; V is the volume of sample taken for analysis, L (equal to 1 L).

Table 6 shows the measured OP contents in extracts recalculated to the OP content in sea water contaminated with oil sludge after interaction with the sorbent, as well as the data necessary to establish the efficiency of sorption of surface OPs.

Thus, the content of residual OPs was 12.0 mg/L, which corresponds to a sorption efficiency of surface OPs of more than 95%. During the experiment, it was found that the sorption process does not depend on the matrix (salinity) of water.

At the final stage, a comparative experiment was carried out on oil spill response using quartz sand, calcined and modified sorbents (Fig. 5).

A thin film of 1.00 g of oil sludge was applied to the surface of the watch glass. Next, 1.00 g of calcined sorbent, modified sorbent, and quartz sand were applied. After 30 min, the mixture was collected with a spatula. When visually assessing the color intensity of the residual oil sludge stain, it was concluded that there is a significant content of OPs in the case of sorption of oil sludge by quartz sand; a residual yellow layer of oil sludge is visible. In the case of sorption of oil sludge by calcined and modified sorbents, residual oil residues are insignificant. Instrumental analysis of samples of spent modified and calcined sorbents showed the presence of OPs in 1.00 g of sorbent, equal to 0.97 g and 0.95 g, respectively. Thus, the efficiency of cleaning solid surfaces from oil sludge with a calcined sorbent was 97%, and with a modified sorbent—95%.

A comparative analysis of data on the effectiveness of the developed sorbent and currently available analogues based on sludge and slag is given in Table 7. Analysis of the sorption capacity for AI-92 gasoline shows that modifying sludge and slag with various HSLs can increase their sorption properties. The sorption capacity of such sorbents fluctuates at the level of 1 g/g.

The methods presented in [20], [21], [22], and [23] for studying the sorption capacity of sorbents are based on measuring the mass of OPs adsorbed by the sorbent provided they are kept in the thickness of the OPs under complete immersion, which shows the value of the total possible sorption capacity. This article experimentally studied the efficiency of sorption of the working volume of the sorbent during elimination of oil spills of various petroleum products on water and solid surfaces. The methodology for studying sorption capacity contains a stage of drying a sorbent sample with adsorbed OPs in the open air for about a day, in order to remove water and OPs not adsorbed by the sorbent. This demonstrates the ability of the sorbent to reta in adsorbed OPs for a long time.

Based on the research results, sorbent modified with Tiprom K HSL based on the ASWs of the *Novocherkasskaya GRES* power station is recommended for use in eliminating oil spills of various petroleum products on the surfaces of any type of water, including sea water.

Table 6. Efficiency of sorption of surface OPs in a sea water sample based on measured and calculated residual oil product contents

Mass of OPs added to the 1 L water, mg	Measured content of OPs in the extract, mg/L	Eluate dilution factor	Concentration of OPs after sorption, mg/L	Sorption efficiency, %
1000	40.0	10	12.0	98.8

Fig. 5. Oil sludge sorption on a hard surface: from left to right: oil product sample, quartz sand, calcined sorbent, and modified sorbent.

Table 7. Characteristics of sorbents based on sludge and slag (production waste)

Sorbent	Sorption capacity for AI-92 gasoline, g/g	Sorption capacity research method	Source
Activated carbon AG-3	0.48	–	[20]
Granular sorbent based on chemical water treatment sludge at *Kazanskaya TETS-1*:		Gravity method by immersing a sorbent sample in a sample of pure OPs	
impregnated with a 3% aqueous solution of HSL-11N	0.62		[20]
impregnated with a 5% aqueous solution of HSL-94N	0.68		
impregnated with a 5% aqueous solution of HSL-94N + Silor	0.648		[21]
Sorbent based on soda production sludge of *Bereznikovsky Sodovy Zavod* (formed at the boundary of the water surface, finely dispersed, pasty, white):		Ratio of the absorbed OP mass to the known mass of dry sorbent	
original	0.95		[22]
processed with HSL-11P	1.13		
treated with *Akvasila* solution	1.2		[23]
Sorbent based on ash and slag from *Novocherkasskaya GRES* power station (modified HSL brand Tiprom K)	0.89	Measurement of the mass content of OPs in the sorbent using infrared spectrometric methods	Current article

CONCLUSIONS

An environmentally friendly modified sorbent was developed based on thermal power ASWs accumulated in ash dumps. This has high buoyancy when saturated with OPs and the ability to retain them for a long time.

The physicochemical properties of sorbent modified with Tiprom K HSL were determined: bulk density was 0.621 g/mL; ash content was 97.1%; total pore volume in water was less than 0.05 mL/g, abrasion was 8.8%, humidity was less than 0.5%, sorption capacity, in g/g: for *n*-hexane, 0.86; for AI-92 gasoline, 0.89; for nefras, 0.93; for kerosene, 0.99; for oil sludge, 1.18; for fuel oil, 1.46.

A study of oil sludge sorption on a water surface showed an efficiency of more than 95%. The efficiency of cleaning solid surfaces from oil sludge with the calcined sorbent was 97%, and with the modified sorbent—95%.

The resulting modified sorbent is recommended for eliminating spills of OPs and oil-containing waste at production sites and soils. The use of a modified sorbent will make it possible to effectively purify wastewater before discharging it into a reservoir to acceptable quality standards with minimal economic costs.

Acknowledgments

The research is carried out with the financial support of the Kuban Science Foundation in the framework of the scientific project MFI-20.1/57.

Authors' contribution

All authors equally contributed to the research work.

The authors declare no conflicts of interest.

REFERENCES

1. Fedorova N.V., Shaforost D.A., Krivobok E.A. The possibility of using of the ash and slag waste coal-fired power plants in the Rostov region as acarbonaceous sorbents. *Ekologiya promyshlennogo proizvodstva = Industrial Ecology.* 2016;1(93):20–24 (in Russ.).

2. Cherentsova A.A., Olesik S.M. Evaluation of ash waste as a source of pollution and as a source of secondary raw materials. *Gornyi informatsionno-analiticheskii byulleten' = Mining Informational and Analytical Bulletin*. 2013;(S3):230–243 (in Russ.).

3. Afanaseva O.V., Mingaleeva G.R., Dobronravov A.D., Shamsutdinov E.V. Integrated use of ash and slag waste. *Izvestiya vysshikh uchebnykh zavedenii. Problemy energetiki = Power Engineering: Research, Equipment, Technology*. 2015;(7–8):26–36 (in Russ.). https://doi.org/10.30724/1998-9903-2015-0-7-8-26-36

4. Podgoretskii G.S., Gorbunov V.G., Agapov E.A., Erokhov T.V., Kozlova O.N. Processing ash and slag wastes from thermal power stations. Part 1. *Steel in Transl*. 2018;48(6):339–345. http://doi.org/10.3103/S0967091218060074

[Original Russian Text: Podgoretskii G.S., Gorbunov V.G., Agapov E.A., Erokhov T.V., Kozlova O.N. Processing ash and slag wastes from thermal power stations. Part 1. *Izvestiya vysshikh uchebnykh zavedenii. Chernaya metallurgiya.* 2018;61(1):439–446 (in Russ.). https://doi.org/10.17073/0368-0797-2018-6-439-446]

5. Khudyakova L.I., Zalutskii A.V., Paleev P.L. Use of ash and slag waste from thermal power plants. *XXI vek. Tekhnosfernaya bezopasnost' = Technosphere Safety. The 21st Century*. 2019;4(3):375–391 (in Russ.). https://doi.org/10.21285/2500-1582-2019-3-375-391

6. Pichugin E.A. Analytical review of the experience of involving ash slag waste of thermal power plants in economic circulation in the Russian Federation. *Problemy regional'noi ekologii = Problems of Regional Ecology*. 2019;(4):77–87. https://doi.org/10.24411/1728-323X-2019-14077

7. Cherentsova A.A. Ecological and technological evaluation of composition and properties of ash waste (Case study of Khabarovskaya TETS-3). *Vestnik Tambovskogo universiteta. Seriya: Estestvennye i tekhnicheskie nauki = Tambov University Reviews. Series: Natural and Technical Sciences.* 2014;19(5):1733–1736 (in Russ.).

8. Korotkova T.G., Ksandopulo S.Ju., Bushumov S.A., Burlaka S.D., Say Yu.V. Quantitative Chemical Analysis of Slag Ash of Novocherkassk State District Power Plant. *Oriental J. Chem*. 2017;33(1):186–198. http://doi.org/10.13005/ojc/330121

9. Bushumov S.A., Korotkova T.G., Ksandopulo S.Ju., Solonnikova N.V., Demin V.I. Determination of the Hazard Class of Ash After Coal Combustion by the Method of Biotesting. *Oriental J. Chem*. 2018;34(1):276–285. http://doi.org/10.13005/ojc/340130

10. Korotkova T.G., Bushumov S.A., Ksandopulo S.Yu., Istoshina N.Yu. Determination of the Hazard Class of Ash-And-Slag from a Thermal Power Plant Accumulated on Ash Dumps Under the Scheme Hydraulic Ash Removal. *Int. J. Mech. Eng. Technol*. (*IJMET*). 2018;9(10):715–723. URL: https://iaeme.com/MasterAdmin/Journal_uploads/IJMET/VOLUME_9_ISSUE_10/IJMET_09_10_074.pdf. Accessed October 12, 2023.

11. Vasiliev A.M. Use of the waste of slag in devices of cleaning of the drains. *Izvestiya vysshikh uchebnykh zavedenii. Severo-Kavkazskii region. Tekhnicheskie nauki = Bulletin of Higher Educational Institutions. North Caucasus region. Technical Sciences*. 2012;(6):120–122 (in Russ.).

СПИСОК ЛИТЕРАТУРЫ

1. Федорова Н.В., Шафорост Д.А., Кривобок Е.А. О возможности использования золошлаковых отходов угольных электростанций Ростовской области в качестве углеродсодержащих сорбентов. *Экология промышленного производства*. 2016;1(93):20–24.

2. Черенцова А.А., Олесик С.М. Оценка золошлаковых отходов как источник загрязнения окружающей среды и как источник вторичного сырья. *Горный информационно-аналитический бюллетень*. 2013;(S3):230–243.

3. Афанасьева О.В., Мингалеева Г.Р., Добронравов А.Д., Шамсутдинов Э.В. Комплексное использование золошлаковых отходов. *Известия высших учебных заведений. Проблемы энергетики.* 2015;(7–8):26–36. https://doi.org/10.30724/1998-9903-2015-0-7-8-26-36

4. Подгорецкий Г.С., Горбунов В.Г., Агапов Е.А., Ерохов Т.В., Козлова О.Н. Проблемы и перспективы утилизации золошлаковых отходов ТЭЦ. Часть 1. *Известия высших учебных заведений. Черная металлургия.* 2018;61(1):439–446. https://doi.org/10.17073/0368-0797-2018-6-439-446

5. Худякова Л.И., Залуцкий А.В., Палеев П.Л. Использование золошлаковых отходов тепловых электростанций. *XXI век. Техносферная безопасность*. 2019;4(3):375–391. https://doi.org/10.21285/2500-1582-2019-3-375-391

6. Пичугин Е.А. Аналитический обзор накопленного в российской федерации опыта вовлечения в хозяйственный оборот золошлаковых отходов теплоэлектростанций. *Проблемы региональной экологии*. 2019;(4):77–87. https://doi.org/10.24411/1728-323X-2019-14077

7. Черенцова А.А. Эколого-технологическая оценка состава и свойств золошлаковых отходов (на примере Хабаровской ТЭЦ-3). *Вестник Тамбовского университета. Серия: Естественные и технические науки.* 2014;19(5):1733–1736.

8. Korotkova T.G., Ksandopulo S.Ju., Bushumov S.A., Burlaka S.D., Say Yu.V. Quantitative Chemical Analysis of Slag Ash of Novocherkassk State District Power Plant. *Oriental J. Chem*. 2017;33(1):186–198. http://doi.org/10.13005/ojc/330121

9. Bushumov S.A., Korotkova T.G., Ksandopulo S.Ju., Solonnikova N.V., Demin V.I. Determination of the Hazard Class of Ash After Coal Combustion by the Method of Biotesting (Определение класса опасности золы от сжигания углей методом биотестирования). *Oriental J. Chem.* 2018;34(1):276–285. http://doi.org/10.13005/ojc/340130

10. Korotkova T.G., Bushumov S.A., Ksandopulo S.Yu., Istoshina N.Yu. Determination of the Hazard Class of Ash-And-Slag from a Thermal Power Plant Accumulated on Ash Dumps Under the Scheme Hydraulic Ash Removal. *Int. J. Mech. Eng. Technol*. (*IJMET*). 2018;9(10):715–723. URL: https://iaeme.com/MasterAdmin/Journal_uploads/IJMET/VOLUME_9_ISSUE_10/IJMET_09_10_074.pdf. Дата обращения 12.10.2023.

11. Васильев А.М. Обоснование возможности использования золошлаковых отходов в сооружениях очистки поверхностного стока. *Известия вузов. Северо-Кавказский регион. Технические науки*. 2012;(6):120–122.

12. Singh P., Tripathi P., Chauhan S., Mishra A. Domestic Waste Water Treatment Using Fly Ash Alone or in Combined Form. *IOSR J. Electric. Electron. Eng.* (*IOSR-JEEE*). 2016;11(3):34–39. https://www.semanticscholar.org/paper/Domestic-Waste-Water-Treatment-Using-Fly-Ash-Alone-Singh-Tripathi/a78118b380742750b59e8822570e9c2298dbadcf. Дата обращения 12.10.2023.

12. Singh P., Tripathi P., Chauhan S., Mishra A. Domestic Waste Water Treatment Using Fly Ash Alone or in Combined Form. *IOSR J. Electric. Electron. Eng*. (*IOSR-JEEE*). 2016;11(3):34–39. https://www.semanticscholar.org/paper/Domestic-Waste-Water-Treatment-Using-Fly-Ash-Alone-Singh-Tripathi/a78118b380742750b59e8822570e9c2298dbadcf. Accessed October 12, 2023.

13. Lin C.-Y., Yang D.-H. Removal of pollutants from wastewater by coal bottom ash. *J. Environ. Sci. Health. A: Tox. Hazard. Subst. Environ. Eng*. 2002;(6):1509–1522. https://doi.org/10.1081/ese-120013273

14. Dabi N., Patwa N. Flyash: an Effective Method for Treatment of Wastewater. *Int. J. Eng. Res. Technol*. (*IJERT*). 2015;3(23. Special Issue – 2015. NCETRASECT-2015 Conference Proceedings). URL: https://www.ijert.org/research/flyash-an-effective-method-for-treatment-of-wastewater-IJERTCONV3IS23014.pdf. Accessed October 12, 2023.

15. Sanas M.M.V., Gawande S.M. Fly Ash using in Waste Water Tratment. *Int. J. Emerging Eng. Res. Technol.* 2016;4(6):11–14. http://www.ijeert.org/pdf/v4-i6/2.pdf. Accessed October 12, 2023.

16. Singh N.B., Agarwal A., De A., Singh P. Coal fly ash: an emerging material for water remediation. Review. *Int. J. Coal Sci. Technol*. 2022;9:Article number: 44. https://doi.org/10.1007/s40789-022-00512-1

17. Batabyal D., Sahu A., Chaudhuri S.K. Kinetics and mechanism of removal of 2, 4-dimethyl phenol from aqueous solutions with coal fly ash. *Sep. Technol*. 1995;5(4):179–186. https://doi.org/10.1016/0956-9618(95)00124-7

18. Kao P.C., Tzeng J.H., Huang T.L. Removal of chlorophenols from aqueous solution by fly ash. *J. Hazard. Mater*. 2000;76(2–3):237–249. https://doi.org/10.1016/S0304-3894(00)00201-6

19. Bushumov S.A., Korotkova T.G. Determination of physical and chemical properties of the modified sorbent from ash-and-slag waste accumulated on ash dumps by hydraulic ash removal. *RASÃYAN J. Chem*. 2020;13(3):1619–1626. http://doi.org/10.31788/RJC.2020.1335454

20. Nikolayeva L.A., Vdovin E.A., Golubchikov M.A., Mavliyev L.F. Methods of Recovery of Used Sorbents from Petroleum Products on the Basis of Chemical Treatment of Water's Sludge from Kazan CHP-1. *Ekologiya i promyshlennost' Rossii = Ecology and Industry of Russia*. 2014;(7):18–20 (in Russ.). https://www.ecology-kalvis.ru/jour/article/view/452. Accessed October 12, 2023.

21. Nikolaeva L.A., Golubchikov M.A., Zakharova S.V. Granulated hydrophobic adsorbents based on carbonate slag of HVO clarifiers KTETS-1 for post-treatment of sewage from oil products. *Energosberezhenie i vodopodgotovka= Energy Saving and Water Treatment*. 2012;4(78):24–29 (in Russ.). URL: https://www.elibrary.ru/item.asp?id=17959087. Accessed October 12, 2023.

22. Karmanova E.N., Kalinina E.V. Clean-up of emergency spills of oil and oil products from solid surfaces by modified waste of soda production. *Transport. Transportnye sooruzheniya. Ekologiya = Transport. Transport Facilities. Ecology*. 2018;(4):53–60 (in Russ.). URL: https://www.elibrary.ru/item.asp?id=36746277. Accessed October 12, 2023.

23. Kalinina E.V., Glushankova I.S., Rudakova L.V. Modification of the sludge from soda production for producing oil sorbents. *Teoreticheskaya i prikladnaya ekologiya = Theoretical and Applied Ecology*. 2018;(2):79–86. https://doi.org/10.25750/1995-4301-2018-2-079-086

13. Lin C.-Y., Yang D.-H. Removal of pollutants from wastewater by coal bottom ash. *J. Environ. Sci. Health. A: Tox. Hazard. Subst. Environ. Eng*. 2002;(6):1509–1522. https://doi.org/10.1081/ese-120013273

14. Dabi N., Patwa N. Flyash: an Effective Method for Treatment of Wastewater. *Int. J. Eng. Res. Technol*. (*IJERT*). 2015;3(23. Special Issue – 2015. NCETRASECT-2015 Conference Proceedings). URL: https://www.ijert.org/research/flyash-an-effective-method-for-treatment-of-wastewater-IJERTCONV3IS23014.pdf. Дата обращения 12.10.2023.

15. Sanas M.M.V., Gawande S.M. Fly Ash using in Waste Water Tratment. *Int. J. Emerging Eng. Res. Technol.* 2016;4(6):11–14. URL: http://www.ijeert.org/pdf/v4-i6/2.pdf. Дата обращения 12.10.2023.

16. Singh N.B., Agarwal A., De A., Singh P. Coal fly ash: an emerging material for water remediation. Review. *Int. J. Coal Sci. Technol*. 2022;9:Article number: 44. https://doi.org/10.1007/s40789-022-00512-1

17. Batabyal D., Sahu A., Chaudhuri S.K. Kinetics and mechanism of removal of 2, 4-dimethyl phenol from aqueous solutions with coal fly ash. *Sep. Technol*. 1995;5(4):179–186. https://doi.org/10.1016/0956-9618(95)00124-7

18. Kao P.C., Tzeng J.H., Huang T.L. Removal of chlorophenols from aqueous solution by fly ash. *J. Hazard. Mater*. 2000;76(2–3):237–249. https://doi.org/10.1016/S0304-3894(00)00201-6

19. Bushumov S.A., Korotkova T.G. Determination of physical and chemical properties of the modified sorbent from ash-and-slag waste accumulated on ash dumps by hydraulic ash removal. *RASÃYAN J. Chem*. 2020;13(3):1619–1626. http://doi.org/10.31788/RJC.2020.1335454

20. Николаева Л.А., Вдовин Е.А., Голубчиков М.А., Мавлиев Л.Ф. Способы утилизации отработанного сорбента нефтепродуктов на основе шлама химводоочистки Казанской ТЭЦ-1. *Экология и промышленность России*. 2014;(7):18–20. URL: https://www.ecology-kalvis.ru/jour/article/view/452. Дата обращения 12.10.2023.

21. Николаева Л.А., Голубчиков М.А., Захарова С.В. Гранулированные гидрофобные адсорбенты на основе карбонатного шлама осветлителей ХВО КТЭЦ-1 для доочистки сточных вод от нефтепродуктов. *Энергосбережение и водоподготовка*. 2012;4(78):24–29. URL: https://www.elibrary.ru/item.asp?id=17959087. Дата обращения 12.10.2023.

22. Карманова Е.Н., Калинина Е.В. Ликвидация аварийных разливов нефти и нефтепродуктов с твердых поверхностей модифицированными отходами содового производства. *Транспорт. Транспортные сооружения. Экология*. 2018;(4):53–60. URL: https://www.elibrary.ru/item.asp?id=36746277. Дата обращения 12.10.2023.

23. Калинина Е.В., Глушанкова И.С., Рудакова Л.В. Модификация шламов содового производства для получения нефтяных сорбентов. *Теоретическая и прикладная экология*. 2018;(2):79–86. https://doi.org/10.25750/1995-4301-2018-2-079-086

About the authors:

Svyatoslav A. Bushumov, Junior Researcher, Department of Life Safety, Kuban State Technological University (2, Moskovskaya ul., Krasnodar, 350072, Russia). E-mail: bushumov@list.ru. Scopus Author ID 57192814144, RSCI SPIN-code 9871-2551, https://orcid.org/0000-0001-7227-0614

Tatyana G. Korotkova, Dr. Sci. (Eng.), Professor, Department of Life Safety, Kuban State Technological University (2, Moskovskaya ul., Krasnodar, 350072, Russia). E-mail: korotkova1964@mail.ru. Scopus Author ID 56195415000, ResearcherID AAQ-3126-2021, RSCI SPIN-code 3212-7120, https://orcid.org/0000-0001-9278-871X

Об авторах:

Бушумов Святослав Андреевич, младший научный сотрудник, кафедра безопасности жизнедеятельности, ФГБОУ ВО «Кубанский государственный технологический университет (350072, Россия, г. Краснодар, ул. Московская, д. 2). E-mail: bushumov@list.ru. Scopus Author ID 57192814144, SPIN-код РИНЦ 9871-2551, https://orcid.org/0000-0001-7227-0614

Короткова Татьяна Германовна, д.т.н. доцент, профессор кафедры безопасности жизнедеятельности ФГБОУ ВО «Кубанский государственный технологический университет (350072, Россия, г. Краснодар, ул. Московская, д. 2). E-mail: korotkova1964@mail.ru. Scopus Author ID 56195415000, ResearcherID AAQ-3126-2021, SPIN-код РИНЦ 3212-7120, https://orcid.org/0000-0001-9278-871X

The article was submitted: November 16, 2022; approved after reviewing: February 17, 2023; accepted for publication: October 12, 2023.

Translated from Russian into English by H. Moshkov
Edited for English language and spelling by Dr. David Mossop

CHEMISTRY AND TECHNOLOGY OF INORGANIC MATERIALS

ХИМИЯ И ТЕХНОЛОГИЯ НЕОРГАНИЧЕСКИХ МАТЕРИАЛОВ

ISSN 2686-7575 (Online)

https://doi.org/10.32362/2410-6593-2023-18-5-461-470

UDC 661.931; 620.92

RESEARCH ARTICLE

Reduction of hydrogen absorption into materials of membrane electrode assemblies in hydrogen generators

Marina V. Lebedeva, Alexander V. Ragutkin, Ivan M. Sidorov, Nikolay A. Yashtulov✉

MIREA – Russian Technological University (M.V. Lomonosov Institute of Fine Chemical Technologies), Moscow, 119454 Russia

✉*Corresponding author, e-mail: yashtulovna@mail.ru*

Abstract

Objectives. *To investigate the possibility of preventing hydrogen absorption into the functional structural materials of hydrogen-generating membrane electrode assemblies based on porous nickel, carbon black, and reduced graphene oxide with platinum–nickel and palladium–nickel nanoparticles.*

Methods. *The hydrogen absorption into materials of membrane electrode assemblies of alkaline electrolyzers was evaluated using an electrolyzer with variable temperature, reagent feed rate, and gas content.*

Results. *The study established the need to use reduced graphene oxide, in order to reduce hydrogen absorption and degradation of hydrogen-generating membrane electrode assemblies.*

Conclusions. *The service life test results and performance of the designed variants of prototypes of membrane electrode assemblies with nanostructured electrodes based on reduced graphene oxide, preventing hydrogen absorption into functional materials and their degradation, demonstrated the creation of hydrogen generators with high energy efficiency shows potential.*

Keywords: *hydrogen generation, hydrogen absorption into metals, membrane electrode assemblies, nanocomposite electrodes, reduced graphene oxide, energy efficiency*

For citation: Lebedeva M.V., Ragutkin A.V., Sidorov I.M., Yashtulov N.A. Reduction of hydrogen absorption into materials of membrane electrode assemblies in hydrogen generators. *Tonk. Khim. Tekhnol. = Fine Chem. Technol.* 2023;18(5):461–470. https://doi.org/10.32362/2410-6593-2023-18-5-461-470

НАУЧНАЯ СТАТЬЯ

Снижение наводораживания материалов мембранно-электродных блоков генераторов водорода

М.В. Лебедева, А.В. Рагуткин, И.М. Сидоров, Н.А. Яштулов✉

МИРЭА – Российский технологический университет (Институт тонких химических технологий им. М.В. Ломоносова), Москва, 119454 Россия
✉*Автор для переписки, e-mail: yashtulovna@mail.ru*

Аннотация

Цели. *Исследование возможности предотвращения наводораживания функциональных конструкционных материалов мембранно-электродных блоков генерации водорода на основе пористого никеля, сажи и восстановленного оксида графена, модифицированных наночастицами платина-никель и палладий-никель.*
Методы. *Для оценки степени наводораживания материалов мембранно-электродных блоков щелочных электролизеров была использована установка электролизера с возможностью контроля температуры, скорости подачи реагентов и содержания газов.*
Результаты. *Обоснована необходимость применения восстановленного оксида графена с целью снижения наводораживания и деградации мембранно-электродных блоков генерации водорода.*
Выводы. *Результаты ресурсных испытаний и рабочие характеристики сконструированных вариантов макетов мембранно-электродных блоков с наноструктурированными электродами на основе восстановленного оксида графена, нивелирующие наводораживание и деградацию функциональных материалов, демонстрируют перспективность конструирования генераторов водорода с высокой энергоэффективностью.*
Ключевые слова: *генерация водорода, наводораживание металлов, мембранно-электродные блоки, нанокомпозитные электроды, восстановленный оксид графена, энергоэффективность*

Для цитирования: Лебедева М.В., Рагуткин А.В., Сидоров И.М., Яштулов Н.А. Снижение наводораживания материалов мембранно-электродных блоков генераторов водорода. *Тонкие химические технологии*. 2023;18(5):461–470. https://doi.org/10.32362/2410-6593-2023-18-5-461-470

INTRODUCTION

The development of new efficient energy systems using the latest achievements of nano- and chemical technologies, as well as hydrogen energy, is an important objective for energy saving [1–5]. The most promising trend in the design of autonomous energy sources is the creation of integrated energy systems of electrolysis cells with chemical energy converters [3–6]. During the operation of the electrolysis cell, hydrogen and oxygen are formed at the cathode and anode, respectively:

Cathodic reaction: $2H_2O + 2\bar{e} \rightarrow H_2 + 2OH^-$ (1)

Anodic reaction: $2OH^- - 2\bar{e} \rightarrow 1/2O_2 + H_2O$ (2)

Overall reaction: $H_2O \rightarrow H_2 + 1/2O_2$ (3)

In order to convert the chemical energy of fuel into electricity in autonomous power sources, high-purity (more than 99.95%) hydrogen obtained in alkaline water electrolyzers (AWEs) [2, 7–11] must be used. To improve the energy performance of membrane electrode assemblies (MEAs), as a key component of AWEs, nanostructured functional materials are used [4–6, 12–17]. The MEA design is based on metal gas diffusion electrodes, anode and cathode catalytic layers separated by a polymer membrane (diaphragm). Industrial electrolysis plants have a high level of energy consumption, due to high overvoltages of the hydrogen evolution reaction. This factor contributes to the intense degradation of metal electrodes and electrocatalysts [1–3]. In order to ensure an increased service life of electrolyzers, methods need to be developed to stabilize the functional structural metals for MEAs [4, 18–22].

One of the main causes of the degradation of structural metals in contact with hydrogen in industrial plants can be found in the complex multistep processes of hydrogen dissolution in metals. Hydrogen absorption into metals can cause such phenomena as hydrogen embrittlement of steels, hydrogen hardening, and hydrogen damage during friction [2, 3, 8, 23].

Hydrogen absorption into metals is an integral result of the action of many factors. Its mechanism is mainly determined by the following: the rate of diffusion and transfer of hydrogen in the metal; the localization and concentration of hydrogen in certain regions; the ability of the metal to interact with hydrogen in places of its localization; and the behavior of the quality parameters of the bulk of the metal (and to a greater extent, the surface layer) which control the ability of materials to adapt to further impacts [23].

Experimental studies into the processes of diffusion, permeability, and solubility of hydrogen in metals confirmed the possibility of penetration and diffusion of hydrogen deep into the material through the crystal lattice. Possessing a high level of energy, hydrogen atoms can be adsorbed on the interface, nonmetallic inclusions, microvoids, and other collectors. In this case, the rate of diffusion is comparable to the rate of crack development.

The mechanisms of hydrogen absorption, as well as the effect of hydrogen embrittlement and hydrogen transfer on the destruction of the crystal lattice of materials and on the changes in physicochemical properties, are studied using various diffusion models. In this case, the contact surface of the materials can be considered, on the one hand, as the surface of a metal catalyst capable of forming hydrides and, on the other hand, of a catalyst which causes the destruction of substances. Analysis of data on these processes is especially necessary when constructing models of degradation of MEAs of hydrogen generators and searching for efficient methods to increase their service life.

In this work, the support in MEAs was porous nickel (PN) formed by the nanotemplate method on an aluminum matrix, and the electrocatalysts were platinum–nickel and palladium–nickel bimetallic nanoparticles (anode and cathode, respectively). The control of flows of gases (hydrogen and oxygen) is one of the most important technological stages of MEA operation. In industrial electrolyzers at high current densities, it is the use of PN with a large active surface area that ensures the efficient removal of gas bubbles to prevent hydrogen absorption into metals for the efficient operation of catalysts [13, 18–22, 24–26].

Various techniques are used [23–29] to increase the degradation resistance of metal electrodes when exposed to hydrogen. The modification of metals with trace amounts of platinum metals, in particular, as well as alloying of metals with copper, aluminum, and calcium, can enhance the resistance of metals to hydrogen absorption. This can also prevent the formation of reactive hydrogen species on the surface of metals, and inhibit corrosion processes by the formation of oxide–hydroxide films. One promising trend to prevent intense hydrogen absorption into metal structures is the possibility of using graphene, which has a high volumetric density of hydrogen storage [28, 29].

This study aimed at assessing the possibility of preventing hydrogen absorption into functional structural metals of nanostructured hydrogen-generating MEAs by using electrocatalytic matrices based on reduced graphene oxide (rGO). The basic criteria for hydrogen absorption into metals were energy efficiency and stability of the hydrogen generation process.

EXPERIMENTAL

The MEA electrodes were produced of platinum–nickel (Pt–Ni) and palladium–nickel (Pd–Ni) bimetallic particles. The precursors for the synthesis of nanoparticles were aqueous solutions of K_2PtCl_4, $PdCl_2$, and $NiCl_2$ (*Sigma-Aldrich*, USA). PN with a thickness of 2 mm and an average pore diameter of less than 50 μm was used as the main support [22]. The molar ratio of bimetallic particles was 1 : 1 at a mass loading of palladium at the cathode of m_s = 0.5 mg/cm^2 and a mass loading of platinum at the anode of 0.8 mg/cm^2. The sizes of palladium–nickel and platinum–nickel bimetallic nanoparticles ranged from 4 to 9 nm.

In order to estimate the degree of degradation of the electrodes, XC-72 carbon black (*Cabot*, USA) and rGO, obtained according a published procedure [6], were studied as supports.

The energy efficiency and stability of hydrogen generation were assessed using a 600 ETS Electrolyzer Test System (*Scribner Associates Inc*., USA), consisting of a controller with a potentiostat, a power supply, gas reagent supply systems, and sensors of temperatures, flows, and contents of hydrogen and oxygen. The controller was connected to the electrolyzer by cables for electropositive and electronegative currents (I+, I–), voltage power cables (V+, V–), and auxiliary wires (A+, A–) (Fig. 1). Voltammograms were recorded and the stability of the MEA operation was tested using a two-electrode circuit (Fig. 1).

The MEA was a key part of the electrolysis cell. The MEA consisted of 7 × 7 cm PN-based gas diffusion bimetallic electrodes with the ability to control the process temperature from 25 to 80°C, as well as a commercial Sustainion® X37-50 anion exchange membrane (*Fuel Cell Store*, USA) placed between the anode and cathode materials [14]. The stability of the MEA during the electrolysis of water was tested at current densities from 0.05 to 0.6 A/cm^2 for 180 h. The operating voltage was varied in the range from 1.3 to 3 V.

Electrolyzers can use MEAs of two types: standard and zero-gap [19, 21]. The disadvantages of the second type of MEA include the need

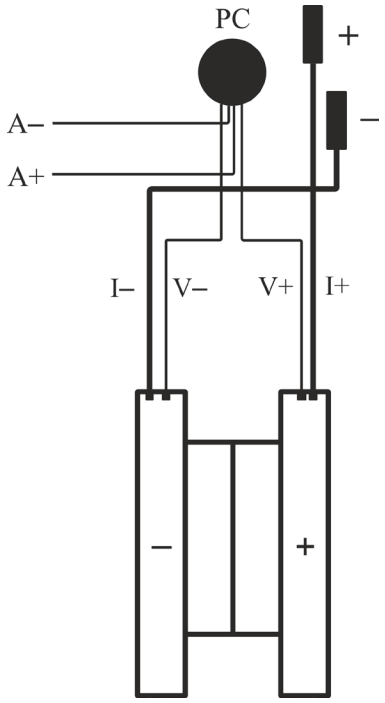

Fig. 1. Two-electrode cell connection diagram: (+), positive electrode (anode); (−), negative electrode (cathode); A, auxiliary electrode; and PC, power cable.

to remove hydrogen and oxygen from the electrodes. In this work, the standard variant (Fig. 2) of the design was chosen due to its ease of assembly and low degradation of the electrolyte. The removal of gaseous reaction products was facilitated by using electrode matrices based on PN with a developed pore system and carbon materials in the gas diffusion layer.

RESULTS AND DISCUSSION

This work studied the effect of the localization of electrocatalysts on the process of hydrogen absorption into structural functional materials of MEAs during hydrogen generation. Three variants of localization of bimetallic nanocatalysts in the MEA during cathodic hydrogen evolution were considered. The three variants differ in the type of support matrix, on which the electrocatalysts are located, i.e., in the localization of hydrogen release and the place of contact with the structural material. The following support matrices were used: PN, an electrode material; carbon black, a standard component of the gas diffusion layer; and rGO, the first proposed component of the gas diffusion layer for studying the hydrogen absorption process.

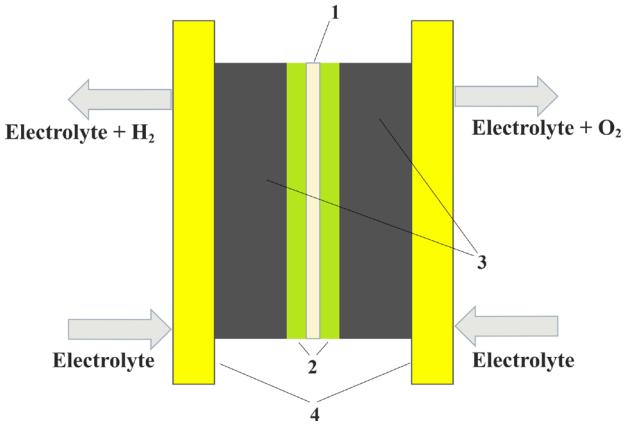

Fig. 2. Scheme of membrane electrode assembly (MEA): (1) anion exchange membrane, (2) gas diffusion layers, (3) electrodes based on porous nickel (PN), and (4) bipolar plates.

Variant 1: the support matrix is PN; Pd–Ni bimetallic nanocatalyst with a mass loading of metals of m_s = 0.5 mg/cm^2.

Variant 2: the support matrix is XC-72 carbon black; Pd–Ni bimetallic nanocatalyst with a mass loading of metals of m_s = 0.5 mg/cm^2.

Variant 3: the support matrix is rGO; Pd–Ni bimetallic nanocatalyst with a mass loading of metals of m_s = 0.5 mg/cm^2.

A characteristic of the efficient operation of the MEA is the specific energy consumption W (kW·h/m^3 H_2) of the AWE process, determined by the ratio of the power P (kW) of the electrolysis process to a unit volume of generated hydrogen:

$$P = I \times U_n. \quad (4)$$

Herein, I is the current in the MEA, A; and U_n is the rated voltage of the electrolysis process, V.

When an electric current passes through the MEA, the energy consumption potential of the electrodes shifts due to additional energy consumption to compensate for the slow transfer of electrical charges and the destruction of structural metals in the process of hydrogen generation. With increasing current density, the voltage increases, and so does the energy consumption for electrolysis. The change in the electrode potential caused by the flow of electric current through the system relative to its value in the absence of current is determined by overvoltage:

$$\eta = U_j - U_0, \quad (5)$$

wherein U_j and U_0 are the voltages in the presence and absence of electric current, respectively. The hydrogen evolution overvoltage η can be calculated by the Tafel equation

$$\eta = b \cdot (\lg j - \lg j_0), \quad (6)$$

wherein j is the operating current density, A/cm^2; j_0 is the exchange current density, A/cm^2; b is the temperature-dependent constant, V.

Figure 3 presents the experimental dependences of the hydrogen overvoltage on the current density for three variants of MEA with different localization of hydrogen evolution using electrodes based on rGO. It also shows comparison with samples based on carbon black and PN at a temperature of t = 80°C in a 7 M KOH electrolyte. The results demonstrating a decrease in the overvoltage of cathodic hydrogen evolution are typically interpreted as an increase in the exchange current density j_0 (see Eq. (6)).

In order to assess the stability of hydrogen generation, the above three variants of MEA were tested for 180 h, temperatures of 60 and 80°C, and current densities up to 600 mA/cm^2. Figure 4 shows the time dependence of the operating voltage in three variants of MEA at a temperature of 80°C and a current density of 600 mA/cm^2.

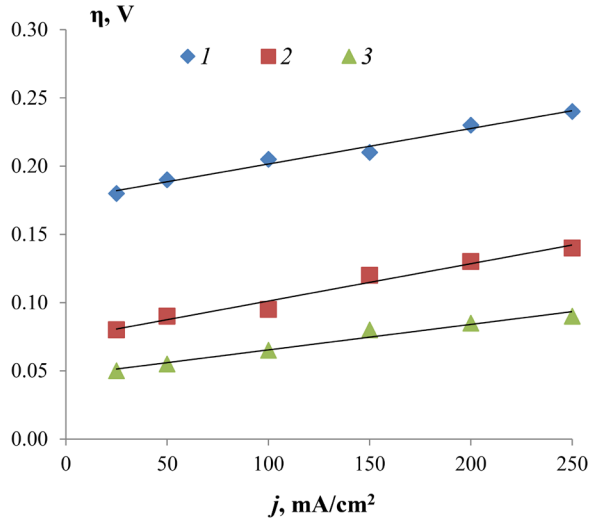

Fig. 3. Polarization curves of cathodic hydrogen evolution for three variants of MEA: (*1*) PN, (*2*) XC-72 carbon black, and (*3*) reduced graphene oxide (rGO).

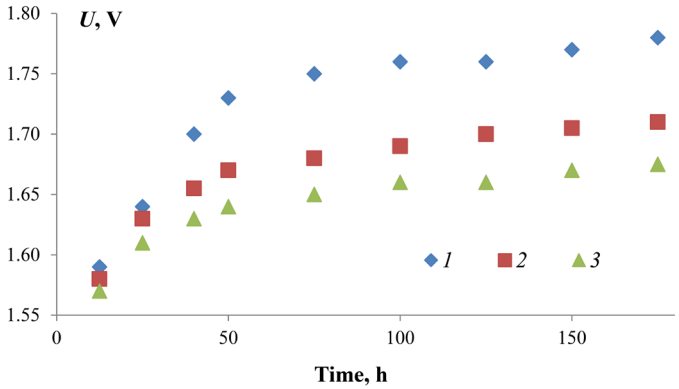

Fig. 4. Dependence of the voltage in three variants of MEA on the operating time of the alkaline water electrolyzer (AWE) at a current density of 600 mA/cm^2 and a temperature of 80°C: (*1*) PN, (*2*) XC-72 carbon black, and (*3*) rGO.

At the first stage of service life tests (up to 15–20 h), the voltages in all MEAs corresponded to the same content of the Pd–Ni electrocatalyst and differed insignificantly. However, at the next stage of hydrogen generation, the voltage in the MEA with the support matrix based on PN (variant *1*) increased significantly in comparison with the carbon variants of support matrices (variants *2* and *3*). At the same time, after 15 h of testing, the minimum voltage was observed for variant *3* of MEA with the rGO-based support matrix. This trend continued throughout the service life tests.

The main disadvantages of industrial hydrogen generators are: firstly, high specific energy consumption (more than 4 kWh for generation of 1 m^3 H_2 with a long service life and elevated temperatures); and secondly, an increased content of platinum metals (more than 1–2 mg/cm^2). Table 1 presents the specific energy consumption in three variants of nanocomposite MEAs for hydrogen generation at current densities of 500 and 600 mA/cm^2 and temperatures of 60 and 80°C.

The table provides specific energy consumption data for three variants of nanocomposite MEAs at current densities of 500 and 600 mA/cm^2, temperatures of 60 and 80°C, and a service life of up to 180 h. These results correspond to the process of generation of high-purity hydrogen with a maximum hydrogen productivity of more than $14 \cdot 10^{-3}$ m^3/h. At a hydrogen generation temperature above 90°C and a current density above 700 mA/cm^2, intense agglomeration of Pt–Ni and Pd–Ni bimetallic nanoparticles was observed in the first 30–40 h of the service life tests. The energy efficiency of hydrogen-generating MEAs obtained with carbon nanocomposite electrodes exceeds the characteristics of commercial hydrogen generation electrolyzers and is on a par with promising modern pilot plants [4, 6, 12, 13].

The rGO-based variant of MEA demonstrated the best results in energy efficiency and stability of hydrogen generation, especially in comparison with the PN-based one. However, the question arises about the causes of this phenomenon and the effect of the structure of the support matrix on increasing the rate of hydrogen formation in the cathodic evolution reaction. This reaction is a complex multistep process and is necessary to resolve problems of energy saving and create anti-corrosion coatings. For most metals, the reaction rate of hydrogen formation is determined by the rate of discharge of hydrogen ions. The removal of adsorbed hydrogen occurs by the Heyrovsky reaction, i.e., the mechanism of electrochemical desorption:

$$H_2O_{ads} + \bar{e} \rightarrow H_{ads} + OH^- \quad (7)$$

Table. Specific energy consumption of electrolysis cells per 1 m^3 of H_2 (pressure 1 bar) at different current densities

t, °C	Specific energy consumption per 1 m^3 of H_2, kWh·m^3 of H_2					
	j = 500 mA/cm^2			*j* = 600 mA/cm^2		
	1	*2*	*3*	*1*	*2*	*3*
80	4.01	4.05	4.10	4.06	4.08	4.13
60	3.98	4.18	4.24	4.14	4.21	4.28

$$H_{ads} + H_2O_{ads} + \bar{e} \rightleftarrows H_2 + OH^- \quad (8)$$

The dependence of the binding energy of adsorbed hydrogen on the metal surface on the overvoltage at the electrode suggests that cathodic hydrogen evolution can also occur through other mechanisms:

$$H_2O_{ads} + \bar{e} \rightleftarrows H_{ads} + OH^- \quad (9)$$

$$2H_{ads} \rightarrow H_2 \quad (10)$$

Thus, the electrochemical desorption reaction can also be the rate-limiting step of the process.

On platinum catalysts at low overpotentials, the rate-limiting step of the process is the recombination of hydrogen atoms [27]. Due to the significant heterogeneity of the electrode surface, the reaction can occur by various mechanisms. This can have a significant impact on the shape of the polarization curves. This confirms the presence of excess surface hydrogen concentration on the polarization side, caused by the rate-limiting step of hydrogen removal and hydrogen penetration through the metal.

When analyzing the causes of the decrease in the energy efficiency and stability of hydrogen generation, the hydrogen saturation of structural materials of MEA needs to be taken into account. The hydrogen saturation of metals occurs by the dissociation on the surface of the support. In similar cases, the saturation of metals is caused by the penetration of hydrogen atoms into them as a result of corrosion reactions, or during cathodic polarization. Metals lose their physicochemical properties, causing degradation of the functional materials of the MEA. Measures are needed to prevent the formation of reactive hydrogen species and ensure the efficient removal of the generated hydrogen from electrocatalysts. In this work, rGO was chosen as the material for preventing these degradation processes. Figure 5 presents the model of the structure of unreduced graphene oxide. Figure 6 shows a micrograph of the rGO support matrix with Pd–Ni nanoparticles.

Hydrogen generation involves the reduction of the initial graphene oxide to rGO, preventing the formation of reactive hydrogen species (atoms, radicals) and hydrogen absorption into the active surface of metals (see Eq. (7)). The efficiency of the removal of the generated hydrogen from electrocatalysts and nickel electrodes is ensured by two factors: the high volumetric density of hydrogen storage in both the layered structure of rGO (Fig. 6); and the porous structure of individual graphene layers. Moreover, the hydrogen production by the alkaline electrolysis of aqueous solutions is carried out at elevated temperatures (60–80°C). This leads to hydrogen desorption by thermal fluctuation vibrations and hydrodynamic deformation of graphene layers [28, 29]. Intensification of the removal of molecular hydrogen from the zone of the electrocatalytic process increases the rate of the rate-limiting stage of recombination of adsorbed hydrogen atoms on platinum group metals (platinum, palladium) [27] and reduces the hydrogen absorption of metallic structural materials of MEA by reactive hydrogen species.

CONCLUSIONS

The research studies the possibility of preventing hydrogen absorption into functional structural materials of nanostructured hydrogen-generating MEAs. The criteria for process of hydrogen absorption of metals were energy efficiency and stability of the hydrogen generation process. For the first time, the results of service life tests using electrocatalytic matrices based on rGO demonstrated the stability and high electrocatalytic activity of functional nanocomposite electrodes at elevated temperatures (up to 80°C) and current densities (more than 600 mA/cm^2). The specific

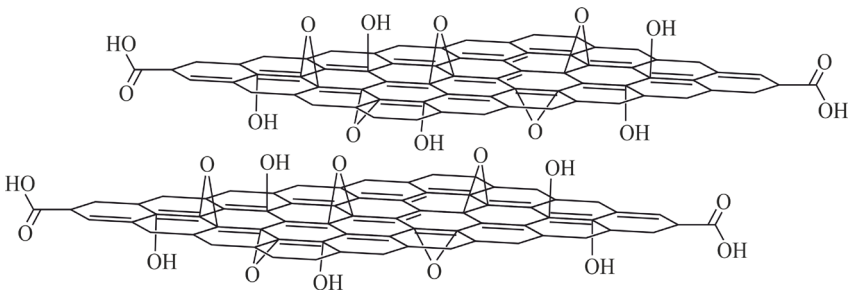

Fig. 5. Model of graphene oxide.

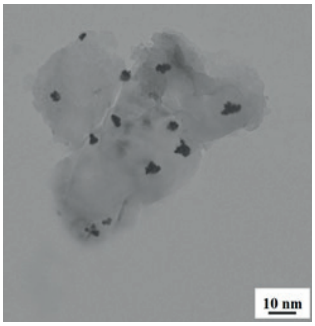

Fig. 6. Micrograph of the rGO support matrix with Pd–Ni nanoparticles.

energy consumption and performance characteristics of the developed prototypes of AWEs with nanocomposite electrodes based on rGO, preventing the hydrogen absorption and degradation of functional materials, indicate that it shows the potential to create hydrogen generators with a high level of energy efficiency.

Acknowledgments

The work was carried out using the equipment of the RTU MIREA Central Research Center. The work was financially supported by the grant of the State Task of the Russian Federation № FSFZ-2023-0003.

Authors' contributions

M.V. Lebedeva – planning and conducting experiments, drawing up methods;

A.V. Ragutkin – formulation of the scientific concept, goals and objectives of the work, processing and interpretation of experimental results;

I.M. Sidorov – analysis of experimental data;

N.A. Yashtulov – writing the manuscript and leading a scientific group.

Financial disclosure

No author has a financial or property interest in any material or method mentioned.

The authors declare no conflicts of interest.

REFERENCES

1. Burton N.A., Padilla R.V., Rose A., Habibullah H. Increasing the efficiency of hydrogen production from solar powered water electrolysis. *Renew. Sust. Energ. Rev*. 2021;135:110255. https://doi.org/10.1016/j.rser.2020.110255

2. Antropov A.P., Ragutkin A.V., Lebedeva M.V., Yashtulov N.A. Nanocomposite micro-power alternative power energy sources for electronic technology. *Therm. Eng*. 2021;68(1):17–24. https://doi.org/10.1134/S0040601521010109

[Original Russian Text: Antropov A.P., Ragutkin A.V., Lebedeva M.V., Yashtulov N.A. Nanocomposite micro-power alternative power energy sources for electronic technology. *Teploenergetika*. 2021;68(1):21–29 (in Russ.). https://doi.org/10.1134/S0040363621010100]

3. Zeng K., Zhang D. Recent progress in alkaline water electrolysis for hydrogen production and applications. *Prog. Energy Combust. Sci*. 2010;36(3):307–326. https://doi.org/10.1016/j.pecs.2009.11.002

4. Haverkort J.W., Rajaei H. Electro-osmotic flow and the limiting current in alkaline water electrolysis. *J. Power Sources Adv*. 2020;6:100034. https://doi.org/10.1016/j.powera.2020.100034

5. Smirnov S.E., Yashtulov N.A., Putsylov I.A., Smirnov S.S., Lebedeva M.V. Polysulfone Copolymer as Polymer Electrolyte for Alkaline Fuel Cell and Li-Ion Battery Applications. *J. Eng. Appl. Sci*. 2019;14(9):2928–2935. https://doi.org/10.36478/jeasci.2019.2928.2935

6. Yashtulov N.A., Lebedeva M.V., Patrikeev L.N., Zaitcev N.K. New polymer-graphene nanocomposite electrodes with platinum-palladium nanoparticles for chemical power sources. *eXPRESS Polym. Lett*. 2019;13(8):739–748. https://doi.org/10.3144/expresspolymlett.2019.62

7. Yashtulov N.A., Lebedeva M.V. Hydrogen energy renewable current sources. *Russ. Technol. J*. 2017;5(3):58–73 (in Russ.). https://doi.org/10.32362/2500-316X-2017-5-3-58-73

8. Spiridonov N.V., Ivashko V.S., Kudina A.V., Kurash V.V. Hydrogen absorption and structure destruction of machinery and mechanism steel parts in hydrogen-containing medium. *Nauka i tekhnika = Science & Technique*. 2014;(2):72–77 (in Russ.).

9. Delvaux A., Lumbeeck G., Idrissi H., Proost J. Effect of microstructure and internal stress on hydrogen absorption into Ni thin film electrodes during alkaline water electrolysis. *Electrochimica Acta*. 2020;340:135970. https://doi.org/10.1016/j.electacta.2020.135970

10. Jiang X.G., Zhang Y.P., Song C., Xie Y.C., Liu T.K., Deng C.M., Zhang N.N. Performance of nickel electrode for alkaline water electrolysis prepared by high pressure cold spray. *Int. J. Hydrogen Energy*. 2020;45(58):33007–33015. https://doi.org/10.1016/j.ijhydene.2020.09.022

11. Mayerhöfer B., McLaughlin D., Böhm T., Hegelheimer M., Seeberger D., Thiele S. Bipolar Membrane Electrode Assemblies for Water Electrolysis. *ACS Appl. Energy Mater*. 2020;3(10):9635–9644. https://doi.org/10.1021/acsaem.0c01127

12. Liu Z., Sajjad S.D., Gao Y., Yang H., Kaczur J.J., Masel R.I. The effect of membrane on an alkaline water electrolyzer. *Int. J. Hydrogen Energy*. 2017;42(50):29661–29665. https://doi.org/10.1016/j.ijhydene.2017.10.050

13. López-Fernández E., Gil-Rostra J., Espinós J.P., González-Elipe A.R., de Lucas Consuegra A., Yubero F. Chemistry and Electrocatalytic Activity of Nanostructured Nickel Electrodes for Water Electrolysis. *ACS Catal*. 2020;10(11):6159–6170. https://doi.org/10.1021/acscatal.0c00856

14. Koj M., Qian J., Turek T. Novel alkaline water electrolysis with nickel-iron gas diffusion electrode for oxygen evolution. *Int. J. Hydrogen Energy*. 2019;44(57):29862–29875. https://doi.org/10.1016/j.ijhydene.2019.09.122

15. Le Formal F., Yerly L., Potapova Mensi E., Da Costa X.P., Boudoire F., Guijarro N., Spodaryk M., Züttel A., Sivula K. Influence of Composition on Performance in Metallic Iron–Nickel–Cobalt Ternary Anodes for Alkaline Water Electrolysis. *ACS Catal.* 2020;10(20):12139–12147. https://doi.org/10.1021/acscatal.0c03523

16. Rauscher T., Bernäcker C.I., Mühle U., Kieback B., Röntzsch L. The effect of Fe as constituent in Ni-base alloys on the oxygen evolution reaction in alkaline solutions at high current densities. *Int. J. Hydrogen Energy*. 2019;44(13):6392–6402. https://doi.org/10.1016/j.ijhydene.2019.01.182

17. Yashtulov N.A., Ragutkin A.V., Lebedeva M.V., Smirnov S.S. Functional characteristics of electrode materials based on porous silicon for micro-power current sources. *Tsvetnye Metally*. 2017;(5):58–63 (in Russ.). https://doi.org/10.17580/tsm.2017.05.09

18. Wang S., Zou X., Lu Y., Rao S., Xie X., Pang Z. Electrodeposition of nano-nickel in deep eutectic solvents for hydrogen evolution reaction in alkaline solution. *Int. J. Hydrogen Energy*. 2018;43(33):15673–15686. https://doi.org/10.1016/j.ijhydene.2018.06.188

19. Kraglund M.R., Aili D., Jankova K., Christensen E., Li Q., Jensen J.O. Zero-gap alkaline water electrolysis using ion-solvating polymer electrolyte membranes at reduced KOH concentrations. *J. Electrochem. Soc*. 2016;163(11):F3125. https://doi.org/10.1149/2.0161611jes

20. Sulka G.D., Brzozka A., Liu L. Fabrication of diameter-modulated and ultrathin porous nanowires in anodic aluminum oxide templates. *Electrochimica Acta*. 2011;56(14):4972–4979. https://doi.org/10.1016/j.electacta.2011.03.126

21. Antropov A.P., Zaitsev N.K., Ryabkov E.D., Yashtulov N.A., Mudrakova P.N. Manufacturing of nanopillar (ultra-dispersed) catalytically active materials through chemical engineering. *Tonk. Khim. Technol. = Fine Chem. Technol*. 2021;16(2):105–112. https://doi.org/10.32362/2410-6593-2021-16-2-105-112

22. Lebedeva M.V., Antropov A.P., Ragutkin A.V., Zaitsev N.K., Yashtulov N.A. Development of electrode nanomaterials for alkaline water electrolysis. *Theor. Found. Chem. Eng*. 2021;55(5):952–961. https://doi.org/10.1134/S0040579521050262

[Original Russian Text: Lebedeva M.V., Antropov A.P., Ragutkin A.V., Zaitsev N.K., Yashtulov N.A. Development of electrode nanomaterials for alkaline water electrolysis. *Teoreticheskie Osnovy Khimicheskoi Tekhnologii*. 2021;55(5):642–651 (in Russ.). https://doi.org/10.31857/S0040357121050079]

23. Stavrovskii M.E., Sidorov M.I., Albagachiev A.Yu., Ragutkin A.V., Lukashev P.E. *O roli vodoroda v protsessakh razrusheniya materialov* (*On the Role of Hydrogen in the Processes of Destruction of Materials*). Moscow: Eko-Press; 2020. 208 p. (in Russ.). ISBN 978-5-6044018-7-3

24. Lukashev E.A., Stavrovskii M.E., Sidorov M.I., Emelyanov S.G., Poserenin S.P. Model of topochemical kinetics of interaction of materials. *Izvestiya Yugo-Zapadnogo gosudarstvennogo universiteta. Seriya: Tekhnika i tekhnologii = Proceedings of the Southwest State University. Series: Engineering and Technology*. 2016;2(19):9–20 (in Russ.).

25. Vagin A.V., Sidorov M.I., Albagachiev A.Y., Stavrovskii M.E. Improving the life of artillery systems. *Russ. Engin. Res*. 2017;37(3):211–217. https://doi.org/10.3103/S1068798X17030212

26. Lebedeva M.V., Antropov A.P., Ragutkin A.V., Yashtulov N.A. Platinum nanoelectrocatalysts for hydrogen-air energy sources. *Computational Nanotechnology*. 2020;7(1):26–29 (in Russ.). https://doi.org/10.33693/2313-223X-2020-7-1-26-29

27. Damaskin B.B., Petri O.A., Cirlina G.A. *Elektrokhimiya* (*Electrochemistry*). St. Petersburg: Lan; 2015. 672 p. (in Russ.). ISBN 978-5-8114-1878-7

28. Krylova K.A., Baimova J.A., Mulyukov R.R. Effect of deformation on dehydrogenation mechanisms of crumpled graphene: molecular dynamics simulation. *Lett. Mater*. 2019;9(1):81–85. https://doi.org/10.22226/2410-3535-2019-1-81-85

29. Chuah C.Y., Lee J., Bae T.-H. Graphene-based Membranes for H_2 Separation: Recent Progress and Future Perspective. *Membranes*. 2020;10(11):336. https://doi.org/10.3390/membranes10110336

About the authors:

Marina V. Lebedeva, Cand. Sci. (Eng.), Associate Professor, Ya.K. Syrkin Department of Physical Chemistry, M.V. Lomonosov Institute of Fine Chemical Technologies, MIREA – Russian Technological University (86, Vernadskogo pr., Moscow, 119571, Russia). E-mail: lebedevamv2030@gmail.com. Scopus ID 57197593059, Research ID P-3661-2017, RSCI SPIN-code 1146-0867, https://orcid.org/0000-0003-0637-1745

Alexander V. Ragutkin, Cand. Sci. (Eng.), Vice-Rector for Innovative Development, MIREA – Russian Technological University (78, Vernadskogo pr., Moscow, 119454, Russia). E-mail: ragutkin@mirea.ru. Scopus ID 56871217700, RSCI SPIN-code 7531-7376, https://orcid.org/0000-0001-8256-1941

Ivan M. Sidorov, Cand. Sci. (Eng.), Head of the IT Solutions Development Department of the Mobile Solutions Engineering Center, MIREA – Russian Technological University (78, Vernadskogo pr., Moscow, 119454, Russia). E-mail: sidorov@mirea.ru. RSCI SPIN-code 6774-8834

Nikolay A. Yashtulov, Dr. Sci. (Eng.), Professor, Head of the S.S. Voyutsky Department of Nanoscale Systems and Surface Phenomena, M.V. Lomonosov Institute of Fine Chemical Technologies, MIREA – Russian Technological University (86, Vernadskogo pr., Moscow, 119571, Russia). E-mail: yashtulovna@mail.ru. Scopus ID 6507694451, Research ID U-8825-2017, RSCI SPIN code 3919-5844, https://orcid.org/0000-0002-7709-4186

Об авторах:

Лебедева Марина Владимировна, к.х.н., доцент кафедры физической химии им. Я.К. Сыркина Института тонких химических технологий им. М.В. Ломоносова ФГБОУ ВО «МИРЭА – Российский технологический университет» (119571, Россия, Москва, пр-т Вернадского, д. 86). E-mail: lebedevamv2030@gmail.com. Scopus ID 57197593059, Research ID P-3661-2017, SPIN-код РИНЦ 1146-0867, https://orcid.org/0000-0003-0637-1745

Рагуткин Александр Викторович, к.т.н., проректор по инновационному развитию ФГБОУ ВО «МИРЭА – Российский технологический университет» (119454, Россия, Москва, пр-т Вернадского, д. 78). E-mail: ragutkin@mirea.ru. Scopus ID 56871217700, SPIN-код РИНЦ 7531-7376, https://orcid.org/0000-0001-8256-1941

Сидоров Иван Михайлович, к.т.н., начальник отдела разработки ИТ-решений Инжинирингового центра мобильных решений, ФГБОУ ВО «МИРЭА – Российский технологический университет» (119454, Россия, Москва, пр-т Вернадского, д. 78). E-mail: sidorov@mirea.ru. SPIN-код РИНЦ 6774-8834

Яштулов Николай Андреевич, д.х.н., профессор, заведующий кафедрой наноразмерных систем и поверхностных явлений им. С.С. Воюцкого Института тонких химических технологий им. М.В. Ломоносова ФГБОУ ВО «МИРЭА – Российский технологический университет» (119571, Россия, Москва, пр-т Вернадского, д. 86). E-mail: yashtulovna@mail.ru. Scopus ID 6507694451, Research ID U-8825-2017, SPIN-код РИНЦ 3919-5844, https://orcid.org/0000-0002-7709-4186

The article was submitted: December 13, 2022; approved after reviewing: May 25, 2023; accepted for publication: October 06, 2023.

Translated from Russian into English by V. Glyanchenko
Edited for English language and spelling by Dr. David Mossop

CHEMISTRY AND TECHNOLOGY OF INORGANIC MATERIALS

ХИМИЯ И ТЕХНОЛОГИЯ НЕОРГАНИЧЕСКИХ МАТЕРИАЛОВ

ISSN 2686-7575 (Online)

https://doi.org/10.32362/2410-6593-2023-18-5-471-481

UDC 544.7

RESEARCH ARTICLE

Emergent properties of magnetic ions and nanoparticles in micellar solutions of surfactants: Use in fine technologies[1]

Yuri A. Mirgorod✉, Nikolay A. Borsch, Anastasia M. Storozhenko, Liliya S. Ageeva

Southwest State University, Kursk, 305040 Russia
✉Corresponding author, e-mail: yu_mirgorod@mail.ru

Abstract

Objectives. *To establish expected emergent (unexpected) properties of magnetic materials when obtained in aqueous micellar solutions of surfactants (aqueous quantum materials), and their use in fine technologies.*

Methods. *Chemical synthesis of magnetic nanoparticles in aqueous micellar solutions of surfactants of various nature. Characterization of magnetic solutions and nanoparticles by magnetic measurements, spectroscopy, diffractometry, small-angle X-ray diffraction, scanning probe microscopy, and others.*

Results. *The term "water quantum material" refers to materials (micellar solutions) whose properties are mainly determined by the nuclear quantum effect on macroscopic scales (emergent property). Micellar solutions exhibit phenomena and functionality not always consistent with the classical theory of micellization. The article presents in detail the experimental results that suggest the manifestation of the emergent properties of magnetic materials obtained in aqueous micellar solutions of surfactants. In particular, Gd^{3+} ions in an aqueous micellar solution of sodium dodecyl sulfate exhibit paramagnetic properties, possibly indicating their random arrangement in solution contrary to the classical theory of micellization with an ordered adsorption layer on micelles. Hybrid Pt–Gd nanoparticles are formed in a quantum material*

This is the revised and translated from Russian into English language variant of the original article published in *Izvestiya Yugo-Zapadnogo gosudarstvennogo universiteta. Seriya: Tekhnika i tekhnologii = Proceedings of the Southwest State University. Series: Engineering and Technology*. Russian Text © The Authors, 2022. For citation: Mirgorod Yu.A., Borsch N.A., Storozhenko A.M., Ageeva L.A. Emergent Properties of Magnetic Ions and Nanoparticles in Micellar Solutions of Surfactants. *Izvestiya Yugo-Zapadnogo gosudarstvennogo universiteta. Seriya: Tekhnika i tekhnologii = Proceedings of the Southwest State University. Series: Engineering and Technology*. 2022;12(4):222–238 (in Russ.).

with cetylpyridinium chloride as a matrix, although Gd^{3+} ions must be repelled by CP^{+} ions on micelles. Nanosized powders of cobalt ferrite and nickel ferrite obtained in a micellar solution of sodium dodecyl sulfate have superparamagnetic properties, although the presence of their precursor ions in the adsorption layer in classical micelles should lead to ferromagnetic properties.
Conclusions. *The synthesis of nanoparticles in a quantum material opens up the possibility of reducing ions of different signs in one stage during the processing of metallurgy waste, in order to obtain nanoparticles of various metals and their composites. Magnetic nanoparticles obtained in a quantum surfactant material self-assemble on various substrates, enabling the creation of materials whose residual magnetization and coercive field can be controlled at room temperatures.*

Keywords: *magnetic nanoparticles, nuclear quantum effects, water quantum materials, emergent properties, metallurgy waste processing*

For citation: Mirgorod Yu.A., Borsch N.A., Storozhenko A.M., Ageeva L.S. Emergent properties of magnetic ions and nanoparticles in micellar solutions of surfactants: Use in fine technologies. *Tonk. Khim. Tekhnol. = Fine Chem. Technol.* 2023;18(5):471–481. https://doi.org/10.32362/2410-6593-2023-18-5-471-481

НАУЧНАЯ СТАТЬЯ

Эмерджентные свойства магнитных ионов и наночастиц в мицеллярных растворах ПАВ: Использование для тонких технологий

Ю.А. Миргород✉, Н.А. Борщ, А.М. Стороженко, Л.С. Агеева

Юго-Западный государственный университет, Курск, 305040 Россия
✉Автор для переписки, e-mail: yu_mirgorod@mail.ru

Аннотация

Цели. *Выявить предполагаемые эмерджентные (неожиданные) свойства магнитных материалов при их получении в водных мицеллярных растворах поверхностно-активных веществ (ПАВ) (водных квантовых материалах), которые можно использовать для тонких технологий.*
Методы. *Химический синтез магнитных наночастиц в водных мицеллярных растворах ПАВ различной природы; характеризация магнитных растворов и наночастиц методами магнитных измерений, спектроскопии, дифрактометрии, малоугловой рентгеновской дифракции, сканирующей зондовой микроскопии и другими.*
Результаты. *Термин «водный квантовый материал» относится к материалам (мицеллярным растворам), свойства которых в основном определяются ядерным квантовым эффектом в макроскопических масштабах (эмерджентное свойство). Мицеллярные растворы демонстрируют явления и функциональные возможности, не всегда соотносимые с классической теорией мицеллобразования. В статье подробно представлены экспериментальные результаты, которые позволяют предположить проявление*

эмерджентных свойств магнитных материалов, получаемых в водных мицеллярных растворах ПАВ. В частности, ионы гадолиния Gd^{3+} в водно-мицеллярном растворе додецилсульфата натрия проявляют парамагнитные свойства, что, возможно, указывает на их беспорядочное расположение в растворе вопреки классической теории мицеллообразования с адсорбционным упорядоченном слое на мицеллах. Гибридные наночастицы Gd–Pt образуются в квантовом материале с хлоридом цетилпиридиния в качестве матрицы, хотя ионы Gd^{3+} должны отталкиваться ионами цетилпиридиния $ЦП^{+}$ на мицеллах. Наноразмерные порошоки феррита кобальта и феррита никеля, получаемые в мицеллярном растворе додецилсулфата натрия, обладают суперпарамагнитными свойствами, хотя присутствие их прекурсорных ионов в адсорбионном слое в классических мицеллах должно было бы привести к ферромагнитным свойствам.

Выводы. *Синтез наночастиц в квантовом материале открывает возможность восстановления ионов разных знаков за одну стадию при переработке отходов металлургии с целью получения наночастиц различных металлов и их композитов. Магнитные наночастицы, получаемые в квантовом материале ПАВ, самоорганизуются на различных подложках, что позволяет создавать материалы, остаточная намагниченность и коэрцитивное поле которых можно регулировать при комнатных температурах. Таким образом, показано, каким образом эмерджентные свойства квантовых материалов можно применять для тонких технологий.*

Ключевые слова: *магнитные наночастицы, ядерный квантовый эффект, водные квантовые материалы, эмерджентные свойства, переработка отходов металлургии*

For citation: Mirgorod Yu.A., Borsch N.A., Storozhenko A.M., Ageeva L.S. Emergent properties of magnetic ions and nanoparticles in micellar solutions of surfactants: Use in fine technologies. *Tonk. Khim. Tekhnol. = Fine Chem. Technol*. 2023;18(5):471–481. https://doi.org/10.32362/2410-6593-2023-18-5-471-481

INTRODUCTION

Ionic surfactants are often used to obtain magnetic nanoparticles. They play the role of matrices for the localization of d-block elements ions [1–4]. According to classical theory, direct surfactant micelles in water have the structure of a hydrocarbon core with a double electric layer of ions [5]. The electrical double layer consists of an adsorption and a diffuse layer. The ions of the adsorption layer are densely packed and organized. The degree of ionization of micelles and the energy of Gibbs micelle formation can thus be established. The ions of the diffuse layer, on the contrary, are washed out by thermal energy. Based on such an organization of magnetic ions in the adsorption layer, a strong exchange interaction between them can be expected with the manifestation of ferromagnetic properties. However, this is not observed [6]. Another emergent property is associated with the synthesis of metal nanoparticles from positive ions in micelles of cetylpyridinium chloride $C_{16}H_{33}C_5H_5NCl$ [7–9]. Gadolinium ions Gd^{3+} should not penetrate into the hydrocarbon core of a classical micelle, since they are repelled by the positive $C_{16}H_{33}C_5H_5N^+$ ions of the micelle. Therefore, the matrix or protective properties of micelles should not appear. However, these properties are used very successfully.

For more purposeful application, these and other contradictions or emergent properties require a more detailed study. This is especially important for *in vivo* use, where synergism and antagonism of drugs or magnetic probes with the quantum properties of a biological cell is possible [10–12].

We previously conducted similar studies with the same goal, but the mystery of the nature of this phenomenon did not allow us to explain the contradictions we observed. The time has come now to return to the causes of the magnetic properties of ions and nanoparticles obtained in the matrices of quantum materials.

Let us briefly dwell on the probable mechanism of this phenomenon. Solid quantum materials operate at low temperatures where quantum fluctuations are more pronounced. Solid quantum materials reveal completely new phenomena and functions in the Mott transition, high-temperature superconductivity, topological superconductivity, colossal magnetoresistance, and giant magnetoelectric effect [13].

The quantum properties of water have been the focus of intensive study, in order to understand the role of quantum phenomena in the properties of water. However, these studies are based on calculations of various water models and depend on the choice of parameters proposed by the researchers themselves. Therefore, the results are very inconsistent. Water does not have the properties of a quantum material. The quantum fluctuations in it need to be "woken up".

The unravelling of the mystery of quantum phenomena in aqueous solutions was made possible by the fact that for the first time the presence of accompanying phenomena was shown. This consisted namely of an extended phase transition in an ensemble of small aqueous systems and micellization [14–17]. The micelle formation process and the accompanying liquid-liquid phase transition are two sides of the same coin. Strong fluctuations of the extensive properties of water (thermal fluctuations) appear in the area of formation of spherical micelles, due to the smallness of the ensemble of water (6–14 molecules), corresponding to the size of surfactant molecules. They, in turn, stimulate the manifestation of quantum fluctuations of water molecules and charges. Organized chaos or correlation of thermal and quantum fluctuations arises. Quantum fluctuations at a size of 0.2–0.3 nm with the duration of a picosecond form thermal fluctuations (cavities) for micelles with the capture of water molecules at a size of 4–6 nm with diffusion coefficients of the order of $4 \cdot 10^{-6}$ cm·s^{-1} [17].

Magnetic ions and nanoparticles in micellar aqueous solutions are assumed to be present inside a quantum micelle or an organized chaos of water and surfactants. When attempting to measure electrical conductivity or electromotive force, the electromagnetic field of the device destroys quantum fluctuations and the micelle shows classical behavior. The reducing agent hydrazine hydrate does not affect the nuclear quantum effect. Such a theoretical explanation of the manifestation of emergent properties is still debatable. Nevertheless, these properties can already be used for practical purposes.

In this article, as part of the discussion, we consider only the supposed emergent properties of magnetic materials when they are obtained in micellar surfactant solutions. The first part of the article discusses the magnetic properties of ions, then we will consider the features of self-organization and behavior of magnetic nanoparticles. In conclusion, we will show how a micellar surfactant solution can be used in a hybrid waste processing technology to obtain metal nanoparticles, metal oxides, and to create self-assemblies of magnetic nanoparticles.

MATERIALS AND METHODS

The main reagents used were cetylpyridinium chloride $C_{16}H_{33}C_5H_5NCl$ (CPC) (99%, *Sigma-Aldrich*, USA), sodium dodecyl sulfate (SDS) (99%, *Shostka Chemical Plant*, Russia), gadolinium acetate $Gd(CH_3COO)_3 \cdot 3H_2O$ (chemically pure, *Vekton*, Russia), platinum hydrochloric acid $H_2[PtCl_6] \cdot 6H_2O$ (99%, *SilverSalt*, Russia), hydrazine hydrate $N_2H_4 \cdot H_2O$ (100%, *Clearsynth*, India), $FeSO_4 \cdot 7H_2O$ (chemically pure, *Russian Vitriol Company*, Russia), $CoCl_2 \cdot 6H_2O$ (chemically pure, *Fairsky Industrial Co*., China) and $NiCl_2 \cdot 6H_2O$ (chemically pure, *Fairsky Industrial Co*., China) were used to obtain $CoFe_2O_4$ and $NiFe_2O_4$ nanoparticles. A mixture of toluene and isoamyl alcohol in a volume ratio of 4:1 (purified grade reagents from *Fluka*, Switzerland) was used as the organic phase in the process of flotation extraction.

For the synthesis of nanoparticles, an ultrasonic disperser UZDN-2 (*Techcenter*, Russia) was used. The diffraction patterns of the nanopowders were recorded on a DRON 3M X-ray diffractometer (*Burevestnik*, Russia) with a copper emitter. The size and shape of nanoparticles were determined using a JEOL JEM-1011 transmission electron microscope (TEM) (*JEOL*, Japan) at an accelerating voltage of 100 kV. The content of platinum in the Pt–Gd nanopowder was determined using a Kvant-Z atomic absorption spectrometer (*Kortek*, Russia) with an electrothermal atomizer (graphite furnace). Magnetic studies were carried out on magnetic balances by the ponderomotive method, as well as on the universal "Cryogenic high field measurement system" (CFMS, *Cryogenic*, United Kingdom). In addition to the usual measurements of the magnetic moment as a function of the magnetic field and temperature, we used the technique of measuring the magnetic susceptibility after cooling in zero (zero field cooling, ZFC) and low (field cooling, FC) magnetic

fields. The characteristic maximum on the ZFC branch at the blocking temperature was used to estimate the sizes, as well as the size distribution of nanoparticles. Topographic and elemental analyzes were performed on a Philips SEMS 515 scanning electron microscope (*Philips*, Netherlands) with an EDAX ECON IV microanalyzer. The photographs of the obtained powder particles were taken with an Olympus GX71 metallographic microscope (*Olympus*, Japan).

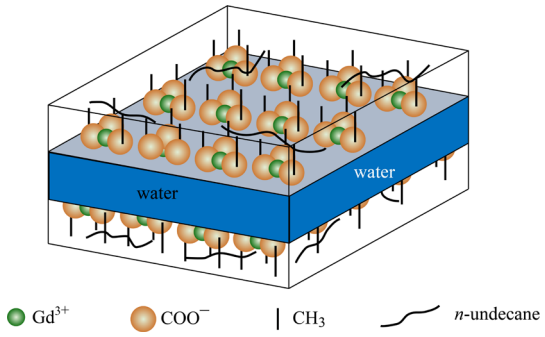

Fig. 1. Lamellar micelle (liquid crystal) in the GA–water–*n*-undecane system.

RESULTS AND DISCUSSION

Magnetic properties of Gd^{3+} obtained in a quantum material with sodium dodecylsulfate (SDS)

We tested the magnetic ordering of Gd^{3+} ions by adding gadolinium acetate $(CH_3COO^-)_3Gd^{3+}$ (GA) to SDS in the ratio (1:1, mol) [6]. Solutions of 0.05 M GA at 298 K had a magnetic susceptibility equal to $1.8\cdot10^{-7}$ $m^3\cdot kg^{-1}$, i.e., they were diamagnetic. When GA was added to a solution of SDS (1:1), no precipitation was observed. The micellar solution of gadolinium dodecyl sulfate obtained in this way became paramagnetic with a magnetic susceptibility equal to $2.0\cdot10^{-7}$ $m^3\cdot kg^{-1}$ (Table). If we assume that gadolinium dodecyl sulfate at such a concentration is soluble in an aqueous solution of GA, then without the action of a magnetic field, the Gd^{3+} ions, and, consequently, Na^+ ions in solutions with spherical micelles, are completely randomly oriented. They do not have the structure of the adsorption layer of a classical micelle. The paramagnetic properties of such solutions are preserved in the temperature range of 275–315 K.

On the other hand, if the Gd^{3+} ions are built into an order characteristic of a lamellar micelle (liquid crystal) (Fig. 1), as in the GA–water–undecane system, the Gd^{3+} ion has ferromagnetic properties.

When the aqueous solution of GA is saturated with *n*-undecane, the temperature dependencies of the specific inverse magnetic susceptibility $\chi^{-1}(T)$ indicate the appearance of magnetic ordering of another type. The projection of the function $\chi^{-1}(T)$ on the abscissa axis is positive. This indicates that the ferromagnetic order is typical for metallic gadolinium. Figure 2 shows the temperature dependence of the specific inverse magnetic susceptibility for liquid crystals of the GA (0.1 M)–water–*n*-undecane system. In this case, the approximate linear function is:

$$\chi^{-1}(T) = 2.5\cdot10^5 T - 2.5\cdot10^7.$$

When comparing the magnetic properties of Gd^{3+} ions in a quantum material and with organized ions of liquid crystal, we can conclude that they are different. Using the classical theory of the formation micelles in water, they possess the structure of a hydrocarbon core with a double electric layer of ions. The double electrical layer consists of an adsorption layer and a diffuse layer. The ions of the adsorption layer are dense and organized. Based on such an organization of magnetic ions in the adsorption layer, we can rightly expect a strong exchange interaction between them with the manifestation of ferromagnetic properties. However, we observed the paramagnetic properties of gadolinium ions with random motion in solution.

Table. Specific magnetic susceptibility of GA aqueous solutions without micelles and with SDS spherical micelles at 298 K

Aqueous solutions	GA concentration, [M]	$\chi\cdot10^{-7}$, [m^3/kg]
GA	0.0005	−6.0
GA	0.005	−4.0
GA	0.05	−1.8
GA + SDS (1:1)	0.0005	−4.0
GA + SDS (1:1)	0.005	−2.1
GA + SDS (1:1)	0.05	2.0

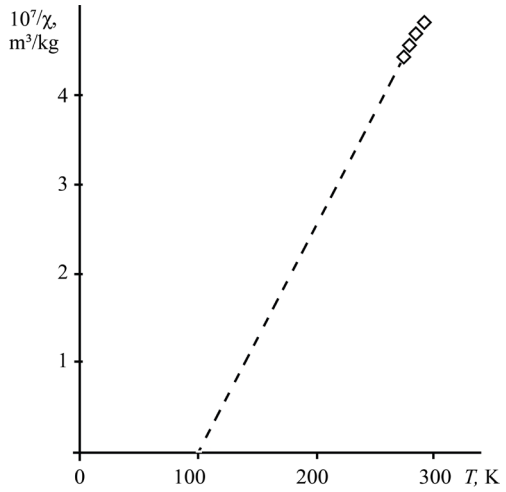

Fig. 2. Inverse magnetic susceptibility *vs* temperature for the lamellar micelle of the GA (0.1 M)–water–*n*-undecane system.

Magnetic properties of Pt–Gd nanoparticles obtained in a quantum material with cetylpyridinium chloride (CPC)

For the synthesis of hybrid nanoparticles, we chose $H_2[PtCl_6]$ and $Gd(CH_3COO)_3$ with CPC concentration of 0.0293 M. This is greater than critical micelle concentration (CMC) = 0.002 M [18]. We passed nitrogen through the mixture of dissolved substances, in order to remove dissolved oxygen, followed by stirring. A yellow solution was obtained, the color of which is due to the interaction of the cetylpyridinium$^+$ ion with $[PtCl_6]^{2-}$. The ions in micellar solution and alkaline medium were reduced with hydrazine hydrate. After reduction, a dispersion with dark brown nanoparticles was obtained, represented by the TEM image in the middle (Fig. 3a) and along the edges of the dried suspension (Fig. 3b).

The content of Pt in the washed dry nanoparticles corresponded to the complete reduction of ions, 2.4 wt % Pt. The 82% content of Gd instead of 97.6% indicates the presence of organic impurities in the nanoparticles. These can be assumed to be CPC molecules. As can be seen from Fig. 3, the nanoparticles are 5–10 nm in size. The nanoparticles are self-organized in the quantum material (Fig. 3a) and this organization is visible in the dried material on the carbon substrate (TEM). The granular equidistant structure of the hybrid nanoparticles is also clearly visible. After the redox reaction and preparation for TEM, nitrogen and water disappeared from the reaction mixture, thus it can be assumed that the hybrid nanoparticles are distributed between CPC molecules.

In order to understand and compare this with our magnetic nanoparticles, we have presented the mechanism of photoreduction of Au and Pt ions in a micellar solution of SDS without the addition of a chemical reducing agent. Such a research method avoids pollution of the production of nanoparticles by reaction products and makes the study of the reaction mechanism purer. Micelles and nanoparticles have been investigated using small-angle X-ray scattering, extended X-ray absorption fine structure, and TEM [19]. The authors have provided evidence that SDS micelles are preserved with the inclusion of nanoparticles of the "nanoparticle core–surfactant shell" type. Au and Pt metal nanoparticles were formed photochemically in the cores of micelles, and had no significant effect on the micelle morphology. Before reduction, the ions were randomly distributed in solution, and after reduction, their reduced forms ended up inside micelles.

Our studies [8] have also proved the formation of condensation centers and magnetic nanoparticles

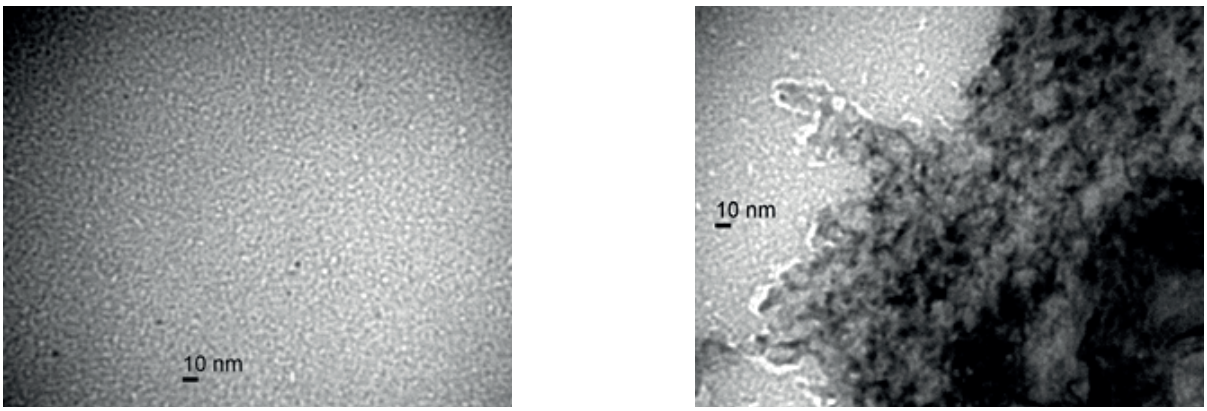

(a) (b)

Fig. 3. TEM images of hybrid Pt–Gd nanoparticles obtained in a quantum material and dried on a graphite substrate.

of manganese and cobalt in micelles. This behavior of ions indicates their participation in the quantum nuclear effect, as confirmed by our and other studies.

Let us compare the magnetic properties of crystalline Gd and powder Pt–Gd. According to reference data, the specific magnetization of bulk crystals Gd in a magnetic field 0.5–1.7 T in a nitrogen atmosphere is 240 A·m^2/kg and bulk crystals has a Curie point of about 293 K. Specific magnetization of the synthesized powder Pt–Gd in a magnetic field 0.86 T is two orders of magnitude lower than those of Gd crystals and has the value 1.92 A·m^2/kg. The Curie point of the studied Pt–Gd nanopowder is equal to ~270 K, which is ~23 K below the Curie point of the bulk sample. There is no blocking temperature on the ZFC curve which is typical for superparamagnetic nanoparticles.

Thus, taking into account the results obtained in the study of magnetic properties, it can be assumed that using such a synthesis method and without thorough purification of nanoparticles from surfactants, the Pt–Gd powder has an atypical magnetic behavior.

Magnetic properties of cobalt ferrite nanoparticles obtained in a quantum material with SDS

Cobalt ferrite nanoparticles were obtained by ion flotation extraction, in order to demonstrate the production of nanoparticles from waste using our integrated technology [20]. SDS were dissolved in a 1.5-liter solution, 0.0002 M $CoCl_2$ and 0.0004 M $FeSO_4$ and 0.0008 M. A micellar solution (quantum material) of a mixture of salts of cobalt, iron, sodium, and pink-colored SDS due to the presence of hydrated cobalt ion is formed. After 10 min of ionic flotation extraction, the pink color of the aqueous solution disappeared: the mixture of toluene extractant with isoamyl alcohol turned pink. The extraction was stopped. After flotation, the extractant with iron cobalt salts and SDS was separated. The extractant was removed by distillation, the salt precipitate was dried under vacuum and over paraffin powder. Then the mixture of salts was treated with sodium hydroxide solution until complete precipitation of iron and cobalt hydroxides. This was washed with water and dried in air to obtain possible $CoFe_2O_4$. We deliberately did not shape the crystal lattice of $CoFe_2O_4$ by heating to thermally decompose SDS.

In order to obtain X-ray diffraction (XRD) and TEM images, the composite was preliminarily dispersed in ethyl alcohol using ultrasound. Received the dispersion was applied to a copper substrate coated with carbon. The diffraction pattern showed that the formation of the $CoFe_2O_4$ crystal lattice was either incomplete (i.e., the dense packing of the spinel structure was not formed) or a strongly defective structure was formed. This is indicated by slightly higher interplanar spacing and broadened diffraction peaks. Moreover, X-ray reflections are shifted towards larger angles, i.e., for a crystal cell with smaller parameters. Nanoparticles self-organize into a periodic colloidal structure on a carbon substrate (Fig. 4a) and have a maximum size distribution in the range of 4 to 6 nm (Fig. 4b).

Thus, the following conclusions can be drawn about the structure and magnetic properties of the formed nanoparticles. Surfactants adsorbed and included in the powder system interfere with the creation of an “ideal” crystal lattice of $CoFe_2O_4$.

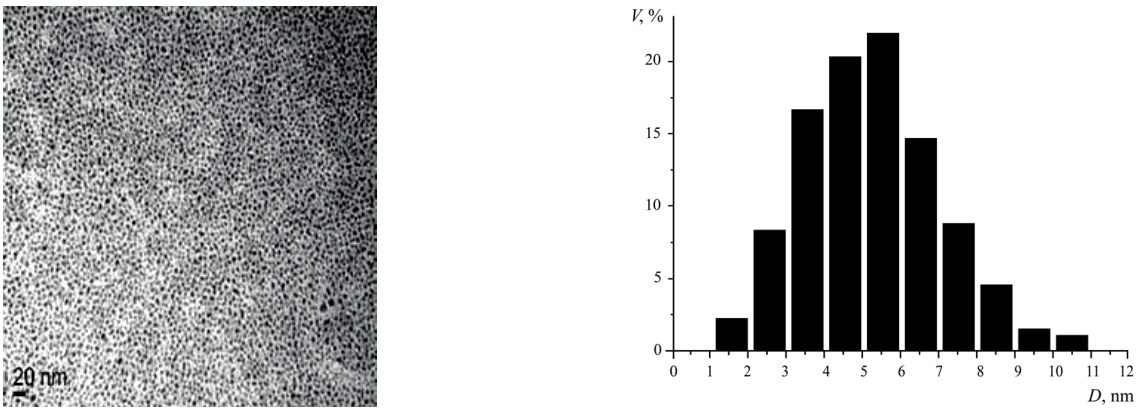

(a) (b)

Fig. 4. TEM image of self-organization into a periodic colloidal structure of cobalt ferrite powder nanoparticles obtained in a quantum material and dried on a graphite substrate (a) and size distribution of nanoparticles (b); *V* is the relative frequency, %; *D* is the nanopaticle size, nm.

The particles consist of two components: a well-formed $CoFe_2O_4$ phase and its amorphous counterpart. Nanoparticles have a maximum size distribution in the range from 4 to 6 nm and self-organize into a periodic colloidal structure on a carbon substrate. As established from the ZFC–FC magnetization curves, the nanosized powder possesses a blocking temperature of 45 K with a magnetic moment of 0.85–0.9 μ_B[2] at a temperature of ~0 K, and the Néel temperature lies in the range of 110–250 K.

Magnetic properties of nickel ferrite nanoparticles obtained in a quantum material with SDS

The results of experimental elemental analysis of the synthesized powder of the expected nickel ferrite showed an increased content of iron and oxygen relative to stoichiometric nickel ferrite ($NiFe_2O_4$) [21]. The composition of the powder corresponds to $NiFe_{4.6}O_{14.8}$. The method described above for obtaining cobalt ferrite in the case of nickel leads to the formation of self-organizing nanoparticles of nonstoichiometric nickel ferrite (Fig. 5). This is because the synthesis process with the addition of alkali was accompanied by the partial removal of amphoteric nickel hydroxide. In addition, the resulting powder, in addition to iron and nickel hydroxides, possibly contained $(C_{12}H_{25}SO_4)_3Fe$, $(C_{12}H_{25}SO_4)_2Fe(OH)$, and $(C_{12}H_{25}SO_4)\cdot Fe(OH)_2$. They were difficult to isolate at the stage of filtering the precipitate after the addition of alkali. The 3% carbon content confirms such assumptions.

The XRD pattern of the synthesized powder had no sharp peaks; something which does not prove that ideal crystals were obtained. Elemental analysis and XRD data of the powder convincingly prove that it consisted of X-ray amorphous non-stoichiometric ferrite and SDS. Furthermore, heat treatment at 600°C caused the appearance of diffraction peaks of crystalline nickel ferrite.

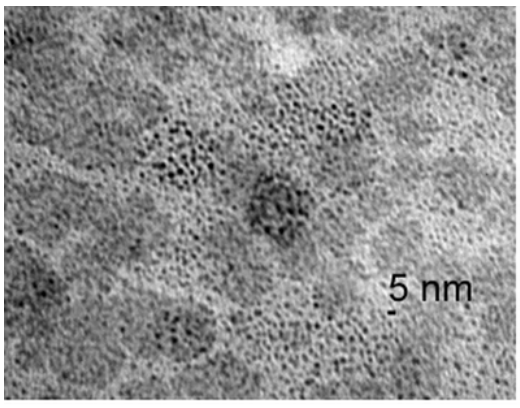

Fig. 5. TEM image of self-organization into a periodic colloidal structure of nickel ferrite powder nanoparticles obtained in a quantum material and dried on a graphite substrate.

[2] μ_B is the Bohr magneton.

The magnetic susceptibility of the material after ZFC or FC was measured [21, 22], in addition to standard magnetization versus magnetic field. In the ZFC procedure, the sample was cooled to 4 K without applying a magnetic field and measurements were made in a static magnetic field. Then the temperature was slowly raised and the magnetization was recorded. The FC procedure differed from the ZFC measurements only in that the sample was cooled in a non-zero magnetic field. FC and ZFC curves of magnetically inhomogeneous magnetic materials typically coincide at high temperatures while differing below their blocking temperature T_b. Their ZFC curves have a maximum at T_b, whereas their FC curves usually rise monotonically down to very low temperatures. At temperatures above T_b = 25 K, the synthesized nickel ferrite nanoparticles possess superparamagnetic properties (Fig. 6), characteristic of magnetic nanomaterials.

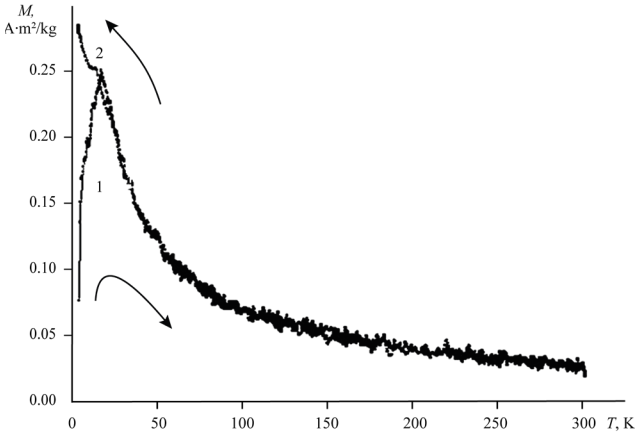

Fig. 6. Temperature dependence of the specific magnetization of nickel ferrite powder in magnetic field of 300 Oe: 1 – ZFC, 2 – FC.

Another important characteristic of a magnetic nanomaterial is its specific saturation magnetization. That of the synthesized ferrite nanoparticles is 15.0 A·m²/kg at 5 K which is slightly below the saturation magnetization of bulk $NiFe_2O_4$ (17.6 A·m²/kg).

From the experiment of synthesis of nanoparticles in a quantum material, the following conclusions can be drawn. It is possible to reduce metal ions of different signs of complex and simple $[PtCl_6]^{2-}$ and Gd^{3+} ions in a quantum material in a single step. This is very important when processing

waste to obtain nanoparticles of different metals [23, 24]. There are no differences in the recovery of supposedly "organized" ions of the adsorption layer and the diffuse layer of an ionic surfactant micelle. All ions are randomly distributed in the water quantum material.

The listed methods for the synthesis of nanoparticles were created in order to illustrate the production of nanoparticles from waste. This technology consists of three stages: firstly, aqueous solutions of simple or complex metal ions are obtained from waste; secondly, they are extracted by the method of ion flotation; at the third stage, ions are reduced to nanoparticles in an aqueous micellar solution.

Magnetic nanoparticles in a quantum material are necessary for their organization into long-range and dynamic assemblies on various substrates. Experiments show that nanoparticles in a quantum material self-organize well when dried on substrates in the second minimum of the dependence of their potential energy on distance. This technology will open up possibilities for a wide range of applications. In particular, materials can be created for which the remanent magnetization and coercive field are controlled at room temperature. For this, liquid crystals containing ions can also be used [25].

Self-organized structures are well-formed from dispersions of nanoparticles in a quantum material on any substrate. Further annealing on the substrate preserves this organization and allows the formation of a different mesoscopic order with emergent properties: an increase in the blocking temperature and the behavior of superspin glass [26, 27].

In terms of further potential, other emergent properties of quantum materials that can be used for the synthesis and application of magnetic materials found by other researchers may be a focus in the future.

Thus, there is an increase in the optical rotation of SDS solutions in the concentration range from 0.002 mol/L to CMC, followed by a decrease after CMC to a constant value at 0.015 mol/L and higher [28]. The existence of a strong anisotropic structure around the CMC of ionic surfactants is confirmed [29]. Sonication increases the viscosity and solubilization in micellar solutions [30]. Interaction of quantum fluctuations of water with excitons of quantum dots with intense luminescence was established [30–32]. Films and foams obtained from surfactant solutions near CMC exhibit extreme properties [33].

CONCLUSIONS

Nano magnetic materials synthesized in aqueous micellar solutions of surfactants (aqueous quantum materials) exhibit emergent properties. This opens up the possibility of reducing ions of different signs in a single stage during the processing of metallurgy waste, in order to obtain nanoparticles of various metals and their composites. Magnetic nanoparticles obtained in a quantum surfactant material self-assemble on various substrates, enabling the creation of materials whose residual magnetization and coercive field can be controlled at room temperatures.

Acknowledgments

The study was financially supported by the Ministry of Education and Science of the Russian Federation (state assignment 2020, No. 0851-2020-0035). The study was carried out as part of the Priority 2030 strategic academic leadership program (Agreement No. 075-15-2021-1213).

Authors' contributions

Yu.A. Mirgorod – analysis and generalization of the results of studying the behavior of magnetic nanoparticles obtained in micellar solutions of surfactants.

N.A. Borsch – planning an experiment on the synthesis of magnetic nanoparticles in micellar solutions of surfactants.

A.M. Storozhenko – characterization of magnetic nanoparticles.

L.S. Ageeva – synthesis of magnetic nanoparticles in micellar solutions of surfactants.

The authors declare no conflicts of interest.

REFERENCES

1. Hatakeyama W., Sanchez T.J., Rowe M.D., *et al.* Synthesis of Gadolinium Nanoscale Metal−Organic Framework with Hydrotropes: Manipulation of Particle Size and Magnetic Resonance Imaging Capability. *ACS Appl. Mater. Interfaces*. 2011;3(5):1502–1510. https://doi.org/10.1021/am200075q

2. Lu A.H., Salabas E.L., Schüth F. Magnetic nanoparticles: synthesis, protection, functionalization and application. *Angew. Chem.* 2007;46(8):1222–1244. https://doi.org/10.1002/anie.200602866

3. Leem G., Sarangi S., Zhang S., *et al*. Surfactant-Controlled Size and Shape Evolution of Magnetic Nanoparticles. *Crystal. Growth Des*. 2009;9(1):32–34. https://doi.org/10.1021/cg8009833

4. Shamim N., Hong L., Hidajat K., *et al*. Thermosensitive polymer (*N*-isopropylacrylamide) coated nanomagnetic particles: Preparation and characterization. *Colloids Surf. B: Biointerfaces*. 2007;55(1):51–58. http://doi.org/10.1016/j.colsurfb.2006.11.007

5. Holmberg K., Jönsson B., Kronberg B., *et al.* Surfactants and Polymers in Aqueous Solutions. UK: Wiley; 2003. 568 p. ISBN 978-0-470-85642-0

6. Mirgorod Yu.A., Chekadanov A.S., Yanushkevich A.M., *et al*. Magnetic properties of Gd (III) in aqueous micellar systems. *Magnetohydrodynamics*. 2018;54(3):299–308. https://doi.org/10.22364/mhd.54.3.9

7. Mirgorod Yu.A., Borshch N.A. *Method of Producing nanoparticles of metal or hybrides of nanoparticles of metals*: RF Pat. 2369466 RU. Publ. 10.10.2009 (in Russ.).

8. Mirgorod Yu.A., Borshch N.A., Borodina V.G., Yurkov G.Yu. Production and characterization of cotton fabric modified with copper nanoparticles. *Khimicheskaya promyshlennost' = Chemical Industry*. 2012;89(6):310–316 (in Russ.).

9. Vorobiova I.G., Borshch N.A., Mirgorod Yu.A. The structure of Mn and Co nanoparticles obtained in direct surfactant micelles. *Journal of Nano- and Electronic Physics.* 2017;9(5):05036-1–05036-4. http://doi.org/10.21272/jnep.9(5).05036

10. Geesink H.J.H., Jerman I., Meijer D.K.F. Water, the Cradle of Life via its Coherent Quantum Frequencies. *Water.* 2020;(11):78–108. http://doi.org/10.14294/WATER.2020.1

11. Krause W. *Contrast Agents I: Magnetic Resonance Imaging*: Pt. 1. Berlin, Heidelberg: Springer; 2002. 249 p.

12. Salt C., Lennox A.J., Takagaki M. Boron and gadolinium neutron capture therapy. *Rus. Chem. Bull.* 2004;53(9):1871–1888. https://doi.org/10.1007/s11172-005-0045-6

13. Tokura Y., Kawasaki M., Nagaosa N. Emergent functions of quantum materials. *Nature Phys*. 2017;13:1056–1068. https://doi.org/10.1038/nphys4274

14. Mirgorod Yu.A., Emelyanov S.G., Pugachesky M.A. *Method for Measuring the Parameters of Liquid-Liquid Phase Transition and Micellization*: RF Pat. 2730433 RU. Publ. 08.21.2020 (in Russ.).

15. Mirgorod Yu.A. *Method for Measuring the Parameters of the Liquid-Liquid Phase Transition*: RF Pat. 2720399 RU. Publ. 04.29.2020 (in Russ.).

16. Mirgorod Yu.A. Quantum nuclear effect in aqueous ionic surfactant and polyelectrolytes solutions. In: *Proc. Bio-Inspired Nanomaterials – Nature Conferences* (*Nov. 14–15, 2021*). Seoul, South Korea. http://doi.org/10.13140/RG.2.2.32364.08325

17. Mirgorod Yu.A. Strongly correlated electronic states in aqueous micellar surfactant systems. *Preprint*. 2021. https://doi.org/10.21203/rs.3.rs-660013/v1

18. Mirgorod Yu.A., Borshch N.A., Reutov A.A., Yurkov G.Yu., Fedosyuk V.M. Synthesis of gadolinium-based nanoparticles in a system of direct surfactant micelles and study of their magnetic properties. *Russ. J. Appl. Chem.* 2009;82(8):1357–1363. http://doi.org/10.1134/S1070427209080072

19. Harada M., Saijo K., Sakamotoet N., *et al*. Small-angle X-ray scattering study of metal nanoparticles prepared by photoreduction in aqueous solutions of sodium dodecyl sulfate. *Colloids and Surfaces A: Physicochem. Eng. aspects*. 2009;345(1–3):41–50. http://doi.org/10.1016/j.colsurfa.2009.04.015

20. Mirgorod Yu.A., Borsch N.A., Fedosyuk V.M., Yurkov G.Yu. The structure and magnetic properties of cobalt ferrite nanoparticles synthesized in a system of direct micelles of amphiphiles by means of ion flotoextraction. *Russ. J. Phys. Chem. A*. 2012;86(3):418–423. https://doi.org/10.1134/S0036024412030211

21. Mirgorod Yu.A., Borsch N.A., Fedosyuk V.M., Yurkov G.Yu. Magnetic properties of nickel ferrite nanoparticles prepared using flotation extraction. *Inorg. Mater.* 2013;49(1):109–114. https://doi.org/10.1134/S0020168512110064

22. Hansen M.F., Mørup S.J. Estimation of blocking temperatures from ZFC/FC curves. *J. Magn. Magn. Mater*. 1999;203:214–216. https://doi.org/10.1016/s0304-8853(99)00238-3

23. Mirgorod Yu.A., Borsch N.A., Yurkov G.Yu. Preparation of nanomaterials from aqueous solutions imitating the hydrometallurgy waste. *Russ. J. Appl. Chem*. 2011;84(8):1314–1318. http://doi.org/10.1134/S1070427211080039

24. Mirgorod Yu.A., Emelyanov S.G. Integrated technology for production of nanomaterials from poor ore and waste. *J. Min. Sci*. 2015;51(1):164–173. http://doi.org/10.1134/S1062739115010226

25. Matt B., Pondman K.M., Asshoff S.J., *et al.* Soft Magnets from the Self-Organization of Magnetic Nanoparticles in Twisted Liquid Crystals. *Angew. Chem. Int. Ed*. 2014;53(46):12446–12450. https://doi.org/10.1002/anie.201404312

26. Lisiecki I. From the Co Nanocrystals to Their Self-Organizations: Towards Ferromagnetism at Room Temperature. *Acta Phys. Polonica. A*. 2012;121(2):426–433. URL: http://przyrbwn.icm.edu.pl/APP/PDF/121/a121z2p58.pdf

27. Darling S.B., Yufa N.A., Cisse A.L., *et al*. Self-Organization of FePt Nanoparticles on Photochemically Modified Diblock Copolymer Templates. *Adv. Mater.* 2005;17(20):2446–2450.https://doi.org/10.1002/adma.200500960

28. Rusanov A.I., Nekrasov A.G. One more extreme near the critical micelle concentration: optical activity. *Langmuir.* 2010;26(17):13767–13769. https://doi.org/10.1021/la102514a

29. Farinato R.S., Rowell R.L. Transient light scattering in aqueous surfactant systems. *J. Colloid and Interface Sci.* 1978;66(3):483–491. http://doi.org/10.1016/0021-9797(78)90069-3

30. Yusof N.S.M. The effect of sonication on the ion exchange constant, K_X^{Br} of CTABr/chlorobenzoates micellar systems. *Ultrason. Sonochem*. 2021;71:105360. https://doi.org/10.1016/j.ultsonch.2020.105360

31. Maestro L.M., Marqués M.I., Camarillo E., *et al.* On the Existence of Two States in Liquid Water: Impact on Biological and Nanoscopic Systems. *Int. J. Nanotech.* 2016;13(8–9):667–677. http://doi.org/10.1504/IJNT.2016.079670

32. Fan H., Leve E.W., Scullin C., *et al*. Surfactant-Assisted Synthesis of Water-Soluble and Biocompatible Semiconductor Quantum Dot Micelles. *Nano Lett.* 2005;5(4):645–648. https://doi.org/10.1021/nl050017l

33. Rusanov A.I., Krotov V.V., Nekrasov A.G. Extremes of some foam properties and elasticity of thin foam films near the critical micelle concentration. *Langmuir.* 2004;20(4):1511–1516. https://doi.org/10.1021/la0358623

About the authors:

Yuri A. Mirgorod, Dr. Sci. (Chem.), Leading Researcher, Regional Center for Nanotechnology, Southwest State University (94, 50 Let Oktyabrya ul., Kursk, 305040, Russia). E-mail: yu_mirgorod@mail.ru. Scopus Author ID 87243112000, ResearcherID P-7243-2015, RSCI SPIN-code 7494-3982, https://orcid.org/0000-0003-0370-2465

Nikolay A. Borsch, Cand. Sci. (Chem.), Senior Researcher, Regional Center of Nanotechnology, Southwest State University (94, 50 Let Oktyabrya ul., Kursk, 305040, Russia). E-mail: nborsch@mail.ru. Scopus Author ID 55975582000, RSCI SPIN-code 6136-8418, https://orcid.org/0000-0002-8156-593X

Anastasia M. Storozhenko, Cand. Sci. (Phys.-Math.), Senior Researcher, Regional Center of Nanotechnology, Southwest State University (94, 50 Let Oktyabrya ul., Kursk, 305040, Russia). E-mail: storogenko_s@mail.ru. Scopus Author ID 36440356800, ResearcherID D-6103-2013, RSCI SPIN-code 9559-8284, https://orcid.org/0000-0002-4995-7407

Liliya S. Ageeva, Cand. Sci. (Chem.), Researcher, Regional Center of Nanotechnology, Southwest State University (94, 50 Let Oktyabrya ul., Kursk, 305040, Russia). E-mail: millfi@yandex.ru. Scopus Author ID 57016621700, RSCI SPIN-code 8986-8930, https://orcid.org/0000-0002-5644-3367

Об авторах:

Миргород Юрий Александрович, д.х.н., ведущий научный сотрудник Регионального центра нанотехнологий, ФГБОУ ВО «Юго-Западный государственный университет» (305040, Россия, г. Курск, ул. 50 лет Октября, д. 94). E-mail: yu_mirgorod@mail.ru. Scopus Author ID 87243112000, ResearcherID P-7243-2015, SPIN-код РИНЦ 7494-3982, https://orcid.org/0000-0003-0370-2465

Борщ Николай Алексеевич, к.х.н., старший научный сотрудник Регионального центра нанотехнологий, ФГБОУ ВО «Юго-Западный государственный университет» (305040, Россия, г. Курск, ул. 50 лет Октября, д. 94). E-mail: nborsch@mail.ru. Scopus Author ID 55975582000, SPIN-код РИНЦ 6136-8418, https://orcid.org/0000-0002-8156-593X

Стороженко Анастасия Михайловна, к.ф.-м.н., старший научный сотрудник Регионального центра нанотехнологий, ФГБОУ ВО «Юго-Западный государственный университет» (305040, Россия, г. Курск, ул. 50 лет Октября, д. 94). E-mail: storogenko_s@mail.ru. Scopus Author ID 36440356800, ResearcherID D-6103-2013, SPIN-код РИНЦ 9559-8284, https://orcid.org/0000-0002-4995-7407

Агеева Лилия Сергеевна, к.х.н., научный сотрудник Регионального центра нанотехнологий, ФГБОУ ВО «Юго-Западный государственный университет» (305040, Россия, г. Курск, ул. 50 лет Октября, д. 94). E-mail: millfi@yandex.ru. Scopus Author ID 57016621700, SPIN-код РИНЦ 8986-8930, https://orcid.org/0000-0002-5644-3367

The article was submitted: December 13, 2022; approved after reviewing: May 25, 2023; accepted for publication: October 06, 2023.

The text was submitted by the authors in English
Edited for English language and spelling by Dr. David Mossop

MATHEMATICAL METHODS AND INFORMATION SYSTEMS IN CHEMICAL TECHNOLOGY

МАТЕМАТИЧЕСКИЕ МЕТОДЫ И ИНФОРМАЦИОННЫЕ СИСТЕМЫ В ХИМИЧЕСКОЙ ТЕХНОЛОГИИ

ISSN 2686-7575 (Online)
https://doi.org/10.32362/2410-6593-2023-18-5-482-497
UDC 661.71+51-74

RESEARCH ARTICLE

Principles of creating a digital twin prototype for the process of alkylation of benzene with propylene based on a neural network

Konstantin G. Kichatov✉, Tatyana R. Prosochkina, Irina S. Vorobyova

Technological Faculty, Ufa State Petroleum Technological University, Ufa, 450062 Russia
✉Corresponding author, e-mail: kichatov_k@mail.ru

Abstract

Objectives. *To identify the principles of creating digital twins of an operating technological unit along the example of the process of liquid-phase alkylation of benzene with propylene, and to establish the sequence of stages of formation of a digital twin, which can be applied to optimize oil and gas chemical production.*

Methods. *The chemical and technological system consisting of reactor, mixer, heat exchangers, separator, rectification columns, and pump is considered as a complex high-level system. Data was acquired in order to describe the functioning of the isopropylbenzene production unit. The main parameters of the process were calculated by simulation modeling using UniSim® Design software. A neural network model was developed and trained. The influence of various factors of the reaction process of alkylation, separation of reaction products, and evaluation of economic factors providing market interest of the industrial process was also considered. The adequacy of calculations was determined by statistics methods. A microcontroller prototype of the process was created.*

Results. *A predictive neural network model and its creation algorithm for the process of benzene alkylation was developed. This model can be loaded into a microcontroller to allow for real-time determination of the economic efficiency of plant operation and automated optimization depending on the following factors: composition of incoming raw materials; the technological mode of the plant; the temperature mode of the process; and the pressure in the reactor.*

Conclusions. *The model of a complex chemicotechnological system of cumene production, created and calibrated on the basis of long-term industrial data and the results of calculations of the output parameters, enables the parameters of the technological process of alkylation to be calculated (yield of reaction products, energy costs, conditional profit at the output of finished products). During the development of a hardware-software prototype, adapted to the operation of the real plant, the principles and stages of creating a digital twin of the operating systems of chemical technology industries were identified and formulated.*

Keywords: *digital twin, cumene, industrial plant, neural networks, machine learning, ESP8266*

For citation: Kichatov K.G., Prosochkina T.R., Vorobyova I.S. Principles of creating a digital twin prototype for the process of alkylation of benzene with propylene based on a neural network. *Tonk. Khim. Tekhnol. = Fine Chem. Technol.* 2023;18(5):482–497. https://doi.org/10.32362/2410-6593-2023-18-5-482-497

НАУЧНАЯ СТАТЬЯ

Принципы создания прототипа цифрового двойника процесса алкилирования бензола пропиленом на основе нейронной сети

К.Г. Кичатов✉, Т.Р. Просочкина, И.С. Воробьева

Технологический факультет, Уфимский государственный нефтяной технический университет, Уфа, 450062 Россия
✉*Автор для переписки, e-mail: kichatov_k@mail.ru*

Аннотация

Цели. *Выявление принципов создания цифровых двойников реально действующей технологической установки на примере процесса жидкофазного алкилирования бензола пропиленом и установление последовательности этапов формирования цифрового двойника, которая может быть применима для оптимизации работы нефтегазохимического производства.*

Методы. *Рассмотрена в целом химико-технологическая система, состоящая из реактора, смесителя, теплообменников, сепаратора, ректификационных колонн и насоса, как система высокого уровня. Выполнен сбор данных, описывающих функционирование установки получения изопропилбензола алкилированием бензола пропиленом путем расчета основных параметров процесса с помощью имитационного моделирования с применением специализированного программного обеспечения UniSim® Design. Разработана и обучена нейросетевая модель, учитывающая влияние различных факторов реакционного процесса алкилирования, разделения продуктов реакции и оценки экономических факторов, обеспечивающих рыночную привлекательность рассматриваемого промышленного процесса. Определена адекватность результатов расчетов оптимальных параметров процесса методами математической статистики. Создан прототип цифрового двойника процесса, реализованной на микроконтроллере.*

Результаты. *Создана прогностическая нейросетевая модель и алгоритм ее построения для процесса алкилирования бензола пропиленом, позволяющая при загрузке ее в микроконтроллер обеспечить в режиме реального времени определение экономической эффективности работы установки и автоматическую оптимизацию работы установки в зависимости от состава поступающего сырья технологического режима системы, температурного режима проведения процесса и давления в реакторе.*
Выводы. *Созданная модель сложной химико-технологической системы производства кумола, откалиброванная на основании промышленных данных длительного пробега технологической установки и результатов расчетов выходных параметров процесса при помощи нейронной сети, реализованной на микроконтроллере, позволяет рассчитать параметры технологического процесса алкилирования (выход продуктов реакции, энергетические затраты, условную прибыль при выпуске готовой продукции). В процессе разработки прототипа программно-аппаратного комплекса управления установкой алкилирования бензола пропиленом на основе данных, адаптированных к работе реальной установки, были выявлены и сформулированы принципы и этапы создания цифрового двойника производственных систем отраслей химической технологии.*

Ключевые слова: *цифровой двойник, кумол, промышленная установка, нейронные сети, машинное обучение, ESP8266*

Для цитирования: Kichatov K.G., Prosochkina T.R., Vorobyova I.S. Principles of creating a digital twin prototype for the process of alkylation of benzene with propylene based on a neural network. *Tonk. Khim. Tekhnol. = Fine Chem. Technol.* 2023;18(5):482–497. https://doi.org/10.32362/2410-6593-2023-18-5-482-497

INTRODUCTION

The petrochemical industry is one of the largest sectors of the world economy. The main trends in the development of modern petrochemistry are aimed at increasing the capacity of petrochemical plants and the selectivity of chemical reactions, reducing the energy intensity of chemical technological processes, processing of new types of raw materials, and environmental safety of production. The key results of these processes will be to increase the efficiency of petrochemical productions.

The modernization and technical re-equipping of operating plants are carried out, as a rule, on the basis of experimental data without the appropriate scientific study. The methods of chemical technological processes optimization applied do not allow us to cover comprehensively the whole range of characteristics and factors affecting the production process. Existing approaches to the selection of the current operating parameters are based primarily on the experience of operators and process engineers, thus limiting the possibility of eliminating shortcomings associated with the human factor [1].

Currently, digital processes using artificial intelligence technologies are being increasingly introduced, in order to resolve urgent production problems and improve the efficiency of industrial enterprises. One of the most effective ways of solving this problem today is mathematical modeling using neural network technologies using modern hardware and software systems.

The use of neural networks based on Big Data provides a unique opportunity to establish the hidden relationships of the qualitative and quantitative characteristics of feed streams, fuel, cooling water, and electricity consumed by cumene with production efficiency indicators. In the

conditions of existing production, this enables the potential for increasing energy saving in a short time to be identified and the number of measures needed to optimize industrial technological processes to be significantly reduced: redistribution of feed streams, fuel, water, and electricity [2].

At the same time, the application of intelligent systems in the industrial sector is often implemented with the use of cloud data storage and distributed computing. The use of external cloud systems poses certain difficulties and risks:

– high cost of ownership of cloud services infrastructure;

– the possibility of unauthorized access by the provider's personnel due to insufficient data protection;

– temporary loss of access to information may occur as a result of network equipment failures[1].

Industrial companies are concerned about the uninterrupted operation of all plant facilities and services. The risks associated with the transfer of data and calculations for the management of existing production to external cloud resources are a potential threat to the safety of operation of existing fire and explosion hazardous facilities. In this regard, embedded solutions based on industrial controllers and supervisory control and data acquisition (SCADA) systems are currently a fault-tolerant alternative to external cloud services.

The basic unit of a digital intelligent system at an industrial petrochemical enterprise is a digital twin (DT). This is a digital (virtual) model of industrial facilities, systems and processes of an enterprise which accurately reproduces the characteristics and actions of the original and is synchronized with it. The DT is used to simulate events which occur with the original under certain conditions, significantly reducing the time and material costs for testing complex and expensive equipment, thus preventing possible emergencies and ensuring the safety of existing production[2].

Classification of DTs by levels of integration with a real production facility[3,4]:

– DT prototype is a virtual analogue of the facility, including all the data for reproducing the original object;

– DT instance is a database of all characteristics, operational properties, and information about the operation of a physical facility, including its three-dimensional model and functioning in parallel with the original;

– DT aggregate is a collected intelligent cyber physical system including DTs and real facilities, controlled from a single center and exchange data with each other online.

The development of new digital technologies has marked the arrival of the fourth industrial revolution (Industry 4.0) [3] and the trend towards the re-profiling of all sectors of industrial production. Using supply chain management-marketing systems as an example, [4] enabling technologies that enable the transition to Industry 4.0 were identified: advanced manufacturing, additive manufacturing, augmented reality, simulation, cloud computing, industrial Internet of Things (IoT), cyber security, and Big Data analytics and customer profiling. Among these, the most used digital technologies are mobile and cloud computing, IoT, big data analytics, and blockchain [5].

Digital transformation is profoundly changing our way of living, rendering obsolete not only products or services, but also the way in which firms organize their business processes along with how they create and capture value. Thereby, reinventing a business model is mandatory for incumbents in their attempt to survive in the changing digital world [6].

At the same time, [7] notes that information on available assistive technologies and trends is scarce and limits the ability to make appropriate decisions.

The concept of Digital Transformation itself is multifaceted [8]. In [9], the different types of digital transformation impacts on innovation processes are classified, and barriers to integrating digital competencies into traditional companies are described. It should be noted that research on the relationship of digital transformation to innovation processes and innovation management is at an embryonic stage. The concept of DT is analyzed in [10]. It was shown that DTs of technological processes may be used for monitoring.

The effectiveness of digitalization is clear: it enables industry processes to be automated, a variety of information to be stored and data analyzed. It can also predict future incidents and system states [11]. 2021 has been a year of growth in the active involvement of global oil and gas companies in business transformation from upstream to downstream,

[1] "We risk losing data and breaking the law" – why companies are afraid of the clouds. VC.ru. 2021. Available from URL: https://vc.ru/promo/246963-riskuem-poteryat-dannye-i-narushit-zakon-pochemu-kompanii-opasayutsya-oblakov. Accessed January 5, 2022.

[2] Zuykova A. What are digital twins and where are they used. RBC. 2021. Available from URL: https://trends.rbc.ru/trends/industry/6107e5339a79478125166eeb. Accessed January 5, 2022.

[3] Prokhorov A. Digital twins. The concept is evolving. C-News. 2018. Available from URL: https://data.cnews.ru/articles/2018-04-18_tsifrovye_dvojniki_kontseptsiya_razvivaetsya. Accessed January 5, 2022.

[4] Digital twin technology. Future2Day. 2019. Available from URL: https://future2day.ru/texnologiya-cifrovyx-dvojnikov/. Accessed January 5, 2022.

with the re-engineering of production strategies and operating models taking the lead. Ceipek *et al*. [12] conducted an analysis of a 10-year US panel dataset showing that underperforming firms are more willing to engage in the emerging digital transformation, while a superior level of prior performance make firms less inclined to engage in such digital technologies. As a rule, the management of large successful companies is not willing to change and upgrade resources to include digital technologies, because they are inert and inflexible, and the volume of production is high. Such companies lack incentives to adopt advanced digital technologies [13]. Therefore, company boards of directors are often the inhibitor of digital change in this case. Managers also need to actively combat myopia, inertia, or rigidities that ensue from an established product and business logic to ensure the exploration of cutting-edge solutions for future product development [12]. This inertia is partly explained by the fact that according to estimates made by [14], 66% to 84% of digital transformation projects fail, 13% of which is a sizable share considering the costs, both monetary and otherwise, of putting these projects in place. Nevertheless, more and more business leaders have recently begun to understand the importance of using digital data and analytics to improve business performance[5].

Digital transformation can lead to notable advantages for firms, such as helping to create products and services that are more efficient and consistent with customer needs, thus providing a shorter innovation process and time to market, and creating related digital ecosystems [15].

In 2002, Michael Greaves gave a lecture in which he formulated the world's first concept of DTs [16].

Digital twinning in industry was first applied in the aerospace industry [17], but the oil industry has long used only traditional modeling and optimization techniques. Nowadays, in oil and gas chemistry, the use of DTs is becoming increasingly important [18, 19].

The classification of data from the literature on the use of DTs of production systems has shown that three options for their use are possible:

1) modeling the reliability of systems, the ability to plan their maintenance by monitoring anomalies, deformations, fatigue cracks, diagnosis of the state of the existing physical object;

2) study of system behavior at each stage of life cycle and prediction of its characteristics by digital simulation of physical object and control of its life cycle using the IoT concept;

3) optimizing the behavior of the system at the design stage prior to the creation of the physical object, or optimizing and predicting the characteristics of the product life cycle based on its past and present states [17].

In [20], information on various factors enabling the application of DTs in industry and creating barriers to their implementation is systematized. Currently, there are two approaches to describing DTs [21]:

– a full equivalent of a cyber-physical system;

– only one, key and fundamental, component of a cyber-physical system out of several possible ones [22]. This also stresses the opinion that a true DT provides an automatic bidirectional data transfer between the digital and the physical counterparts [23]. This distinguishes DTs from digital models with manual information transfer and from digital shadows, in which the collection of information from the physical object to the digital analogue is automatic and the reverse data transfer is done manually [24].

The authors [25] provide information on existing methods for designing DTs, based on data from a real object[6], or from a real physical system [26], or a combination of these approaches, resulting in the greatest added value and functionality of the twin.

Although Industry 4.0 proposes the use of DTs in industry for predictive maintenance and aftermarket analysis, there are few applications in this area. This is due to imperfect methodology for developing real-time DT models, limited synchronization capabilities between the digital and physical object [27], problems with Big Data collection and processing, a lack of highly accurate models for multilevel object representation, and difficulties in implementing them in production, including due to companies' resistance to change. New generation information technology [28], which provides a continuous exchange of information between DT and production facilities [29], can help to resolve this problem.

There are successful examples of application of DTs for solving problems of optimization of industrial plants. These include the optimization of the reactor unit of styrene production in the Tabriz petrochemical complex using an artificial neural

[5] Booth A., Patel N., Smith M. Digital transformation in energy: Achieving escape velocity. 2020. Available from URL: https://www.mckinsey.com/industries/oil-and-gas/our-insights/digital-transformation-in-energy-achieving-escape-velocity#. Accessed January 5, 2022.

[6] Steve Miller. Predictive Maintenance Using a Digital Twin. 2019. Available from URL: https://www.mathworks.com/company/newsletters/articles/predictive-maintenance-using-a-digital-twin.html. Accessed January 5, 2022.

network and an adaptive neuro-fuzzy inference system [30], improving the energy efficiency of furnace equipment using a DT integrated into the SCADA system [31] and coke formation prediction at a catalytic cracking unit [32].

In this regard, it is thus pertinent to identify the principles of creating a DT of the process of liquid-phase alkylation of benzene with propylene, a prototype of an intelligent industrial process control system.

MATERIALS AND METHODS

Chemical process description

The method of coproduction of phenol and acetone by oxidation of cumene obtained by gas-phase alkylation of benzene with propylene over $AlCl_3$ catalyst, was first developed and introduced into industrial production in the Soviet Union by a group of chemists (P.G. Sergeev, R.Yu. Udris, and B.D. Kruzhalov). At present in global industry, cumene is mainly produced on zeolite catalysts (licensors of the modern alkylation process are such companies as BADGER[7], UOP[8], LUMMUS[9], and IFP[10]) [33, 34]. Processes for the production of cumene, phenol, and acetone from cumene are constantly being improved. Various methods for intensifying the process have been proposed, for example by optimizing the recycle flows in the alkylation process or introducing ozone as an initiator in the cumene oxidation process [35].

Works are known in which the optimization of the alkylation process was carried out by means of traditional technological methods (carrying out the process using a reactive distillation column [36], the introduction of additional separation columns [37]). Other authors have proposed ways of intensification based on the results of mathematical modeling using conventional approaches. Thus, the authors of [38] applied a computer model written in Borland Delphi and defined the optimal parameters of the alkylation process to increase product yield and decrease catalyst consumption. In previous studies [39], we proposed a model of the reactor block in Aspen® HYSYS (*Aspen Technology, Inc.*, USA)[11], which enables the cumene yield in the alkylator to be calculated with sufficient accuracy and optimal parameters of the process conditions to be selected depending on the required productivity. At the same time, the results of such modeling are “idealized”, since it is not possible to take into account all the factors of real production. Therefore, the optimal operating parameters calculated on the basis of such models cannot be directly applied in real faculties and require additional clarification. The regulation of technological mode parameters is performed by means of the SCADA, based on the laws of proportional–integral–derivative regulation. However, the main responsibility for making decisions on the choice of operating parameters lies with operators. This can lead to errors due to human factor, including suboptimal process management and loss of profit share.

Application of DTs based on neural network modeling technologies not only allows all the factors affecting the equipment (including hidden ones) to be taken into account, but also plant operation to be reproduced as accurately as possible and continuously synchronized. As a result, it is possible to regulate process mode parameters by applying a new type of controllers integrated into intelligent cyberphysical systems and automatically to optimize plant operation online without operator intervention. This approach is currently the first step towards the creation of smart manufacturing, or more correctly called intelligent manufacturing.

In [40], for the liquid-phase alkylation process, modeling was performed using two-layer neural networks. The optimum values were calculated for temperature and pressure in the reactor, as well as its length, allowing the maximum yield of cumene to be obtained. The authors [41], simulated the yield and selectivity of benzene alkylation reaction products formation with propylene using two-layer neural networks and compared the calculated data with the experimental results with an average relative error ranging from 3.7% to 7.7%.

However, there is no information in the literature regarding the creation of DTs of the process of liquid-phase alkylation of benzene with propylene based on neural networks, in which the output parameter is the profit of the process unit.

Creating a database of raw data

The creation of a DT of the cumene production process implies the development of a virtual model which enables not only the process conditions to be reliably repoduced, but also, as a result of continuous analysis of stream data, to regulate the process faster than the operator can react to the event.

[7] Badger Licensing LLC. 2021. Available from URL: https://www.badgerlicensing.com/. Accessed January 5, 2022.

[8] UOP. 2022. Available from URL: https://uop.honeywell.com/. Accessed January 5, 2022.

[9] Lummus Technology. 2022. Available from URL: https://www.lummustechnology.com/. Accessed January 5, 2022.

[10] IFP Energies nouvelles (IFPEN). 2022. Available from URL: https://www.ifpenergiesnouvelles.com/. Accessed January 5, 2022.

[11] Aspen Technology, Inc. 2022. Available from URL: https://www.aspentech.com/en. Accessed January 5, 2022.

In order to develop such a virtual model of a chemical technological process, the operation of a complex multiparameter system must be reproduced.

The first step in creating a DT is simulation using data, obtained from the factory set. In order to show the possibility of developing a model of a DT of the process, despite the lack of data from a real process unit, we created our own initial database by simulating the process unit in the Honeywell UniSim® Design[12] software .

The reactor was modeled according to the method described in [39]. In order to form a detailed model of the alkylation reactor, 13 chemical reactions (1 main and 12 side) were used, the kinetic parameters of which are given in Table 1. As part of the creation of a DT model, it was assumed that the kinetic parameters of the reactions were constant in the range of the selected values of temperature and pressure.

In a continuation of studies of the alkylation process, the reactor model was supplemented with a separation system using commercial-grade cumene production.

The design scheme includes three blocks: raw materials preparation, reaction block, and a separation system. The process equipment consisted of a reactor for alkylation and transalkylation reactions, two columns—atmospheric column for extracting benzene from the reaction mass and a vacuum column for separating a mixture of cumene and diisopropylbenzenes, a separator for separating off-gases, six heat exchangers, a mixer, and a pump.

Figure 1 shows a simplified scheme for the production of cumene.

In the feed preparation unit, the initial benzene and propylene are mixed with recycled diisopropylbenzenes (Dcumene) in the mixer M-1, then heated to 60°C. This mixture is fed to the reaction unit, modeled on the basis of the equilibrium reactor R-1 and the separator SK-1. From here unreacted off-gases (propane, ethane) are released. This reactor is characterized by complete conversion of propylene into reaction products. The selectivity for cumene is about 99%.

The separation system is a system of columns RC-1 and RC-2. Column RC-1 is designed to extract benzene from the reaction mass which returns

Table 1. Kinetic parameters of the reactions of the alkylation of benzene with propylene at a temperature of 122°C and a pressure of 1.6 bar

Reaction	A_0, c^{-1}	E_a, kJ/mol	k, c^{-1}
1	2	3	4
$C_6H_6 + C_3H_6 \rightarrow i{-}C_6H_5CH(CH_3)_2$	$1.58 \cdot 10^5$	150.94	$3.74 \cdot 10^{-12}$
$C_6H_5CH(CH_3)_2 + C_3H_6 \rightarrow C_6H_4(CH(CH_3)_2)_2$	$2.26 \cdot 10^5$	128.81	$1.47 \cdot 10^{-9}$
$C_6H_4(CH(CH_3)_2)_2 + C_3H_6 \rightarrow C_6H_3(CH(CH_3)_2)_3$	$1.80 \cdot 10^4$	140.64	$5.81 \cdot 10^{-12}$
$C_6H_6 + C_3H_6 \rightarrow n{-}C_6H_5C_3H_7$	$1.28 \cdot 10^5$	130.41	$5.53 \cdot 10^{-10}$
$2C_3H_6 \rightarrow C_6H_{12}$	$1.97 \cdot 10^5$	116.20	$6.68 \cdot 10^{-13}$
$2C_2H_4 \rightarrow CH_2{=}CH{-}C_2H_5$	$1.65 \cdot 10^6$	166.98	$7.64 \cdot 10^{-10}$
$2\,C_2H_4 \rightarrow CH_3{-}CH{=}CH{-}CH_3$	$2.92 \cdot 10^6$	141.47	$2.00 \cdot 10^{-9}$
$2C_2H_4 \rightarrow CH_2{=}C(CH_3)_2$	$3.95 \cdot 10^6$	138.86	$3.13 \cdot 10^{-8}$
$C_6H_6 + CH_2{=}CH{-}C_2H_5 \rightarrow C_6H_5CHCH_3C_2H_5$	$5.45 \cdot 10^6$	159.90	$1.33 \cdot 10^{-11}$
$C_6H_6 + CH_2{=}C(CH_3)_2 \rightarrow C_6H_5C(CH_3)_3$	$5.65 \cdot 10^5$	158.23	$2.11 \cdot 10^{-12}$
$C_6H_6 + CH_2{=}CH{-}C_2H_5 \rightarrow C_6H_5C_4H_9$	$1.42 \cdot 10^6$	147.95	$7.18 \cdot 10^{-11}$
$C_6H_6 + C_2H_4 \rightarrow C_6H_5C_2H_5$	$7.16 \cdot 10^5$	37.40	$5.15 \cdot 10^{-10}$
$C_6H_5C_2H_5 + C_2H_4 \rightarrow C_6H_4(C_2H_5)_2$	$2.90 \cdot 10^4$	129.58	$1.55 \cdot 10^{-10}$

Note: A_0 is the pre-exponential factor or Arrhenius equation, E_a is the activation energy for the reaction, k is the rate constant.

[12] Honeywell International Inc. 2022. Available from URL: https://honeywell.com. Accessed January 5, 2022.

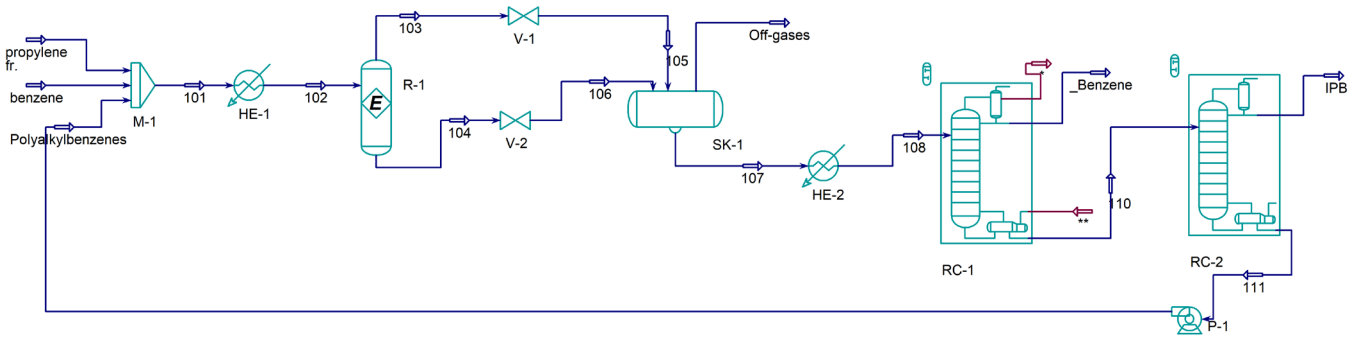

Fig. 1. Simplified scheme for the production of cumene:
M-1 – mixer; HE-1, HE-2 – heat exchangers; R-1 – reactor; SK-1 – separator; RC-1, RC-2 – distillation columns.

to the feed preparation unit (not shown in the diagram). The column has 56 valve trays, the top and bottom temperatures are 108.5 and 186.0°C, respectively. A mixture of cumene and Dcumene is fed into the RC-2 vacuum separation column, where they are separated at a column top pressure of 200 mm Hg. Column RC-2 consists of 23 valve trays, top and bottom temperatures are 134.0 and 189.0°C, respectively. From above, commercial-grade cumene is obtained, and Dcumenes are removed from the cube, which are sent for mixing with the initial benzene and propylene.

The temperature (from 128 to 147°C) and pressure (0.15 to 0.24 MPa) of the process in the reactor, the ratio of benzene to propylene (from 3:1 to 4:1), corresponding to the operating ranges of the installation under consideration were selected as input parameters of the neural network. The output parameter, in contrast to the works of other authors, is the principle profit from the process.

The values of the principal profit from the sale of cumene *PP*, RUR/h, were calculated by Eq. (1), taking into account the income from the sale of cumene and the cost of energy resources of the installation.

$$PP = C \cdot i \cdot P_i - a \cdot P_a - b \cdot P_b - c \cdot P_c, \quad (1)$$

where C is the cumene concentration in a commercial product, i is the amount of cumene produced, kg/h, a is the water vapor consumption, kg/h, b is the circulating water consumption, kg/h, c is the electricity consumption, kW/h, is the calculated data obtained from the model. Constant values: P_i is the price of commercial cumene, accepted at 4.7825 RUR/kg, P_a is the price of water vapor, accepted at 1.19 RUR/kg, P_b is the price of circulating water, accepted at 7.11 RUR/kg, P_c is the price of electric power, accepted at 2.50 RUR/kW.

The energy requirements are determined using the UniSim® Design cumene production plant model. Steam is used as a heat carrier in reboilers of columns RC-1 and RC-2, heat exchangers of propylene fraction and benzene (HE-1, HE-2), and a feed preheater in front of the reactor. Recycled water is used in the condensers of the columns RC-1, RC-2, in order to reduce the temperature in the reactor and cool the bi-Dcumenes after the column RC-2. The P-1 pump consumes electric power.

Selection of the topology and learning algorithm for the neural network

The data obtained as a result of modeling the technological unit in the UniSim® Design software was used to create a predictive neural network model of the process. Based on the structural approach, this enables the principal profit of the unit to be established depending on the feedstock composition, the temperature of the process, and the pressure in the reactor.

We used a two-layer direct communication network with sigmoidal transfer functions (2) of neurons in the hidden layer:

$$\sigma(x) = \frac{1}{1+e^{-x}} \quad (2)$$

and linear transfer functions in the output layer of neurons (Fig. 3). The choice was due to the fact that such a neural network configuration takes into account the non-linear effects of the original process model. However, at the same time, the computational complexity of the sigmoid function allows it to be used in devices with limited performance (embedded solutions, microcontrollers, etc.). The two-layer network was chosen because in the paper [41], when solving a similar problem, reliable results were obtained.

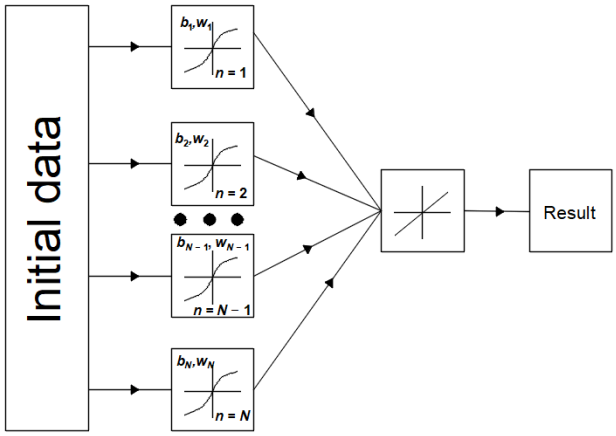

Fig. 3. Model of the used neural network. $b_1 \ldots b_N$ are bias terms of each perceptron, $w_1 \ldots w_N$ are weight vectors of each perceptron, n is the index, N is the number of perceptions in model.

All data was divided into 3 groups: learning curve (70%), training sample (15%), and data for testing the network (15%).

The learning curve is used to train the neural network, after which the neural network is trained in one iteration. Then the learning curves and training samples are mixed and the process is repeated until the minimum value of the standard deviation of the training sample is found. Subsequently the neural network is tested with the calculated values of weights and biases on the data for validation.

We used the Levenberg–Marquardt algorithm (backpropagation algorhythm), Bayesian regularization algorhythm and scaled conjugate gradient algorhythm in the MATLAB® software package[13] (*MathWorks*, USA). The choice of the neural network training algorithm was made by comparing the regression coefficient R.

CALCULATION OF TRANSFER FUNCTIONS COEFFICIENTS

When creating a DT based on a neural network model, the process of continuous receipt at the input of the neural network model of the initial process parameters needs to be organized (in this case, temperature, pressure, reagent ratio) along with their transformation into the output data of the model (in this case, principal profit). In order to produce the model in the form of a computational module of the DT of the process, calculation of transfer functions coefficients is required. This was performed using a program written in Python programming language using the NumPy[14] and Pandas[15] libraries.

When calculating the coefficients, the network topology and the learning algorithm selected in the previous stage in MATLAB® software were used.

RESULTS AND DISCUSSION

After modeling, we obtained a database for creating a DT. Database includes 2100 values by varying the input parameters (temperature, pressure in the reactor and the benzene/propylene ratio) in the operating ranges of the plant under consideration. At each step, UniSim® Design performed calculation of the entire model, the costs of commercial-grade cumene and energy resources were determined, and then the principal profit was calculated.

The model created in UniSim® Design is three-parameter. The assessment of the reliability of the data obtained was carried out by comparing one-factor calculations and known theoretical laws.

With a benzene/propylene ratio equal to 3:1 (Fig. 2a), an increase in the principal profit is observed with an increase in pressure from 0.15 to 0.24 MPa and an increase in temperature from 128 to 140°C. Fluctuations of the principal profit values are explained by the multifactorial influence of energy consumption in the columns of the separation system. Increasing the temperature in the reactor increases the process rate, but is thermodynamically disadvantageous due to the exothermicity of the process. Despite the increase of energy consumption in the reactor and a decrease in the selectivity of the target reaction, with an increase in the process temperature, costs are compensated by reducing the consumption of steam in the separation columns and growth of the principal profit.

An increase in pressure leads to an increase in the principle profit by increasing the product yield from the reactor, reducing steam and cooling water consumption, even though the circulating pump's power consumption increases.

Carrying out the process with a benzene ratio of 4:1 (Fig. 2b) is economically unprofitable for any combinations of temperature and pressure (negative principal profit), since, although feeding more benzene into the reactor leads to greater process selectivity, the cost of benzene separation in the K-1 column exceeds the effect of higher cumene yield.

[13] MATLAB. 2022. Available from URL: https://www.mathworks.com/products/matlab.html Accessed January 5, 2022.

[14] NumPy. 2022. Available from URL: https://numpy.org/. Accessed January 5, 2022.

[15] Pandas. 2022. Available from URL: https://pandas.pydata.org/. Accessed January 5, 2022.

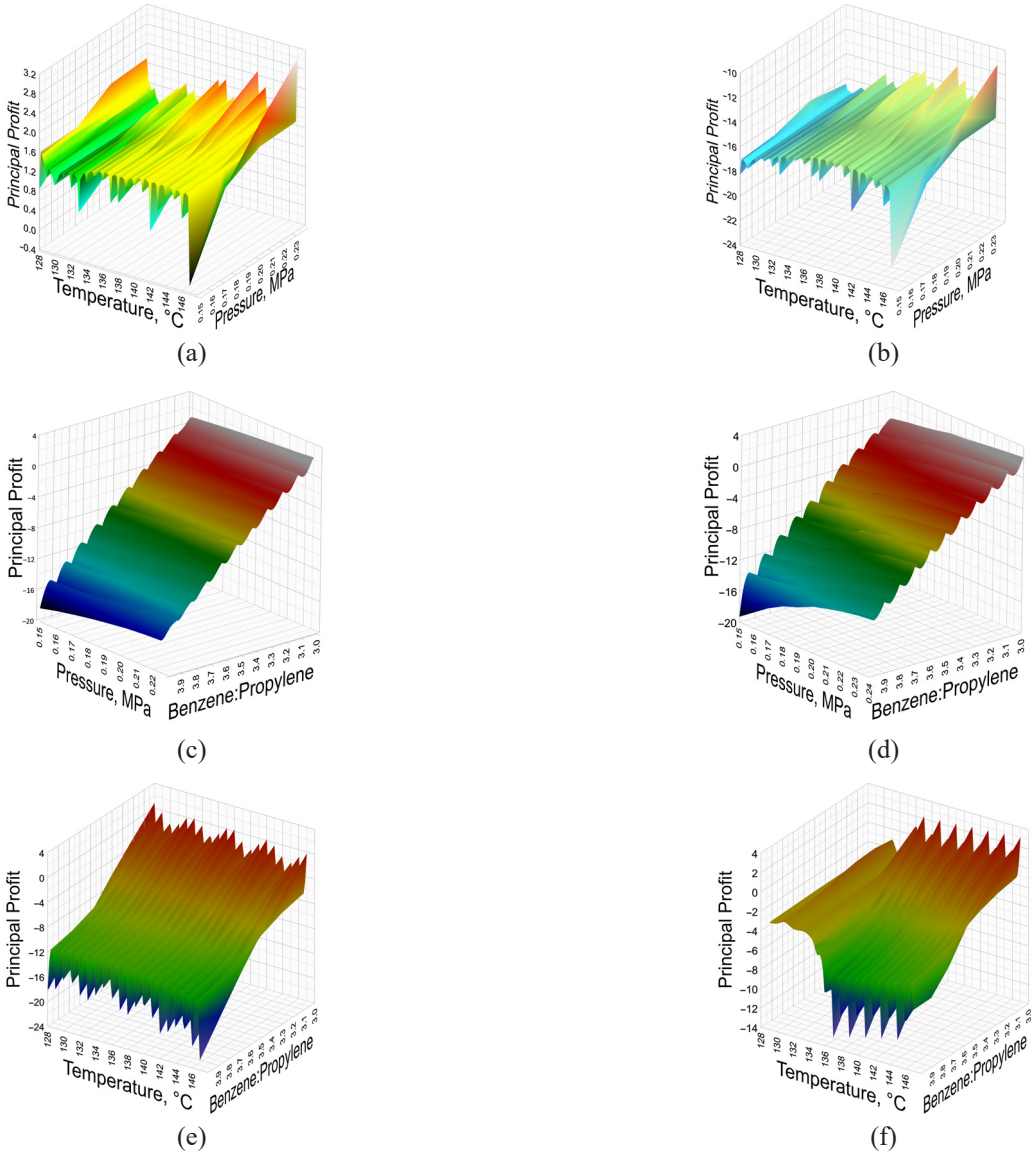

Fig. 2. Dependence of the principal profit on the parameters of the technological process at fixed values: The benzene/propylene ratio = 3:1 (a), 4:1 (b), temperature in the reactor 128°C (c), 140°C (d), pressure in the reactor 0.15 MPa (e), 0.24 MPa (f).

At a fixed temperature of 128 and 140°C (Figs. 2c and 2d), the pressure increase does not lead to a significant increase in the principal profit. At the same time, increasing the amount of fed benzene in relation to propylene significantly reduces the principle profit due to the growth of costs of benzene separation in the column RC-1.

At a minimum fixed pressure of 0.15 MPa (Figs. 2e and 2f), the increase in temperature does not significantly affect the principal profit, while at a pressure of 0.24 MPa, a slight increase in the principal profit is observed.

Thus, the maximum principal profit is achieved with a minimum benzene/propylene ratio of 3:1 and temperatures and pressures of 140°C and 0.25 MPa, respectively. This corresponds to the known theoretical laws.

Nevertheless, in a real process unit, the process is not carried out at the maximum parameter limit (due to triggering of interlocks, the need to ensure the safety of the technological process). Within the ranges, the influence of process parameters on the principal profit is non-linear, therefore, the selection of regression equations describing the process accurately enough is extremely difficult in this case, Optimization requires methods to be used which describe non-periodic series with a trend other than linear, such as neural networks.

The choice of neural network training algorithms (Levenberg–Marquardt algorithm (backpropagation algorhythm), Bayesian regularization algorhythm and scaled conjugate gradient algorhythm) was made by comparing the regression coefficient *R*. The smallest standard deviation corresponds to the

back-propagation algorithm with 12 neurons in the first hidden layer. In this case, the neural network is trained for 54 epochs (Table 2, Fig. 4).

The program allows for the continuous refinement of the transfer functions coefficients, while taking into account the possible arrival of new initial data from production plants (Table 3).

Development of the DT prototype

We chose the ESP8266 microcontroller developed by *Espressif Systems* (Chine) as a prototype of an industrial ACS (automatic control system) controller with an implemented DT: one of the leaders in the development of hardware solutions for the IoT.

The advantages of ESP8266 as a model tool in comparison with other microcontrollers are: prevalence, low price, standard programming language "C", open-source program code, libraries, availability of sensor expansion boards, input-output devices, availability of standard input-output ports (with I2C, SPI, UART, GPIO interfaces), an analog-to-digital converter, which allows for data acquisition and demonstration platform processing, as well as easy integration with industrial controllers. Also, the microcontroller has sufficient computing and communication capabilities for it to be used in solutions for the IoT (single-core 32-bit LX6 microprocessor, up to 160 MHz, program memory 4 MB, ROM 2.4 MB, RAM 32 KB, WiFi module) [43], [44].

This device is programable using specialized software: compiler, linker, and programmer. We used the PlatformIO integrated development environment to create a program [45] to calculate the principal profit of the production unit based on technological parameters. The program was loaded into a microcontroller which will independently receive the initial data from the sensors and produce the result.

Thus, we were able to create a prototype of a DT based on a microcontroller, allowing for the operation of a cumene production unit to be simulated and the process mode optimized. When training a neural network based on data from a real operating plant, the neural network can automatically take into account the specific features of the technological process.

Table 2. Results of neural network modeling

Number of neurons in the hidden layer	Algorithm								
	Backpropagation			Bayesian regularization			Scalable conjugate gradients		
	Number of epochs	Standard deviation MSE	Regression value *R*	Number of epochs	Standard deviation MSE	Regression value *R*	Number of epochs	Standard deviation MSE	Regression value *R*
1	24	1.37	0.9905	48	0.92	0.9926	57	0.76	0.9934
2	94	0.18	0.9986	50	0.12	0.9991	63	0.72	0.9935
3	71	0.23	0.9982	170	0.18	0.9985	200	0.23	0.9982
4	18	0.20	0.9985	72	0.31	0.9976	112	0.55	0.9958
5	45	0.18	0.9986	240	0.11	0.9991	79	0.10	0.9991
6	22	0.36	0.9972	126	0.20	0.9985	66	0.15	0.9989
7	50	0.43	0.9969	258	0.19	0.9986	84	0.36	0.9972
8	17	0.09	0.9993	538	0.31	0.9975	140	0.38	0.9970
9	27	0.37	0.9972	684	0.29	0.9976	62	0.73	0.9940
10	20	0.07	0.9995	673	0.18	0.9985	191	0.42	0.9969
11	43	0.29	0.9977	323	0.08	0.9994	48	1.70	0.9886
12	**54**	**0.03**	**0.9998**	**353**	**0.17**	**0.9986**	**235**	**0.17**	**0.9986**
13	80	0.06	0.9995	1000	0.48	0.9963	211	0.21	0.9982
14	48	0.31	0.9975	1000	0.35	0.9973	222	0.76	0.9940
15	13	0.05	0.9997	803	0.17	0.9985	240	0.27	0.9980

Note: MSE is a mean squared error.

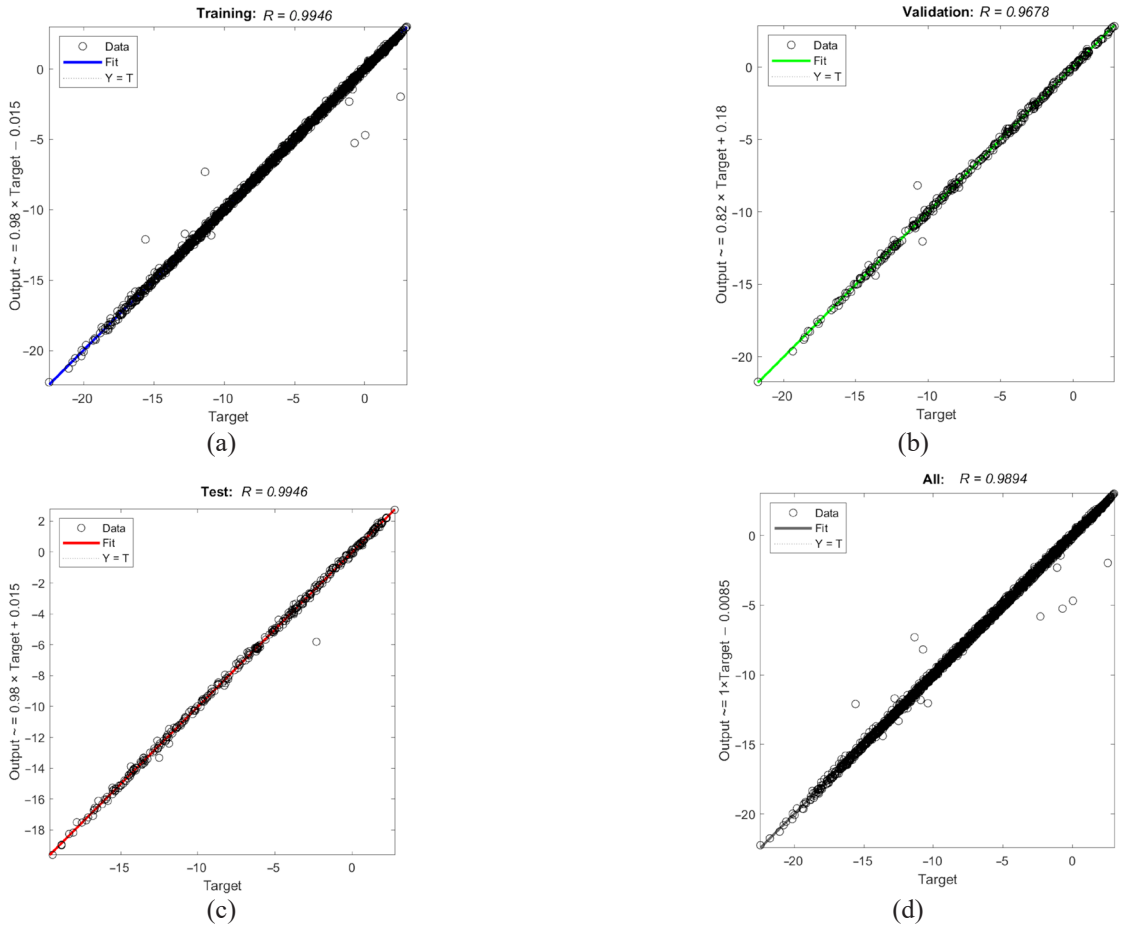

Fig. 4. The results of the selection of the neural network configuration:
(a) on the learning curve (70% of the data), (b) on the test set (15% of the data), (c) on the control sample (15% of the data), (d) on all the data (100% of the data). Target is the target value of the principal profit, Data is the calculated points, Fit is the result of the neural network, Y = T (Output = Target) is the perfect match line.

Table 3. Coefficients of the transfer function of the neural network

First hidden layer					Second hidden layer		
Neuron number	Coefficients				Neuron number	Coefficients	
	b	w_1	w_2	w_3		*b*	*w*
1	2.388	−1.982	−1.258	0.410	1	−0.381	−0.020
2	−2.198	1.085	−1.129	−2.321			0.027
3	−1.643	0.623	−0.406	0.549			−1.196
4	2.214	−2.470	0.227	−0.473			−0.027
5	0.186	−0.254	0.028	−1.003			0.223
6	0.168	0.531	0.207	−0.315			0.547
7	0.338	1.550	−1.577	−1.462			0.023
8	−1.475	−0.512	−0.040	−0.480			0.905
9	1.997	0.659	−2.912	0.074			−0.009
10	1.417	0.409	−0.742	−0.903			0.186
11	−1.433	−1.565	−2.107	1.744			−0.010
12	−2.498	−1.126	−0.720	1.040			−0.145

Note: b is the bias term of each perceptron, w_1, w_2, w_3, *w* are weight vectors of each perceptron.

Based on the prototype, it is planned to create simulators for training production personnel, as well as integrated solutions for optimizing the operation of process units.

The production of cumene is large-scale, so the implementation of the results of this work in terms of the use of new digital technologies may be associated with certain difficulties due to lack of motivation, inertia and lack of obvious need to change the technological base.

Also the promotion of DTs in industry is strongly influenced by the shortage of integrated circuits and financial crises, during which the management seeks to maintain production, while avoiding risks associated with the introduction of innovative technologies and approaches in production. An important factor when creating DTs based on big data from manufacturing, is that the data generated must be professionally and efficiently processed and filtered for subsequent analysis; otherwise the results will be unreliable. There may also be uncertainties associated with errors in the operation of instrumentation, controllers, and actuators of the control system. A partial solution of this problem may be the involvement of a group of qualified specialists, consisting of programmers, technologists, and scientists for screening, classifying and filtering the meaningful data from the database.

A DT obtained using big data, based on a simulation model, cannot in principle take into account all the factors which impact a real plant. Therefore, the DT obtained in this way must be adapted to each specific industrial plant, training it further on data from a real plant.

Our proposed DT prototype can be used in the future to create simulators, useful for training personnel of cumene production.

Further research will be directed towards the creation of an aggregated cumene production twin. This is a cyberphysical system and is characterized by a continuous two-way data exchange with real plants [44]. Data exchange within a cyberphysical system can be organized using a blockchain platform which can serve as a data management tool within the company. With the ever-increasing need for connectedness and security, especially in the petrochemical industry, blockchain may provide the backbone of the manufacturing future [45].

DT creation principles

Based on our research, using the example of the process of liquid-phase alkylation of benzene with propylene, we established the following stages in creating a DT, also applicable for any petrochemical process:

1. The formation of database of information about the functioning of a technological object, which can be performed in two ways:

– collection of process parameters by processing mode sheets of production operators, or collecting data directly from SCADA of a technological facility;

– calculation of the basis process parameters (pressure, temperature, reaction time, reflux ratio, energy consumption, etc.) by modeling the process using specialized software.

2. Defining the preferred algorithm for training a neural network model and calculation of its basic parameters (number of neurons and layers, types of transfer functions, etc.).

3. Assessment of the adequacy of the chosen neural network model using statistical methods criteria.

4. Calculation of the parameters of transfer functions required to predict the optimal parameters of technological modes of production facilities.

5. Selection of an intelligent system (IC) for industrial process control: a prototype of a DT, taking into account the scope and parameters of the application.

6. Programming of an intelligent industrial process control system, testing, pilot tests at an industrial plant.

7. Performing stages 1–6 for all technological objects and production processes.

8. Creation of an aggregated production twinon, including the developed DTs of related technological objects and their continuous data exchange with real installations, in order to clarify the functioning parameters.

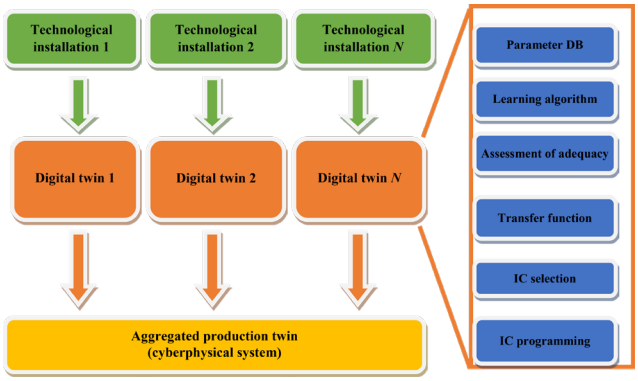

Fig. 5. Cyberphysical system creation algorithm.

CONCLUSIONS

The process of liquid-phase alkylation of benzene with propylene is one of the main large-scale petrochemical processes. At the same time, there is a need to create a cyber-physical system to control and continuously optimize production.

In this article we demonstrated an algorithm aimed at developing a digital production twin as the first step in creating a cyber-physical system. Using the results of the UniSim® Design simulation of the real plant a set of technological data was created and a neural network was built. This allows the economically optimal technological mode of the plant to be defined in online mode. In the process of forming the neural network. the principles of creating a digital duplicate of the process were established, and a prototype of the intelligent process control system was developed.

Given the importance of digital transformation, including the application of DTs and cyber-physical systems in industrial enterprises, the methodology developed to create a DT for the production of cumene by alkylation of benzene with propylene is also significant. The paper systematizes the principles of creating a DT production, as a comprehensive expert system of predictive analysis of production processes.

The practical application of the results of our study is to create a prototype of a DT based on a microcontroller for cumene production unit. A microcontroller control program based on neural network technology was created to enable online optimization of technological mode parameters to be carried out under continuous conditions.

It was shown that it is possible to form a technological database for training of DT in two ways. The first way consists in the processing of technological parameters, acquired from production. In the case of a lack of technological data, they can be obtained simulating the plant, for example, using UniSim® Design.

The implementation of the digital intelligent system will significantly reduce the response time of the operator or control system to changes in technological parameters. It will contribute to reduced costs and the number of measures required to optimize industrial technological processes, as well as improved efficiency and enhanced environmental friendliness of oil and gas chemical production.

Authors' contributions

K.G. Kichatov – writing and editing the text of the research article, methodology, hardware management, microcontroller programming (communication interface, neural network optimization).

T.R. Prosochkina – conceptualization, formal analysis, writing and editing.

I.S. Vorobyova – UniSim® Design simulation, neural network building and training, microcontroller programming.

The authors declare that they have no known competing financial interests or personal relationships that could have influenced the work reported in this document.

REFERENCES

1. Popov N.A. Business process optimization in the digitalization era of production. *Strategic Decisions and Risk Management*. 2019;10(1):28–35. https://doi.org/10.17747/2618-947X-2019-1-28-35

2. Geng Z., Zhang Y., Li C., Han Y., Cui Y., Yu B. Energy optimization and prediction modeling of petrochemical industries: An improved convolutional neural network based on cross-feature. *Energy*. 2020;194(4)116851. https://doi.org/10.1016/j.energy.2019.116851

3. Cozmiuc D., Petrisor I. Industrie 4.0 by Siemens. *J. Cases Inf. Technol*. 2018;20(2):30–48. https://doi.org/10.4018/JCIT.2018040103

4. Ardito L., Petruzzelli A.M., Panniello U., Garavelli A.C. Towards Industry 4.0: Mapping digital technologies for supply chain management-marketing integration. *Bus. Process Manag. J.* 2019;25(2):323–346. https://doi.org/10.1108/BPMJ-04-2017-0088

5. Rindfleisch A., O'Hern M., Sachdev V. The Digital Revolution, 3D Printing, and Innovation as Data. *J. Product Innov. Manag*. 2017;34(5):681–690. https://doi.org/10.1111/jpim.12402

6. D'Ippolito B., Messeni Petruzzelli A., Panniello U. Archetypes of incumbents' strategic responses to digital innovation. *J. Intellectual Capital*. 2019;20(5):662–679. https://doi.org/10.1108/JIC-04-2019-0065

7. Theorin A., Bengtsson K., Provost J., Lieder M., Johnsson C., Lundholm T., *et al.* An event-driven manufacturing information system architecture for Industry 4.0. *Int. J. Prod. Res*. 2017;55(5):1297–1311. https://doi.org/10.1080/00207543.2016.1201604

8. Broekhuizen T.L.J., Broekhuis M., Gijsenberg M.J., Wieringa J.E. Introduction to the special issue – Digital business models: A multi-disciplinary and multi-stakeholder perspective. *J. Bus. Res*. 2021;122:847–852. https://doi.org/10.1016/j.jbusres.2020.04.014

9. Appio F.P., Frattini F., Petruzzelli A.M., Neirotti P. Digital Transformation and Innovation Management: A Synthesis of Existing Research and an Agenda for Future Studies. *J. Product Innov. Manag.* 2021;38(1):4–20. https://doi.org/10.1111/jpim.12562

10. Kholopov V.A., Antonov S.V., Kurnasov E.V., Kashirskaya E.N. Digital Twins in Manufacturing. *Russ. Engin. Res*. 2019;39(12):1014–1020. https://doi.org/10.3103/S1068798X19120104

11. Agrawal A., Gans J., Goldfarb A. *Prediction Machines*: *The Simple Economics of Artificial Intelligence*. Boston, Massachusetts: Harvard Business Review Press; 2018. 272 p.

12. Ceipek R., Hautz J., Petruzzelli A.M., De Massis A., Matzler K. A motivation and ability perspective on engagement in emerging digital technologies: The case of Internet of Things solutions. *Long Range Plann*. 2021;54(5):101991. https://doi.org/10.1016/j.lrp.2020.101991

13. Eggers J.P., Kaul A. Motivation and Ability? A Behavioral Perspective on the Pursuit of Radical Invention in Multi-Technology Incumbents. *Acad. Manage. J.* (*AMJ*). 2018;61(1):67–93. https://doi.org/10.5465/amj.2015.1123

14. Libert B., Beck M., Wind Y. (Jerry). 7 Questions to Ask before Your Next Digital Transformation. *Harvard Bus. Rev*. 2016;12(7):11–13. URL: https://hbr.org/2016/07/7-questions-to-ask-before-your-next-digital-transformation. Accessed January 5, 2022.

15. Correani A., De Massis A., Frattini F., Petruzzelli A.M., Natalicchio A. Implementing a Digital Strategy: Learning from the Experience of Three Digital Transformation Projects. *Calif. Manag. Rev*. 2020;62(4):37–56. https://doi.org/10.1177/0008125620934864

16. Grieves M., Vickers J. Digital Twin: Mitigating Unpredictable, Undesirable Emergent Behavior in Complex Systems. In: Kahlen J., Flumerfelt S., Alves A. (Eds.). *Transdisciplinary Perspectives on Complex Systems*. Cham.: Springer; 2017. P. 85–113. https://doi.org/10.1007/978-3-319-38756-7_4

17. Negri E., Fumagalli L., Macchi M. A Review of the Roles of Digital Twin in CPS-based Production Systems. *Procedia Manuf*. 2017;11:939–948. https://doi.org/10.1016/j.promfg.2017.07.198

18. Zhou X., Eibeck A., Lim M.Q., Krdzavac N.B., Kraft M. An agent composition framework for the J-Park Simulator – A knowledge graph for the process industry. *Comput. Chem. Eng*. 2019;130(2):106577. https://doi.org/10.1016/j.compchemeng.2019.106577

19. Kockmann N. Digital methods and tools for chemical equipment and plants. *React. Chem. Eng*. 2019;4(9):1522–1529. https://doi.org/10.1039/C9RE00017H

20. Perno M., Hvam L., Haug A. Implementation of digital twins in the process industry: A systematic literature review of enablers and barriers. *Comput. Ind*. 2022;134:103558. https://doi.org/10.1016/j.compind.2021.103558

21. Hsu Y., Chiu J.M., Liu J.S. Digital Twins for Industry 4.0 and Beyond. In: *2019 IEEE International Conference on Industrial Engineering and Engineering Management* (*IEEM*). IEEE; 2019. P. 526–530. https://doi.org/10.1109/IEEM44572.2019.8978614

22. Lu Y., Liu C., Wang K.I.K., Huang H., Xu X. Digital Twin-driven smart manufacturing: Connotation, reference model, applications and research issues. *Robot. Comput. Integr. Manuf*. 2020;61:101837. https://doi.org/10.1016/j.rcim.2019.101837

23. Durão L.F.C.S., Haag S., Anderl R., Schützer K., Zancul E. Digital Twin Requirements in the Context of Industry 4.0. In: Chiabert P., Boura A., Noë F., Ríos J. (Eds.). *Product Lifecycle Management to Support Industry 4.0. PLM 2018. IFIP Advances in Information and Communication Technology*. Cham.: Springer; 2018. V. 540. P. 204–214. https://doi.org/10.1007/978-3-030-01614-2_19

24. Kuehner K.J., Scheer R., Strassburger S. Digital Twin: Finding Common Ground – A Meta-Review. *Procedia CIRP*. 2021;104(11):1227–1232. https://doi.org/10.1016/j.procir.2021.11.206

25. Adamenko D., Kunnen S., Pluhnau R., Loibl A., Nagarajah A. Review and comparison of the methods of designing the Digital Twin. *Procedia CIRP*. 2020;91:27–32. https://doi.org/10.1016/j.procir.2020.02.146

26. Zweber J.V., Kolonay R.M., Kobryn P., Tuegel E.J. Digital Thread and Twin for Systems Engineering: Requirements to Design. In: *55th AIAA Aerospace Sciences Meeting*. Reston, Virginia: American Institute of Aeronautics and Astronautics; 2017. https://doi.org/10.2514/6.2017-0875

27. Schleich B., Anwer N., Mathieu L., Wartzack S. Shaping the digital twin for design and production engineering. *CIRP Annals*. 2017;66(1):141–144. https://doi.org/10.1016/j.cirp.2017.04.040

28. Zhou G., Zhang C., Li Z., Ding K., Wang C. Knowledge-driven digital twin manufacturing cell towards intelligent manufacturing. *Int. J. Prod. Res*. 2020;58(4):1034–1051. https://doi.org/10.1080/00207543.2019.1607978

29. Melesse T.Y., Di Pasquale V., Riemma S. Digital Twin Models in Industrial Operations: A Systematic Literature Review. *Procedia Manuf*. 2020;42:267–272. https://doi.org/10.1016/j.promfg.2020.02.084

30. Aghayarzadeh M., Alizadeh R., Shafiei S. Simulation and Optimization of Styrene Monomer Production Using Neural Network. *Iranian Journal of Chemical Engineering* (*IJChE*). 2014;11(1-Serial Number 1, January):30–41. https://dorl.net/dor/20.1001.1.17355397.2014.11.1.3.2

31. Alizadeh M., Sadrameli S.M. Modeling of Thermal Cracking Furnaces Via Exergy Analysis Using Hybrid Artificial Neural Network–Genetic Algorithm. *J. Heat Transfer*. 20161;138(4):042801. https://doi.org/10.1115/1.4032171

32. Xin S., Yingya W., Huajian P., Jinsen G., Xinguing L. Prediction of Coke Yield of FCC Unit Using Different Artificial Neural Network Models. *China Petroleum Processing and Petrochemical Technology*. 2016;18(3):102–109. URL: http://www.chinarefining.com/EN/Y2016/V18/I3/102

33. Meyers R.A. *Handbook of Petrochemicals Production Processes*. 1st ed. New York, Chicago, San Francisco, Athens, London, Madrid, Mexico City, Milan, New Delhi, Singapore, Sydney, Toronto: McGraw-Hill Education; 2005. 744 p.

34. Ananieva E.A., Egorova E.V., Larin L.B. Current status and future tends of combined process producing acetone and phenol. 1. The market review and modern state phenol preparation processes. *Fine Chem. Technol*. 2007;2(2):27–43 (in Russ.).

35. Larin L.B., Egorova E.V., Ananieva E.A. Current status and future tends of combined process for producing acetone and phenol. II. Intensification methods of cumene oxidation process. *Fine Chem. Technol*. 2008;3(3):53–60 (in Russ.).

36. Pathak A.S., Agarwal S., Gera V., Kaistha N. Design and Control of a Vapor-Phase Conventional Process and Reactive Distillation Process for Cumene Production. *Ind. Eng. Chem. Res*. 2011;50(6):3312–3326. https://doi.org/10.1021/ie100779k

37. Zhai J., Liu Y., Li L., Zhu Y., Zhong W., Sun L. Applications of dividing wall column technology to industrial-scale cumene production. *Chem. Eng. Res. Des*. 2015;102:138–149. https://doi.org/10.1016/j.cherd.2015.06.020

38. Chudinova A., Salischeva A., Ivashkina E., Moizes O., Gavrikov A. Application of Cumene Technology Mathematical Model. *Procedia Chem*. 2015;15:326–334. https://doi.org/10.1016/j.proche.2015.10.052

39. Zarutskii S.A., Kichatov K.G., Nikitina A.P., Prosochkina T.P., Samoilov N.A. Simulation of the Process for Cumene Production by Alkylation of Benzene in Equilibrium Reactor. *Pet. Chem*. 2018;58(8):681–686. https://doi.org/10.1134/S0965544118080212

40. Mahmoudian F., Moghaddam A.H., Davachi S.M. Genetic-based multi-objective optimization of alkylation process by a hybrid model of statistical and artificial intelligence approaches. *Can. J. Chem. Eng*. 2022;100(1):90–102. https://doi.org/10.1002/cjce.24072

41. Sun X.Y., Xiang S.G. Product Distributions of Benzene Alkylation with Propylene Estimation Using Artificial Neural Network (ANN). *Adv. Mat. Res*. 2013;772:227–232. https://doi.org/10.4028/www.scientific.net/AMR.772.227

42. Tikhonenkov A.S., Peresypkin A.V., Toporskaya A.S., Suloeva E.S. Modeling of measuring systems based on programmable debugging circuits Arduino. In: *2017 XX IEEE International Conference on Soft Computing and Measurements* (*SCM*). IEEE; 2017. P. 519–521. https://doi.org/10.1109/SCM.2017.7970636

43. Vorobyova I.S., Kichatov K.G., Prosochkina T.R. *Neural network for determining the optimal parameters of the alkylation of benzene with propylene.* Computer program registration certificate RU 2020612986, 03.06.2020. Application № 2020612093 dated February 26, 2020 (in Russ.).

44. Prokhorov A., Lysachev M. *Digital Twin. Analysis, Trends, Global Experience*. 1st ed. Borovkov A. (Ed.). Moscow: AliancePrint; 2020. 401 p. (in Russ.). URL: https://datafinder.ru/files/new4/digital_twin_book.pdf

45. Mandolla C., Petruzzelli A.M., Percoco G., Urbinati A. Building a digital twin for additive manufacturing through the exploitation of blockchain: A case analysis of the aircraft industry. *Comput. Ind*. 2019;109:134–152. https://doi.org/10.1016/j.compind.2019.04.011

About the authors:

Konstantin G. Kichatov, Cand. Sci. (Chem.), Associate Professor, Department of Petrochemistry and Chemical Technology, Ufa State Petroleum Technological University (1, Kosmonavtov ul., Ufa, 450064, Russia). E-mail: kichatov_k@mail.ru. Scopus Author ID 54917537800, SPIN-код РИНЦ 7133-7325, https://orcid.org/0000-0002-5614-3743

Tatyana R. Prosochkina, Dr. Sci. (Chem.), Professor, Head of the Department of Petrochemistry and Chemical Technology, Ufa State Petroleum Technological University (1, Kosmonavtov ul., Ufa, 450064, Russia). E-mail: agidel@ufanet.ru. Scopus Author ID 6508101276, https://orcid.org/0000-0003-0859-3595

Irina S. Vorobyova, Master Student, Department of Petrochemistry and Chemical Technology, Ufa State Petroleum Technological University (1, Kosmonavtov ul., Ufa, 450064, Russia). E-mail: isvorobyeva@mail.ru. https://orcid.org/0009-0006-8254-1733

Об авторах:

Кичатов Константин Геннадьевич, к.х.н., доцент, кафедра нефтехимии и химической технологии, ФГБОУ ВО «Уфимский государственный нефтяной технический университет» (450064, Россия, Республика Башкортостан, Уфа, ул. Космонавтов, д. 1). E-mail: kichatov_k@mail.ru. Scopus Author ID 54917537800, SPIN-код РИНЦ 7133-7325, https://orcid.org/0000-0002-5614-3743

Просочкина Татьяна Рудольфовна, д.х.н., профессор, заведующий кафедрой нефтехимии и химической технологии, ФГБОУ ВО «Уфимский государственный нефтяной технический университет» (450064, Россия, Республика Башкортостан, Уфа, ул. Космонавтов, д. 1). E-mail: agidel@ufanet.ru. Scopus Author ID 6508101276, https://orcid.org/0000-0003-0859-3595

Воробьева Ирина Сергеевна, магистрант, кафедра нефтехимии и химической технологии, ФГБОУ ВО «Уфимский государственный нефтяной технический университет» (450064, Россия, Республика Башкортостан, Уфа, ул. Космонавтов, д. 1). E-mail: isvorobyeva@mail.ru. https://orcid.org/0009-0006-8254-1733

The article was submitted: September 30, 2023; approved after reviewing: January 29, 2023; accepted for publication: October 09, 2023.

The text was submitted by the authors in English
Edited for English language and spelling by Dr. David Mossop

MIREA – Russian Technological University
78, Vernadskogo pr., Moscow, 119454, Russian Federation.
Publication date *October 31*, *2023.*
Not for sale

МИРЭА – Российский технологический университет
119454, РФ, Москва, пр-т Вернадского, д. 78.
Дата опубликования *31.10.2023*.
Не для продажи

www.finechem-mirea.ru